Investigating the Commercial Viability of Stratified Concrete Panels

A thesis submitted in partial fulfilment of the requirements of the Degree of Master in Civil Engineering at the University of Canterbury

By Peter Grange

Supervised by James Mackechnie and Allan Scott

University of Canterbury 2012

Abstract

This thesis investigates the viability of producing stratified concrete panels (SCP) in an industrial setting. SCP comprise a heavyweight structural layer and a lightweight insulating layer. These two distinct strata provide the benefits of both thermal mass, to draw and store excess heat from a room and insulation to prevent rapid heat exchange on the exterior. SCP have been successfully produced in the laboratory under controlled conditions but the viability of commercial production had not been investigated.

The materials chosen for this research differed slightly from past work due to practical constraints of working in a precast yard. These materials include greywacke sandstone and expanded glass beads as the heavyweight and lightweight aggregates respectively. Several panels were cast on site using the vibrating tables of both the precast yard and the university. The panels were initially difficult to produce; consistent results were not achieved and a range of stratification levels were produced. This showed that some capital investment is required to provide more energy for vibration such that sufficient stratification can be reliably attained.

Two of the better stratified panels were then erected as if in service with the exterior facing north to test for warping effects in a practical setting. No measurable warping occurred over a period of two months. This concurred with past work and long-term warping readings that were taken of four year old panels.

Durability, thermal and structural tests were carried out on panels with a range of stratification levels to assess the sensitivity of these properties to the degree of stratification. Where stratification was poor, porosity was increased in the structural layer, due to lightweight aggregate contamination, leading to potential durability issues. Furthermore, it was established that panels with better stratification had significantly better thermal properties than those with moderate to poor stratification. Generally though, the thermal targets for this project were not realised as the total thermal resistance (R-value) readings did not meet the current code requirements. In some cases structural properties were improved with better stratification as the structural layer was stronger through better consolidation. Generally no structural properties suffered from greater stratification. In terms of durability however, the potential for delamination increased with stratification, and with age. This issue requires further research to minimise this effect which may include using fibres across the layer boundary.

It was established that SCP could be produced in the industry but with some changes and better protocols. Perhaps the most important conclusion from this work is that more vertical throw is required from the vibrating table to ensure sufficient stratification is achieved and the requisite properties are achieved. Partial stratification produces relatively poor thermal results, in comparison to well stratified panels, and affects structural properties. Better monitoring of stratification during vibration is also required to ensure consistency of the finished product. It was acknowledged also, that some material substitutions may be required for both technical and financial reasons.

As some investment is required to make industry based SCP production feasible, the most efficient way to produce SCP in the future is likely to be with the use of an assembly line approach such that only one panel is vibrated at a time and conveyed off the table to set. In this case, the vibrating table is only required to be the size of one panel so maximum vibration energy can be provided without excessive capital investment and satisfactory products can be consistently delivered.

Acknowledgements

This research was carried out in the Department of Civil Engineering at the University of Canterbury under supervision of Allan Scott.

Thanks must be given to concrete laboratory manager Tim Perigo for his continued and committed hard work and contribution to the testing solutions used here. Without his involvement the laboratory part of this research would not have run so smoothly. Thanks also to Craig Muir for his assistance with manual work.

A significant contribution to this project was provided by Stahlton Engineered Concrete in Hornby, Christchurch. Thank you to Tim Day, Deon Slatem and several other Stahlton employees for the continued use of your equipment, time and expertise in this development.

A special thanks to Dr. J.R. Mackechnie for his knowledge and passion towards this venture and his continued patience with my personal development throughout the length of this degree.

TABLE OF CONTENTS

TABLE OF FIGURES

TABLE OF TABLES

1 INTRODUCTION

Buildings consume more than 30 percent of the primary energy worldwide, with 65 percent of this attributed to heating, ventilation and cooling (Yang and Li, 2008). Heating residential houses is essential in cold countries while buildings in hot countries need to moderate the temperature by absorbing heat in the façade system and releasing it at night. Panels that are able to provide insulation and thermal benefits are an efficient way of addressing this. This saves heating energy and stabilises internal room temperatures by removing temperature spikes (Bobrowski, 1978). As energy becomes more expensive, the need for better energy efficiency increases as social and political pressure causes regulations to tighten.

Products such as insulating concrete forms have greatly improved insulation of building facades but these products prevent the full thermal mass of concrete being utilised. Thermal mass or fabric energy storage (FES) is a property of the material that enables it to absorb and store thermal energy within its mass. This means that the concrete will absorb heat when the room is hot, store it, and then release it once the internal temperature drops below that of the concrete. This results in cooler feeling rooms in summer and warmer rooms in winter. This means the temperature spikes are removed; interior temperature remains within a comfortable living or operating temperature (CCAA, 1999). Figure 1.1 below shows how internal temperatures can be moderated with the use of thermal mass.

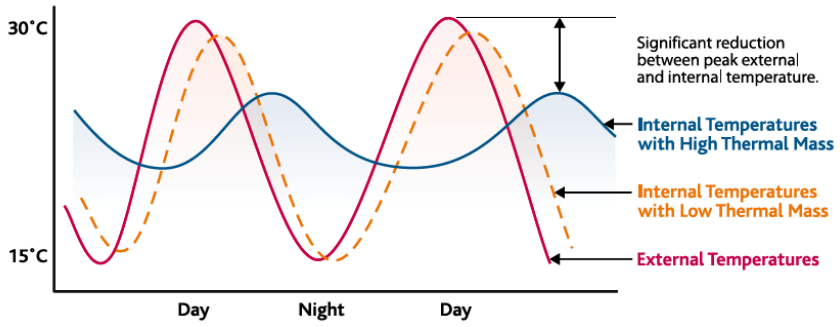

Figure 1.1: Stabilising effect of thermal mass on internal temperature (TheConcreteCentre, 2007)

Stratified Concrete Panels (SCP) are made by combining two different concrete layers to optimise thermal performance. Conventional concrete provides the benefit of thermal mass but has little insulating ability. Lightweight concrete in comparison offers limited thermal mass but has excellent insulating properties due to its low density and high air content. Other important properties of the lightweight layer include good durability and sound insulation as well as reduced energy demand during construction. A facade panel comprising both these layers can provide both thermal mass and insulating properties, leading to a considerable reduction in heating and cooling costs (Mackechnie and Saevarsdottir, 2008). Although in some buildings it is unlikely that mechanical cooling can be completely avoided, this passive alternative to air conditioning can greatly reduce the energy requirement and associated carbon dioxide emissions.

The concept of stratified concrete panels was suggested by Bellamy and McSaveney, combining the thermal storage of normal concrete with the thermal insulation of the lightweight concrete. This means that insulation can be provided without compromising the thermal mass of the concrete (Bellamy and McSaveney, 2003). Combining different concrete mixes within one panel is not easy to control and can provide challenges in consistent production practice. To achieve this however, a single mix containing both lightweight and heavyweight aggregates is cast and vibrated within the formwork using the density difference of the aggregates to form two distinct strata, a light section and a heavy section. Current research shows promising potential for future development of producing variable density panels. These panels can be manufactured with a simple, energy efficient process using mostly recycled materials. Figure 1.2 shows the production and setup of the panels.

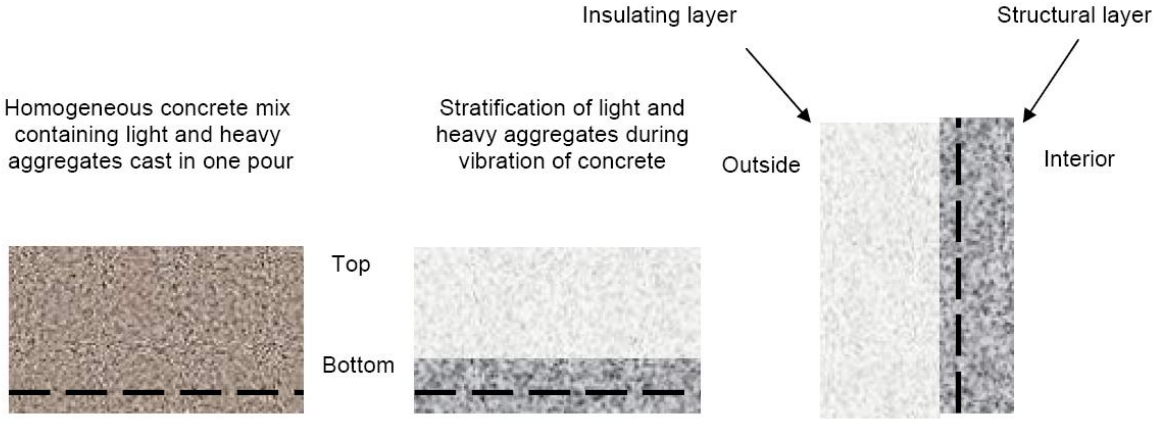

Figure 1.2: Illustration of stratified concrete panel production (Mackechnie et al., 2009)

Stratified concrete panels (SCP) are designed to be 250 mm thick and attempt to provide optimum thermal performance for this wall thickness. The interior face, providing thermal mass, is the heavyweight layer with a depth of approximately one third of the panel. The exterior face as the lightweight layer is two thirds of the panel depth and provides insulation due to its low thermal conductivity.

The thermal performance of buildings is often assessed by using the R-value or total thermal resistance. This property is defined as the thickness divided by the thermal conductivity and is a measure of the insulating ability of the product. A building with a high R-value has more resistance to heat loss in winter and heat gain in summer. New Zealand is divided into three climate zones with different R-value requirements for walls in solid construction (CCANZ, 2007b):

- Zone 1 – Auckland and Northland with minimum R-value of 0.8 m^2K/W
- Zone 2 – Remainder of the North Island with minimum R-value of 1.0 m^2K/W
- Zone 3 – South Island and Central North Island with minimum R-value of 1.2 m^2K/W

Table 1-1 below outlines the basic physical characteristics and properties of SCP showing that these targets can be achievable (Saevarsdottir, 2008).

Table 1-1: Technical objectives for stratified concrete panels

Material Property	Top Layer	Bottom Layer
Thickness (mm)	170	80
Density (kg/m^3)	1000	2250
Compressive Strength (MPa)	2-5	25-35
Thermal Conductivity (W/mK)	<0.25	1.00-1.25
Specific Heat (MJ/m^{3}K)	0.75-1.25	2.00-3.00
R-value panel (m^{2}K/W)	0.8-1.0	

Previous research within the Future Buildings Systems research programme has given the thermal values as shown where an excellent performance demonstrated values as low as 0.2W/mK and R-values of 0.8 and above.

To create these properties, some consideration must be given to the materials used and in what quantities they are mixed. Control of the cohesion of the mix is critical so that the layers are stratified under vibration but the mix remains together during handling. It is also important that sufficient durability and serviceability is provided for satisfactory long-term service of the panels. Materials used in this study were as follows:

- Heavyweight aggregate: Greywacke sandstone
- Lightweight aggregate: Expanded glass beads (EGB)
- Binders: Portland cement and microsilica

Work in the past has included the use of slag aggregate and fly ash as the supplementary binder (Saevarsdottir, 2008). For practicality however, the materials above were chosen as New Zealand precast operators are more familiar with these, reducing variables of production. Also, microsilica has been chosen over fly ash as less is required to attain satisfactory fresh and hardened properties.

Microsilica was used to supplement after the required performance was not attained with conventional constituents alone in the early development of SCP. The use of particular waste products, such as this, in concrete is a sustainable practice as cost reductions and technical benefits are possible. Further environmental benefits result as the relatively porous external façade absorbs a considerable amount of carbon dioxide, offsetting some of that created in the cement production process (Dayaram, 2010).

This development may see a rise in precast concrete wall systems used in residential homes. Precast panels have not been widely used in New Zealand in the past due to poor thermal and acoustic performance. Several concrete wall systems are currently manufactured with improved insulation values with the use of various insulation mediums. A good example of this is polystyrene ‘sandwich panels’ which incorporate a sheet of polystyrene in between two concrete panels to lower the density in the middle and deliver insulating properties. Despite providing adequate insulation properties, sandwich panels are inefficient to produce in terms of labour time, cost, and energy requirements. SCP can be shown to provide equal or better thermal performance while production could be cheaper and quicker.

Before these production and performance benefits can be realised, there are several technical concerns that must be addressed before SCP should be considered for production in the industry:

- The first point of concern is achieving a suitably high level of workability during mixing so that stratification will occur under vibration, whilst maintaining some segregation resistance. This must consider the fact that the different components of the mix have a tendency to separate under handling and transport.
- Once the panels are cast, control of warping and bending must be considered. As the two layers have different properties, there may be some tendency for the panels to bend during drying and thermal stresses.
- As SCP are to be used as façade panels, sufficient strength for service loads must be provided by the panel while the thermal performance is maintained. Sufficient depth of the heavyweight layer is also required to house the mesh at 40 mm cover depth.
- Finally the material must be shown to be durable and serviceable under mild to moderate levels of environmental exposure.

As full-scale research has not been carried out on SCP to date, the next stage in the development of commercial production of SCP is to assess the feasibility of fabricating panels on a large scale at existing precast yards. This involves using the work to date to optimise a mix design that can be cast on site at a Christchurch precast yard and attempting to vibrate this mix to create full scale stratified panels. This will give an indication of the stratification effectiveness of existing vibrating tables in precast yards whilst providing evidence for the best way forward for the commercialisation of SCP.

This document contains the following sections explaining the stages involved in this development:

Chapter 2: Literature Survey

This section considers current knowledge about concrete and concrete production. Special attention is paid to self-compacting concrete due to its relevance for this project. Background on the properties of concrete includes fresh properties, hardened properties, serviceability, durability and thermal properties. Some insight into the development of SCP so far is also given with a focus on the work of Park, 2006 and Saevarsdottir, 2008.

Chapter 3: Materials

This chapter looks at the materials used for SCP, considering the specific properties and benefits of each for SCP application. The material selection for this project was based on previous work in order to meet the rheological targets, but with consideration for the practicalities of the industry. A simple procedure using well understood and easily resourced materials was required to begin the commercialisation process of SCP.

Chapter 4: Test Procedures

This discusses the procedures used at different stages of the project, comprising three main subsections:

- Fresh properties and mix design: A discussion on the rheological targets and how the mix was designed to meet them.
- Site panel tests: An order of events of the various attempts to create satisfactory stratification in large scale panels and the ensuing monitoring
- Hardened property tests: An outline of the testing procedures used to assess the quality of the various panels including structural, thermal and durability tests.

Chapter 5: Mix Design Trials

This chapter provides results of the mix design trials as explained in chapter 4, providing details of the optimisation process with justifications of adjustments to the design at each stage. An eventual final mix design is then provided. This chapter also looks at the vibration mechanism and length of time of vibration to produce well stratified SCP.

Chapter 6: Site Panel Testing

As with chapter 5, this section discusses an iterative optimisation process; in this case the production of SCP in a precast concrete factory. The process of producing satisfactory stratified panels consistently is discussed and justifications for changes to the production approach are outlined. The eventual end product is examined. Results from the monitoring process are then explained and compared with previous work.

Chapter 7: Hardened Properties Tests Results

This chapter outlines the results for each of the tests carried out on the various panels. These tests measure the:

- Degree of stratification/centre of mass
- Density and compressive strength of each layer
- Axial compressive strength
- Flexural tensile strength and displacement
- Delamination strength
- Thermal properties
- Porosity (water sorptivity test)

Comparisons are then drawn between the different panels in terms of both age and degree of stratification. The data is then compared to target measurements to assess the performance quality of the commercially produced SCP.

Chapter 8: Conclusions and Recommendations

This final section summarises the results of the project and discusses them in terms of the commercialisation potential of SCP and market acceptance of new innovations. This looks at both the quality of the product as well as the practical constraints of producing SCP on this scale and larger. Possible suggestions on how to research and develop this technology further are given.

2 LITERATURE REVIEW

Concrete is a multiphase material, the properties of which are dependent on several material, processing and environmental factors. With different combinations and ratios of aggregates, fines, paste and other constituents and additions, concrete can be designed to suit many purposes. Of specific interest to this research study are the following parameters:

- Fresh properties
- Hardened properties
- Serviceability
- Durability
- Thermal properties

The relevance of each of these to stratified concrete panels (SCP) is outlined below.

2.1 Fresh Properties

The finished concrete product is dependent on control and consistency of the fresh concrete properties. If the fresh properties are correctly controlled; transport, placement, compaction and finishing can be more easily achieved to ensure satisfactory performance of the end product. Some important characteristics to consider are workability, rheology and segregation.

2.1.1 Workability

Workability controls the ease and homogeneity with which concrete can be placed. A mix with high workability is required for difficult to reach or highly reinforced areas. Mixes that do not meet workability targets may create voids or weak areas and concrete may not be consistent throughout the placement.

The ability of the concrete to fill the form with available work or vibration depends on the water, air and aggregate content as well as any additives. A higher water/cement ratio will increase the workability but too great an increase will result in bleeding or even segregation. An increase in air content also increases the workability but can reduce strength in the hardened specimen if too much air is entrained. Special additives in the mix can increase the workability of the mix without the requirement for excessive water. This can be a useful way to aid placement while avoiding strength losses later on. Super-plasticisers are used to produce flowing concrete with very high slump without the use of excessive water. Some other chemical admixtures can further aid control of the fresh properties of the concrete such as viscosity modifying mixtures (VMA) (Nanthagopalan and Santhanam, 2010) where others can however, encourage segregation or excessive bleeding if too much is added (Kwan and Ng, 2009). This will obviously reduce the quality of the finished product.

As fresh concrete begins to age, the workability decreases as hydration of cement takes place. This limits the time frame in which concrete can be placed. The relative rate of hydration is shown on Figure 2.1, where placement must be completed before the setting stage begins and workability is lost. This is a function of the constituents of the mix as well as external factors such as weather conditions; air temperature, ground temperature, wind speed and the presence of moisture. Changes to the setting time can be controlled with accelerators and retarders (Neville, 1995).

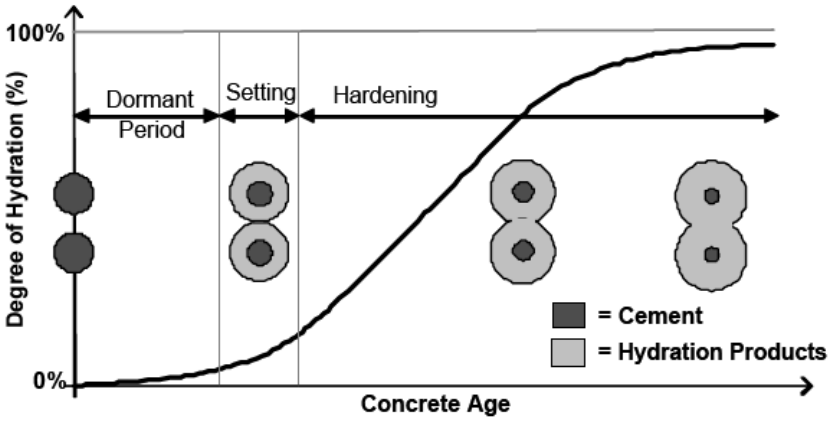

Figure 2.1: Physical interpretation of the degree of hydration development (Schindler, 2003)

Workability is usually measured with the slump test for structural mixes or the spread test for self-compacting concrete (SCC) mixes; both using Abrams cone (Neville, 1995). A relatively stiff, dry sample will hold up and show little slump where a very wet self-compacting mix will flow more freely.

SCP requires sufficient workability to allow for controlled segregation under vibration while segregation during handling and transport is prevented or substantially reduced. Park tested a range of SCP mixes with spread readings ranging from 350 – 630 mm (Park, 2006). The optimum target consistence range for SCP is a spread of 500-520 mm to achieve best rheological properties.

2.1.2 Rheology

Rheology is defined as the scientific description of the flow and deformation of matter. For concrete, rheology is typically used to help describe workability, which is defined as the property describing the ease with which concrete can be mixed, placed, consolidated and finished to a homogenous condition (Koehler, 2009).

More specifically, rheology is a measure of yield shear stress, plastic viscosity and shear rate. The yield stress is a consequence of inter-particle forces. The shear force required to irreversibly break these links is dependent on time and previous shear history as well as shear rate. This yield shear stress can be found with a rheometer where the shear stress needed to initiate flow is measured (Banfill, 2003). The plastic viscosity is then a measure of the resistance to flow once the yield shear stress has been overcome. This can be measured using a rheometer or indirectly by timing the spread of the mix from Abrahm's cone (T500 test). The shear rate is a measure of the rate of strain within the material. In essence this means that the yield stress is the product of the plastic viscosity and the shear rate (Mackechnie, 2010a).

Fresh cement paste has very low yield shear stress of usually less than 100 Pa. With increased aggregate content, the yield stress and the plastic viscosity increase due the greater resistance to flow generated from greater inter-particle interaction. Mortars and flowing concrete have yield shear strengths of 100 – 400 Pa, much lower still than stiff structural concrete mixes with up to 2000 Pa.

Figure 2.2a explains the effects on yield shear stress and plastic viscosity as functions of various influences (Ferraris and Gaidis, 1992). Of particular interest is the effect of increased water

decreasing both yield shear stress and plastic viscosity while greater paste content increases the plastic viscosity and reduces the yield shear stress. Figure 2.2b demonstrates the rheological properties for different fresh concrete consistencies.

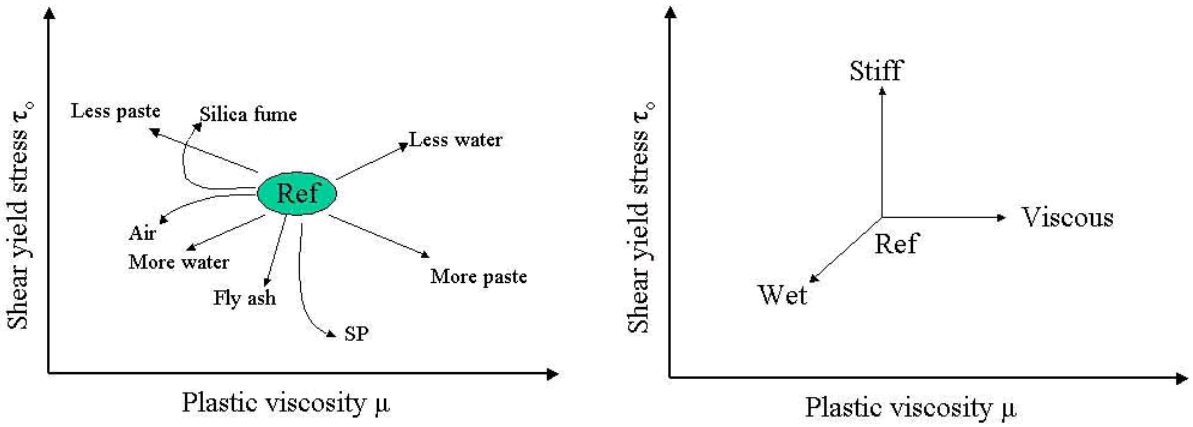

Figure 2.2a: Material effects on rheology (Wallevik and Nielsson, 2003) Figure 2.2b: Physical rheology (Banfill, 2003)

Figure 2.2a also demonstrates the effects that various admixtures and additives can have on the rheology of concrete. For example, super-plasticiser significantly reduces the yield stress while air reduces the plastic viscosity without affecting the yield stress greatly. Fly ash and silica fume both reduce the plastic viscosity, to varying degrees, but have completely opposite effects on the yield shear stress, fly ash reducing it and silica fume increasing it.

The rheology of SCC differs from that of normal and high strength concretes. Figure 2.3 shows the flow rates of the different concrete types. The most important difference is that SCC has almost no yield point (or about zero to 60 Pa) compared to normal or high strength concrete where the yield shear stress ranges from several hundred to a few thousand Pascal. The rate of shear is comparable between SCC and normal concrete, where high strength has a much steeper rate. The low yield shear stress together with a low plastic viscosity of less than 50 Pa.s gives SCC its high flow characteristics.

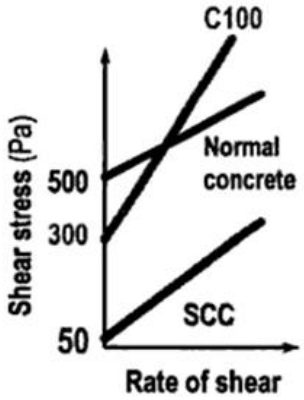

Figure 2.3: Flow curve of normal, high strength and self-compacting concrete (Wallevik and Nielsson, 2003)

For the purpose of SCP, rheological testing has been carried out to locate the optimum zone for controlled segregation. Initial work suggested that a moderately cohesive concrete with good flow characteristics could produce a well stratified concrete (Mackechnie et al., 2009). Figure 2.4 below shows the best rheological range for controlled stratification.

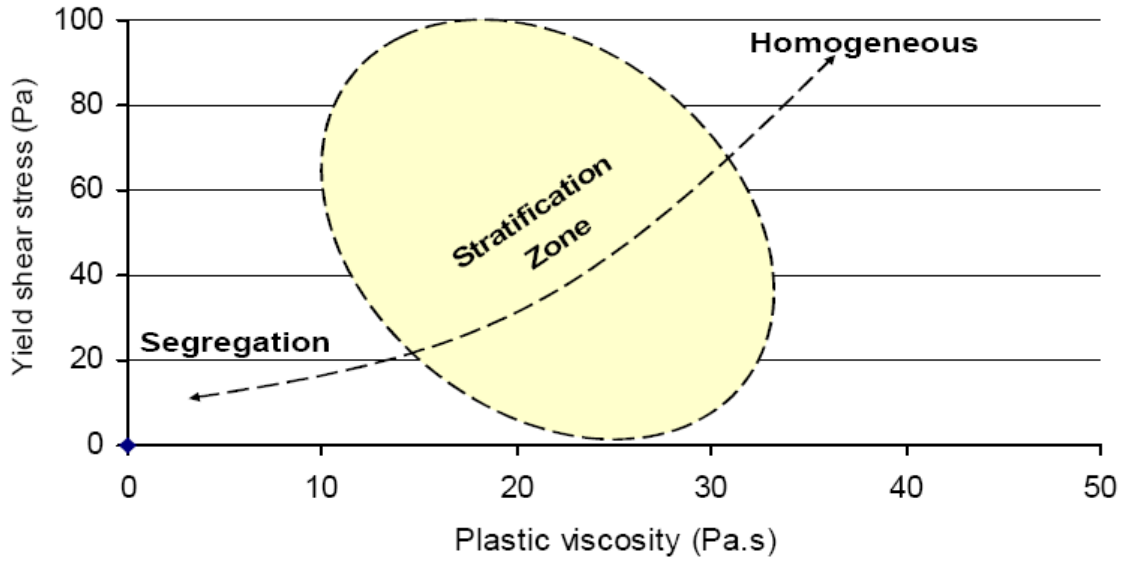

Figure 2.4: Ideal rheological zone for stratification (Mackechnie et al., 2009)

Here a yield shear stress of below 100 Pa and plastic viscosity of between 10 and 35 Pa.s are the target rheological parameters for best control. When the plastic viscosity is too low, uncontrolled segregation occurs during handling and the mix will separate. When it is too high, stratification is unlikely to occur as the mix provides resistance to any segregation.

Concrete begins to gain strength once placed without further agitation as it is an age-stiffening, thixotrophic material. Once initial set occurs, the rheological properties of the fresh concrete are lost as is workability.

2.1.3 Segregation

Segregation describes the tendency for uniformity to be lost across a concrete mix, both horizontally and, more often, vertically. As concrete comprises a wide variety of materials sizes and densities, failure to balance these appropriately can lead to separation when the concrete is subjected to transport loads or even gravity alone. The specific gravity of concrete constituents ranges from 1000 kg/m^3 to 3200 kg/m^3 for normal concrete mixes and can span even greater differences when lightweight materials are used.

A recent trend has seen an increase in the fluidity of concrete mix designs with the development of self-compacting mixes, increasing the ease of placement. This has the potential for segregation when the fluid levels increase as coarser particles can be encouraged to travel further than lighter ones leading to separation, particularly when the grout separates from the mix in excessively wet cases (Roussel, 2006). Although some work has been completed to attempt to model the exact conditions for segregation, the complex structure of concrete makes it very difficult to quantify. Segregation in mortars for example could be predicted by paste rheology and the volume, shape and size of the sand particles. Concrete however, controlled more by grain to grain contacts, is far

more difficult to quantify as the interaction of all particles over a large range of relative sizes must be considered (Larrard and Sedran, 2002).

When the level of workability is increased, the risk of segregation increases as the yield shear stress and plastic viscosity are lowered. Here handling of the mix during transport and placement becomes potentially dangerous for segregation. To help control the risk, a sensible grading must be employed across the mix. This can be assisted by the following recommendations (Neville, 1995):

- Avoiding large aggregates greater than 25 mm in diameter (reduces drag)
- Keeping the fines content high enough for the purpose (increases cohesion)
- Using angled aggregates where possible (round aggregates have lower drag)
- Applying the correct amount of water (maintains a reasonable plastic viscosity)

Concrete with high segregation resistance exposed to normal construction practice will remain consistent in both the horizontal and vertical directions such that the distribution of particles is very close to uniform throughout. Where this is not the case, blocking around reinforcement may occur during placement which can lead to weak areas in the finished concrete where materials may have clumped (Bui et al., 2002).

For the purpose of SCP production, segregation during handling and transport of the fresh concrete is to be minimised by keeping the mix within the recommended rheological constraints. However, once the mix is in the formwork, it is segregation, in a controlled fashion, that provides SCP with the required stratified effect. This process is based on the density difference between the light and heavyweight aggregates. Under the appropriate level of vibration, the heavyweight aggregates with specific gravity of 2.7 g/cm^3, drop through the paste with specific gravity of approximately 2.1 g/cm^3. The heavyweight aggregates are most prone to segregation because of this density difference. The lightweight aggregates rise through the mix as they are displaced by the dropping heavyweight aggregates and are subject to buoyancy effects (Chia et al., 2005).

Theoretically, any two substances with different specific gravities will eventually separate into layers under vibration in the fullness of time, but here the mechanism and rate at which this layering occurs is a function of two factors. The first of these is the vibration mechanism. This is a function of the frequency and direction of the vibration. The optimum vibration frequency for stratification of the panels has been deduced to be between 2500 rpm and 3500 rpm (Saevarsdottir, 2008). Vibration frequency of much below this range moves the mix as a whole and fails to encourage different actions on the individual components of the mix. Anything much higher results in little vertical travel as the direction change is too rapid so does not give the aggregates a chance to sink. The vibration is much more effective when it is predominantly perpendicular to the intended direction of stratification; that is vertically oriented. This means that movement up and down will encourage the aggregates to drop through the mix whereas side to side vibration is much less effective.

The second governing factor is the plastic viscosity of the mix. Once the low yield shear stress of the fresh concrete is broken by the vibration, the plastic viscosity effectively controls the rate of movement of the material. This means when the plastic viscosity or unwillingness to flow, is very high, the aggregates will be held up in the paste and resist segregation. As the intention here is to encourage controlled segregation to create stratification, the plastic viscosity, as discussed in the rheology section, must be kept reasonably low, but without compromising segregation resistance during handling and placing.

2.2 Hardened Properties

The hardened properties ultimately govern the success or failure of the concrete performance. This considers the stiffness and strength as well as deformations; both short term drying shrinkage and long term creep.

2.2.1 Strength

Concrete is used in construction primarily for its high compressive strength. The water/cement ratio of the mix is usually considered to control the strength; that is the lower the ratio, the stronger the concrete (Caldarone, 2008). Aggregates usually make up 60-70 percent of a typical concrete mix but unless they are particularly soft, this is not a limiting factor of the strength of concrete.

Strength can also be affected by weaknesses between different components and materials within the mix. Weak inter-material layers can be minimised by choosing appropriate aggregates. This includes completing a well graded system by considering a sensible maximum size as well as using angled aggregates with sufficient surface texture to form a stronger bond with the surrounding paste than round smooth aggregates that can allow slip, especially in high strength concrete (Hussin and Poole, 2011).

The compressive strength of concrete is very rarely a critical factor for design as it is easy to retain high levels of strength whilst adjusting other parameters. The strength can be varied from 17.5 – 30 MPa, as in most New Zealand residential housing, right up to over 100 MPa for high performance large scale structures. The use of supplementary cementitious materials can improve the compressive strength by densifying the interfacial transition zone (ITZ) and improving interlock with the aggregates. For example, a mix with 20 percent replacement of cement by 10 percent fly ash and 10 percent silica fume reached compressive strengths with an increase of 15-64 percent after 7 days and 13-24 percent after 28 days (Chinnaraju et al., 2010).

Despite the very high compressive strength of concrete, the tensile capacity is much lower at around ten percent of the compressive strength. This means that concrete often fails in tension due to the changing shape of the specimen under excessive compressive loads displacing the concrete out in the perpendicular direction. Many experiments show that for concrete prisms or cylinders under uniaxial compression, the Poisson's ratio increases gradually as the axial strain increases; from 0.2 at low strain and over 0.5 for axial strain above peak-strain and up to 1.0 when loaded to failure (Faxing and Zhiwa, 2006). For structural purposes, concrete is usually reinforced with steel to provide the tensile capacity and confinement.

SCP requires enough strength to carry service loads and to resist moderate levels of abrasion. This means that strength of 20 – 30 MPa must be developed in the structural layer to meet standard requirements for residential construction. As the lightweight aggregates in the mix provide little to no strength contribution, the more pronounced the stratification is, the stronger the structural layer will be. That is a structural layer with minimal contamination of lightweight aggregate will reach sufficient strength. Testing carried out by Saevarsdottir across a range of mix designs produced an average compressive strength of 21 MPa for the structural layer and 10 MPa for the lightweight layer (Saevarsdottir, 2008).

To resist surface abrasion most effectively, a thin layer of paste is required on the top of the panel to shield the lightweight aggregates as they are too soft to resist wear and can pull off the surface if not held in with sufficient paste. This means that over-vibrating the mix can lead to weak or

insufficient weathering resistance by exposing the weak lightweight aggregates on the exterior surface. This can however, be remedied by applying a wearing layer to the panel surface.

2.2.2 Modulus of Elasticity

The elastic modulus of concrete depends on the stiffness of the hardened cement paste, the aggregates, and on the inter-facial transition zone (ITZ) between the two for higher strength concretes. Aggregates have a major influence on the stiffness due to the high proportion present in most concrete mixes and the greater relative stiffness of aggregates compared with the paste. Aggregates from around New Zealand are varied in terms of stiffness due to the geologically active history of the land. Rocks such as greywacke, sandstone, basalt or phonolite produce concrete with consistently higher elastic moduli than the values predicted by NZS 3101 while some volcanic rocks from other areas, such as andesite aggregate from Taranaki, have relatively low stiffness, often less than 25 GPa. This is inherent to the SCP materials so the stiffness of the concrete cannot be increased by bolstering the stiffness of the hardened cement paste (Mackechnie and Fenwick, 2009).

Concrete is a non-linear inelastic material in both tension and compression. As such, caution must be taken when quantifying the modulus of elasticity. As Figure 2.5 demonstrates, the initial stiffness of the concrete sits between the stiffness of the aggregate and the cement paste. This counter intuitive concept can be explained by the tri-axial compression on the cement paste increasing the strength.

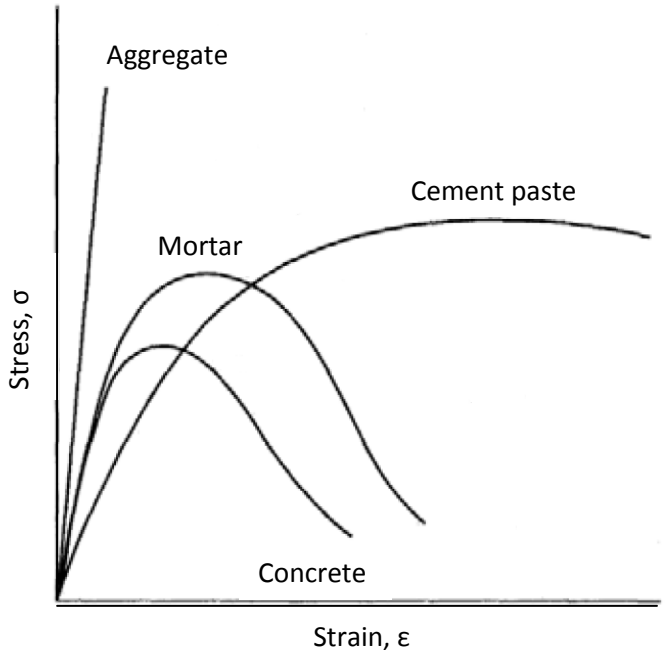

Figure 2.5: Stress-strain curve for normal weight concrete and constituents (Mindess et al., 2003)

Concrete is usually considered to act elastically to up to 40 percent of the ultimate compressive strength. This modulus is often used in sizing structural sections, both reinforced and unreinforced, and computing stress for observed strain (ASTM, 2011). The modulus is given as either a secant or chord modulus by adjoining two appropriate points on the stress-strain curve as not to overestimate the stiffness when concrete begins to crack.

The lightweight aggregate used in SCP contributes little to the stiffness of the panel. As discussed in the above section, the level of stratification governs the performance. This means that a well stratified structural layer will provide sufficient stiffness as a standard concrete panel, where a poorly stratified panel will be riddled with weak inclusions so may perform unsatisfactorily. If the stiffness provided is insufficient, then early deformation or even failure of the panel under structural service loads will result.

Results from previous work on SCP have shown the elastic modulus of the lightweight layer to range from 4.5 to 13 GPa with an average of approximately 8 GPa while the structural layer provides anywhere from 14 to 30 GPa (with the exception of one reading at 8 GPa) with an average of 19 GPa (Saevarsdottir, 2008).

2.2.3 Drying Shrinkage

Drying shrinkage is an important time-dependent property of concrete. It is measured as the strain of an unloaded, unrestrained specimen occurring principally due to loss of water during the drying process. Other shrinkage components, namely autogenous (self-desiccation of concrete during continued hydration) and carbonation are very small compared with drying shrinkage.

Drying shrinkage is often most significant in tall structures as large deflections can result cumulatively over such length or height. This can go on to affect the control of joints and spacing, movement of bearing and loss of prestress. Deflections caused by drying stresses can also produce serviceability issues where cracking, structural deformations and durability concerns can arise (Wong et al., 2007).

Drying shrinkage can be difficult to predict as it can be sensitive to many factors. These include the water/binder ratio, degree of cement hydration, aggregate characteristics, modulus of elasticity and water content while considering that, in general, a greater quantity of aggregates will reduce the overall shrinkage as Figure 2.6 demonstrates. Some correlation can be drawn as to the difference in shrinkage when using lightweight aggregates compared to normal weight aggregates (Zhang et al., 2005). In the first six months, normal weight concrete often displays greater shrinkage than lightweight concrete. This can be attributed to shorter consolidation time for heavier aggregates and reduced autogenous shrinkage of the lightweight aggregate. After an extended period however, lightweight concretes, with lower modulus of elasticity, exercise less resistance to shrinkage at the paste aggregate interface and therefore demonstrate higher levels of shrinkage than normal weight concretes as is shown on Figure 2.7 (Newman, 1993).

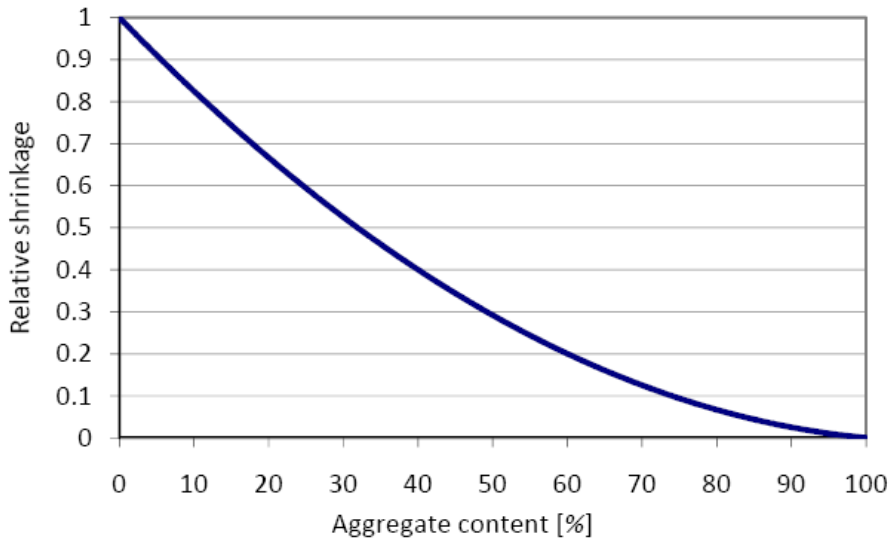

Figure 2.6: Changes in relative shrinkage with aggregate content (Mindess et al., 2003)

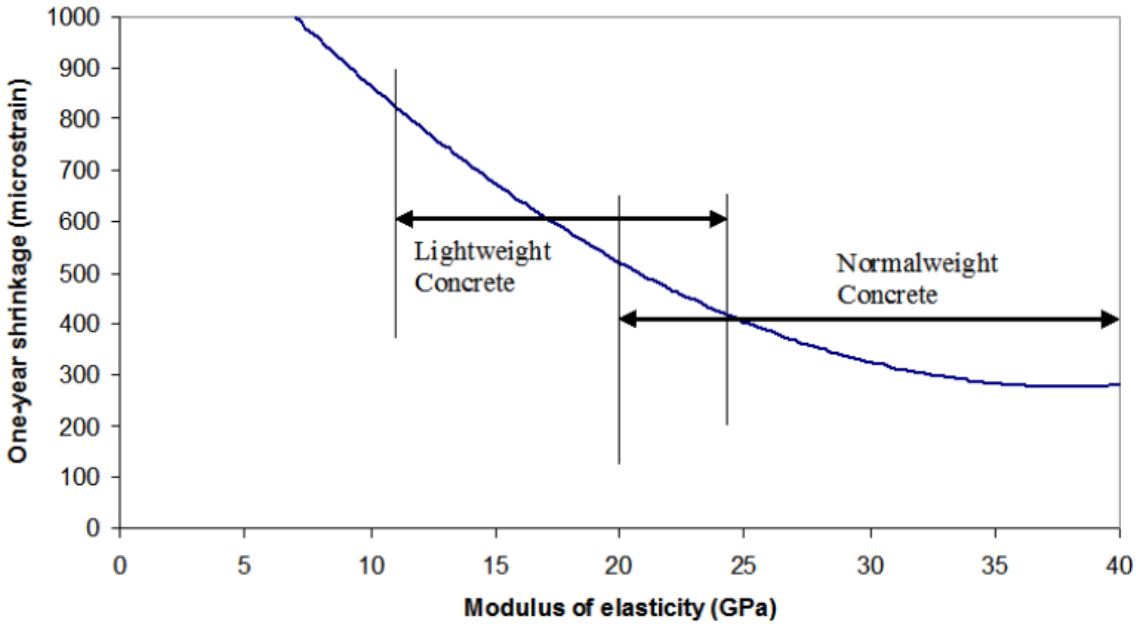

Figure 2.7: Influence of modulus of elasticity of aggregates on drying shrinkage (Mindess et al., 2003)

As well as a function of the material content, drying shrinkage depends on the geometry of the section. It is clear that a thinner cross-section, having greater surface area to volume ratio, will have greater initial shrinkage as the diffusion path is reduced. This then leads to smaller overall ultimate shrinkage. The reverse of this is true meaning that very thick sections may experience significant volume change over time.

Drying shrinkage is a very important consideration for SCP as both heavyweight and lightweight materials are present so differential shrinkage and stresses may be encouraged. For a well stratified panel, the two strata can be considered as two different panels attached in the middle with a

transition phase. If the aggregates demonstrate different drying shrinkage characteristics, the differential between the two layers may cause excessive stress along the interface and even lead to slipping and delamination. This effect could also lead to warping during service as the heavyweight interior layer is subjected to more severe drying; this is covered in greater depth in the section (2.3.1).

Results from previous work show that the shrinkage in the lightweight concrete was typically twice that measured in the structural concrete. All readings for shrinkage were however, very minimal and well within serviceability limits (Saevarsdottir, 2008). Some factors that influenced the shrinkage were dependent on materials and conditions:

- Higher water/binder ratios for otherwise identical mixes increased the shrinkage in both the lightweight and heavyweight layers.
- Using larger lightweight aggregate particles increased the shrinkage in the lightweight layer but decreased the shrinkage in the structural layer, further increasing the differential shrinkage between the two strata.
- Instead of perlite as the lightweight aggregate filler, using fine grade expanded glass beads significantly decreased the shrinkage in both layers due to decreased water movement through the aggregate particles in comparison to the more porous perlite aggregate.

The shrinkage in the structural layer is comparable to normal concrete in the range of 650 to 1100 microstrain after 56 days (Saevarsdottir, 2008). The lightweight layer, though slightly more susceptible to shrinkage, has the capacity to absorb some shrinkage without cracking as would be seen in structural concrete. More specifics about the chosen materials for the commercialisation of SCP are given in chapter 3.

2.2.4 Creep

Creep can be defined as the time-dependent increase in the strain of concrete under a constant and sustained compressive or tensile stress (Wong et al., 2007). Like drying shrinkage, creep is affected by the hydration of cement and drying of the paste; there are many inter-linking facets between the two. This can be seen most prominently in a comparable magnitude of strain as well as a certain degree of irreversibility (Neville, 1995).

As well as continued strain under sustained stress, creep can occur in the form of relaxation. This can be seen as a time-dependent decrease in stress such as prestress loss which can lead to settlements and buckling of columns (Mackechnie, 2010b).

Concrete creep can be divided into basic creep and drying creep. Basic creep is not dependent on the member size or drying environment. It occurs when there is no drying shrinkage or moisture movement between the concrete and the ambient environment. Drying creep is additional creep that occurs when the concrete is still drying while subjected to stress. Like for drying shrinkage, drying creep depends on geometry and drying conditions as it is associated with loss of water. This means drying creep is minimised by thicker elements, specimen maturity upon initial loading, a reduction in temperature, relative humidity and wind. Drying creep can amplify the basic creep by 10-70 percent (Mackechnie and Fenwick, 2009). In practice this distinction is often ignored and creep is simply considered as the deformation under load, a considerable proportion of which is irreversible.

Creep effects can be minimised by optimising the mix design. The most important aspect in minimising creep is the quality and quantity of aggregates used as these act as a direct restraint

against creep. Using more aggregates or those with higher elastic moduli will provide greatest resistance to creep. Secondarily, reducing the water/binder ratio helps to further reduce creep.

As well as concrete constituents, the degree of creep can be controlled with proper site procedures. This is largely a factor of the humidity of the environment. The curing conditions also play a role in the degree of creep. As concrete is more porous at early stages of hydration, creep will be greater if it is loaded before appropriate maturing of the concrete is completed.

The geometry of a concrete specimen also holds some accountability for the creep action. As the surface area to volume ratio is increased, the creep per applied stress increases as the case becomes less dimensionally stable. The temperature of the concrete at loading may cause excessive creep, particularly when is it maintained at between 50 and 90 degrees Celsius, creep tends to develop faster (Mindess et al., 2003). Loading of concrete pushes gel water out of inter-lamina layers to consolidate the material up to about 40 percent of the ultimate load. Up to this point, creep is considered to be a linearly proportional response to the applied stress. Beyond this level however, micro-cracking begins to occur and creep accelerates.

Work completed on lightweight concrete has demonstrated that it provides significantly poorer resistance to creep than normal weight concrete. This was partly attributed to higher shrinkage strains and excess water loss from the saturated lightweight materials (Gesoglu et al., 2004) (Nilsen and Aitcin, 1992). For the purposes of SCP this could give rise to some dimensional stability issues. On the other hand, this could prove to be a useful quality as the willingness of the lightweight layer to creep may provide some stress relief between the two strata rather than cause warping stresses or lead to delamination.

2.3 Serviceability

Serviceability is a measure of the capability of the concrete to remain appropriate for service during its useful life. Though these concerns are often not as important to structural integrity of the hardened properties, ongoing serviceability issues can leave buildings unsuitable for use and can be costly to repair. Warping and delamination are of particular importance to serviceability for SCP.

2.3.1 Warping

The term warping is often used inter-changeably with the term curling and is defined as out of plane deformation of a concrete cross-section such that the member becomes curved or distorted. This is caused, in essence, by differential shrinkage resulting from variations in temperature or moisture content. Warping is most prevalent near joints or edges as these differences are more emphasised. For this reason, other effects such as autogenous shrinkage do not tend to impact on warping as the effects are mostly uniform across a panel or slab so do not cause differential shrinkage.

Curling in concrete slabs is fundamentally caused by differential strain due to humidity difference across the thickness of the slab. Due to the inherent dimensional instability of concrete when subject to moisture content changes, curling upward of the slab edges results. Due to shrinkage, a weightless slab would deform into part of a large sphere with the top surface inside. Flattening of the slab under its self-weight holds this curl to a concave upwards shape as shown below in Figure 2.8 (Mailvaganam et al., 2000), and curling is relieved by cracking.

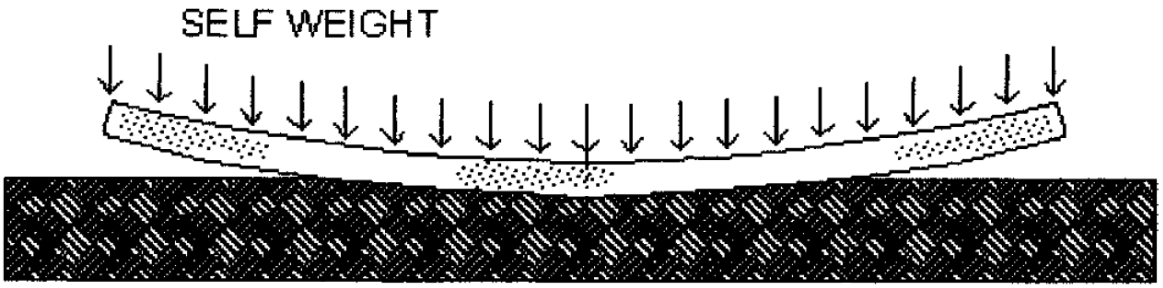

Figure 2.8: Upward concave curling of a concrete slab (Mailvaganam et al., 2000)

This effect can occur from shrinkage on the top surface relative to the bottom surface caused by a lower temperature or dryer conditions on the top surface. Where the temperature is greater or more moisture is present on the top surface then the opposite can occur with convex curling. These effects can result from seasonal temperature variances where the top of a slab is more exposed than the bottom just as the external façade of a wall panel is likely to experience a greater range of temperatures and conditions than the controlled internal face.

Warping is often apparent in the relatively early stages but can occur over an extended time period. Curling straight after placement is often a result of poor curing conditions or excessive bleeding with high relative water content. The moisture gradient created from rapid drying sets up differential shrinkage within concrete. Some finishing techniques that draw fine aggregates and paste to the surface can also increase differential shrinkage.

Warping can be minimised with attention to construction practice and handling as well as using an appropriate mix design. The use of specific aggregate types, shapes and sizes is important as bigger aggregates can reduce curling. The water/cement ratio and the cement type impact greatly on shrinkage so can help control warping if designed properly for the purpose. A well graded system of particles reduces the abruptness of the change in particle density across the mix which lessens potential curling. One good example of a poor mix design in Perth, 1985 showed how excess cement and a lack of sand in the mix can cause problems as significant warping resulted. Inclusions of sand into the mix fixed the issue showing the sensitivity of the mix to poor grading (Shayan, 1985).

SCP has the potential to experience warping to some degree due to the differences in material properties between the two strata. This means there is some chance of differential shrinkage between the two strata from which curling may result. To help minimise this, a mix design with a suitable gradient of particles will be required. Previous research by Saevarsdottir has shown that panels made with inorganic polymers and pumice show slightly more tendency for bending than panels made with Portland cement and expanded glass beads. A potential reason for this is that pumice, with greater strength than expanded glass beads, provides more resistance to creep when following the structural concrete. This means the creep is not ‘absorbed’ here as it is in a softer glass bead layer. The most important warping observation from this research is that every warping reading was below a 0.2 percent threshold so was not considered a concern for the serviceability of SCP produced in the laboratory (Saevarsdottir, 2008).

Some nominated tolerances for warping or bowing in solid or insulated flat structural wall panels are given in the *PCI* Manual: *Tolerance Manual for Precast and Prestressed Concrete*

Construction. Of greatest relevance to this project is the length bowing as shown in Figure 2.9. Here the maximum out-of-plane bowing value is ±0.5 in. (±13 mm) (Sorenson et al., 2000).

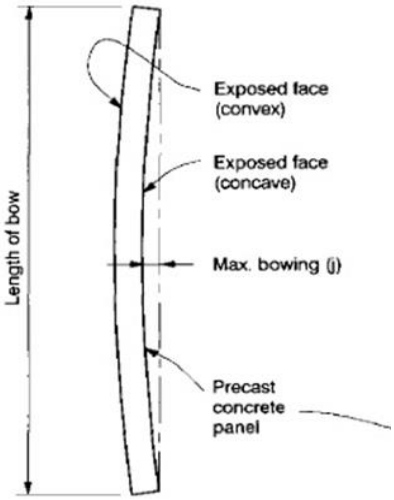

Figure 2.9: Out-of-plane panel bowing (Sorenson et al., 2000)

2.3.2 Cracking and Delamination

Cracking occurs when the tensile strength of the concrete is exceeded. Cracks caused by overloading or structural inadequacies can result in significant strength loss of the material depending on the position of the element in relation to applied loads. Cracks of 0.4 mm or less are controlled with the reinforcing steel but can cause aesthetic issues on exposed facades.

Cracks of little to no structural significance can occur as a result of restraint on long term drying shrinkage. This means where the concrete is held in place by attachment fixings or reinforcement whilst shrinking occurs, cracking will result to relieve the stress. Though this is usually of no concern other than aesthetic detriment, left restrained and untreated, micro cracks can continue to grow to a point where durability issues may ensue (Concrete-Society, 2003).

As SCP has a lightweight, low strength aggregate material in the exterior layer, shrinkage will have minimal restraint. This means that cracking is unlikely to occur on the surface as the lightweight stratum can disperse stresses by slight deformation due to its lower stiffness. The potential for cracking may exist on the interface between the two strata for reasons such as when differential settlements, drying or creep occur. Again this is likely to be a function of the degree of stratification and the abruptness of the change between the two layers. As the amount of shrinkage in the structural layer is expected to be less than that of the lightweight layer, a very well stratified panel may experience a greater degree of differential shrinkage between the two layers potentially leading to cracking.

By extension, the cause of concrete cracking can lead to delamination. Delamination in concrete elements is the process whereby a thin layer of concrete detaches from the surface and breaks down, usually under some extent of service load. Although the exact mechanisms of delamination

are not fully understood, the attributed causes include air content, bleed characteristics and differential setting of the concrete. Delamination resulting from bleeding and setting characteristics can be affected by events such as winds across the surface in open environments (Concrete-Society, 2003).

Delamination is often found in concrete bridge decks caused by corrosion of reinforcing steel or freeze-thaw action. This can affect large areas and can be difficult to detect as the effects are often not immediately visible from the outside. Techniques such as tapping or chain dragging can be used for detection as the resulting gap causes a hollow sound (ASTM, 2007).

SCP is at risk of displaying some delaminating issues due to the different material properties between the two strata. This can be minimised by reducing the smoothness of the band separating the two layers by not over-vibrating the mix. Where the mix is vibrated for too long, the paste layer that forms between the two layers can become too thick creating a weak interface. Previous work on a range of SCP samples has shown that delamination failure is not sensitive to the transition phase between the two strata with all samples tested by Bateman failing in the mid to top of the insulating layer. Further work showed that this result remained the same with various doses of fibre reinforcement (Bateman, 2008).

2.4 Durability

Concrete is a complex composite material that is exposed to a wide range of environmental and service conditions that affect deterioration mechanisms. The hardened properties of concrete are affected by construction practices and environmental factors so deterioration begins almost immediately after casting. Physical and chemical effects can cause damage through a wide range of internal and external mechanisms.

Deterioration in concrete is caused primarily by three main transport mechanisms. The first of these is *absorption* where capillary action draws fluid to the concrete surface, the severity of which depends on pore geometry and degree of saturation. Following this, *diffusion* pulls the high concentration of (salt) ions through the porous medium due to the concentration gradient. The last mechanism is *permeation* which occurs as a result of a hydraulic gradient when pressure is applied externally. This is dependent on the concrete microstructure, the moisture condition of the material, and the characteristics of the permeating fluid.

Movements of all substances are confined to the network set up by the pore system. This includes an intricate system of pores ranging from microscopic gel pores and capillary pores to the discrete bubbles of entrained air and inter-connected compaction pores (Mackechnie and Alexander, 2009).

Concrete durability issues can result from a combination of physical, chemical and electrical attacks. Two of greatest significance and concern for SCP are outlined below; corrosion of reinforcing steel and alkali silica reaction.

2.4.1 Corrosion of Reinforcing Steel

Corrosion of reinforcing steel in concrete is the predominant causal factor in the premature degradation of reinforced concrete structures. This can give the effect of large scale deterioration as mass cracking and spalling can result. This happens when the expansive stress, resulting from the corrosion product, exceeds the low tensile strength of the concrete. Although this is often not critical to the structural integrity of a structure, at least initially, it can incur considerable costs and public disruptions to repair (Li et al., 2005).

Two main threats to durability of reinforcing bars exist, the most severe of which is chloride-induced corrosion. This form of corrosion, usually associated with marine environments, is initiated when chloride levels reach a critical threshold. This type of corrosion is predominant between the tides or where concrete experiences continual wetting and drying. It causes localised breakdown of the passive film that initially forms on steel as a result of the alkaline nature of the pore solution in concrete. Harmful chloride ions can be provided by the surrounding environment or contaminated mix constituents. As the presence of chloride is influenced by many factors, quantifying the critical value for corrosion can be difficult (Montemor et al., 2002). As SCP is not intended for marine environments at this stage, this is not a major concern for current design.

Carbonation-induced corrosion is another important but less aggressive type of steel reinforcing corrosion. In moist environments, carbon dioxide present in the air forms an acid aqueous solution that can react with the hydrated cement paste and neutralise the alkalinity of concrete. Although other acid gases present in the atmosphere, such as sulphur dioxide, can cause a similar reaction, the effect is normally limited to the surface so the same threat to reinforcement corrosion is not posed as for carbonation (Bertolini et al., 2005). If chlorides are not present in the concrete initially, the pore solution following carbonation is reduces pH and depassivation of embedded steel is possible. This means that the steel in humid carbonated concrete corrodes as if it was in contact with water. A further potential consequence of carbonation is that chlorides bound in the form of calcium chloroaluminate hydrates and otherwise bound to hydrated phases may be liberated, making the pore solution even more aggressive (Alonso and Andrade, 1994).

A certain amount of resistance to corrosion is provided by the alkaline nature of the calcium hydroxide in the cement but all forms of reinforcing bar corrosion can be minimised with attention to simple details. Some options for achieving this include increasing the cover depth of the reinforcing, increasing the cement content of the concrete and improving the cover resistance with SCMs. Further corrosion reductions may be made by adopting physical considerations such as member geometry and rebar spacing as well as acknowledging that corrosion may be accelerated in areas of high stress (Mackechnie and Alexander, 2009).

The design of SCP incorporates the steel reinforcing in the structural layer 40 mm from the interior face. This means that the mesh has 40 mm cover on the interior face of the panel and 25-30 mm on the exterior side plus the remaining 160-170 mm of lightweight concrete and the transition phase. Further measures can be taken to reduce this by applying a cover coating for panels in service. As it is anticipated, at this stage, that SCP will be used in non-marine environments, the major corrosion risk is that of carbonation. The exterior lightweight does not provide as much resistance to carbonation, as does the structural layer, due to its high porosity. The 25-30 mm of structural layer on the exterior side of the mesh provides a significant amount of protection for the steel therefore. This means that it is important that sufficient stratification takes place to produce this protective structural cover.

2.4.2 Alkali Silica Reaction (ASR)

Alkali-silica reactivity in concrete involves the alkali hydroxides present in the cement and reactive forms of silica present within aggregates. This combination, in the presence of water, reacts to form a gel which swells with continued moisture absorption. The amount of gel produced and hence the resulting swelling pressures are dependent on reaction temperature, the type and proportion of reacting materials, and gel composition amongst other factors. These swelling pressures often lead to micro-fractures in the concrete which can, in turn, lead to expansion and disruption of the element or structure. In particularly bad cases this can lead to spalling, cracking and structural

misalignment. This reaction usually takes between 5 and 12 years to develop to a deleterious stage but it can be encouraged by such factors as aggregate reactivity and available surface area of an amorphous or cryptocrystalline silicious material (Swamy, 1992).

Although the actual number of structures affected by ASR is quite limited, experience has shown that, when considered in the global context of concrete construction, the effects of ASR can be severely detrimental to concrete structures affecting strength, stiffness, serviceability, safety and stability. While it can be difficult to predict and prevent ASR, some precautions can be taken to minimise the risk. These include using cement with low alkali content, replacing some Portland cement with SCMs such as blast-furnace slag or fly-ash, using suitable non-reactive aggregates and minimising the external source of water coming into contact with the concrete (Neville, 1995).

Expanded glass beads, which are to be used for SCP production, present the risk of ASR reaction due to the potentially reactive silica forms in the glass. The primary counteractive approach against this is the use of microsilica as a supplementary material. This has been proven to improve ASR resistance of concrete through the production of a dense and impermeable matrix which inhibits the movement of water and alkalis and by binding free alkalis in calcium silica hydrates or by absorption on their large specific surface area, thereby reducing the hydroxyl ion concentration of the pore solution, discussed further in chapter 3 (Boddy et al., 2000). Should ASR expansion occur in SCP however, as discussed in the drying shrinkage section above, local crushing of the lightweight layer can relieve the stress. As the strength of the lightweight layer is only about 5 MPa, the stresses produced by the expansive ASR gel are minimised by micro-cracking without causing significant cracking through the whole section.

2.5 Thermal Properties

Temperature management in buildings, residential and otherwise, can be controlled with insulation and suitable thermal properties. Heavy buildings or cladding systems stabilise internal temperatures by absorbing excess heat during the day and releasing it once the temperature has dropped below that of the system. Where the appropriate structural applications are implemented, significant energy savings can be made in terms of heating and cooling. Factors affecting thermal and insulation properties include the weight of the structure, the specific heat capacity of the material, and thermal transmittance.

Testing by CCANZ has demonstrated the benefits of high mass buildings for strong thermal performance in New Zealand weather conditions. This research showed that concrete houses can use up to 15.5 percent less energy than equivalent timber houses. Further to this, concrete buildings demonstrated better control of comfortable temperatures than timber ones where large windows are fitted (CCANZ, 2007a).

The New Zealand Standard (NZS 4218) permits three methods for determining the required insulation for New Zealand homes. These are: (NZS4218, 2009)

- Prescribing R values for various building elements
- Allowing some R value reduction where this is picked up with higher R values elsewhere in the building
- Advanced modelling techniques to model thermal performance more accurately

The main considerations for achieving the required thermal standards are outlined below with discussion as to how SCP is designed to meet these.

2.5.1 Thermal Conductivity

Thermal conductivity is the intrinsic property of a material which quantifies its ability to conduct heat. Heat transfer by conduction involves transfer of energy within a material based on a temperature gradient, without any motion of the material as a whole (Halliday et al., 1997).

Thermal conductivity of concrete, defined as the ratio of heat flux to temperature gradient, is sensitive to specific constituents, particularly the aggregate type. Increased crystallinity of aggregate type can augment conductivity. That is quartz may well maximise thermal conductivity where the crystals are aligned to the direction of flow, while basalt and trachyte provide little conductivity and therefore have greater resistance to heat transfer (Neville, 1995).

The effect of density on thermal conductivity is most notable in lightweight concretes. In oven dried conditions, concrete with greater density and lower porosity will exhibit greater thermal conductivity as there is less air present to inhibit thermal flow. Values as low as 0.115 W/(m.K) can be reached in the ideal setting. As saturation levels increase, the thermal conductivity is greatly increased. It is notable that lighter concrete has the capacity to absorb more moisture, a result of which is a significant increase in thermal conductivity. Once concrete is saturated the thermal conductivity can be as high as 3.6 W/(m.K) (Gawin et al., 2004).

As is the case for any building application, for SCP it is important to restrict the thermal conductivity of the concrete such that comfortable or workable conditions can be easily attained without excessive heating or cooling requirements. As the majority of the resistance to heat transfer through low conductivity is provided by the lightweight layer, the performance of SCP is governed by the degree of stratification. This means that if a considerable amount of heavyweight aggregates are held up in the lightweight layer, then thermal bridging will greatly reduce the effectiveness of the thermal resistance. Where a clean lightweight layer of at least 125 mm is produced, the thermal conductivity will be minimised. This will achieve the greatest possible separation between the exterior and interior climates so stable indoor conditions will be efficiently maintained.

Thermal conductivity values in the insulating layer as low as 0.20 W/mK (1.30 W/mK in heavyweight layer) have been achieved with sufficiently stratified samples made using inorganic polymer (Mackechnie et al., 2009). Specimens made with Portland cement have not reached values this low but for well stratified specimens a range of 0.23-0.25 W/mK (1.10-1.40 W/mK in heavyweight layer) has been attained. Results from research by Park showed a range of thermal conductivity values from as low as 0.24 W/mK up to over 0.40 W/mK (Park, 2006). From each of these research projects, where stratification was not satisfactory, values were significantly compromised with lightweight thermal conductivity values reaching up to and over 0.50 W/mK (Saevarsdottir, 2008). This means that both the thermal mass drawing heat out of the room and the insulation retaining it are notably reduced when stratification is not sufficient.

2.5.2 Specific Heat Capacity

The specific heat capacity is the amount of heat required to change a unit mass of a substance by one degree in temperature. This can be expressed as shown in Equation 2.1 (Halliday et al., 1997).

$$Q = m\ c\ dt \qquad \textbf{(Eq 2.1)}$$

Where: Q = heat supplied (kJ)

m = mass (kg)

c = specific heat (kJ/kg°C)

dt = temperature change (°C)

This is effectively a measure of the concrete to act as a heat storage material; the more energy required to change the temperature, the greater the resistance of the concrete to the change. This means less energy is required inside the building in response.

There is a range of values over which the specific heat of concrete is typically found, depending on the density and other specific properties. The extent of this range is from 0.5-1.17 kJ/kgK (Neville, 1995). This is sensitive to the particular constituents of the concrete however. The type of aggregate used is largely responsible in most cases with less significant influences attributed to the mix proportions, density, water/cement ratio, cement type and the initial temperature of the concrete.

Experimental work has demonstrated that, though the mineralogical aspects of the concrete have an effect on the specific heat as discussed above, a very strong correlation exists between the moisture content and the specific heat capacity, especially for porous lightweight mixes. The relationship between moisture content and specific heat has been found to be almost linear for normal weight and structural lightweight aggregate mixes but begins to deviate from this linearity for lower density mixes (Whiting et al., 1978).

The aggregate materials used for SCP have very different specific heat capacities based on the density difference between the two. As this property effectively defines how quickly heat passes through the panel, the specific heat of both the heavyweight and lightweight aggregates are an important consideration when addressing thermal resistance properties of each layer and the overall panel performance. When considered in conjunction with the mass of the respective materials, the specific heat capacity controls the thermal mass of the SCP panels as outlined in the following section.

As for the thermal conductivity, the specific heat values from the inorganic polymer samples were more preferable with some values as low as 0.44 MJ/m^{3}K (Mackechnie et al., 2009). Portland cement results ranged from 0.50 MJ/m^{3}K (1.35 MJ/m^{3}K in heavyweight layer), for a well stratified sample, up to over 1.1 MJ/m^{3}K (1.3-1.6 MJ/m^{3}K in heavyweight layer) for a moderately/poorly stratified one (Saevarsdottir, 2008). Again this shows the correlation between the thermal properties and the degree of stratification. Where the lightweight layer is less contaminated by heavyweight aggregates, the specific heat capacity of the insulating layer is much lower so less heat is lost through thermal bridging.

2.5.3 Thermal Mass

Building materials that have the ability to absorb, store, and later release significant amounts of heat are said to have thermal mass (or fabric energy storage). Buildings constructed with concrete and masonry have a unique energy saving advantage because of their inherent thermal mass. In comparison to lighter structural materials, these materials absorb energy slowly and hold it for longer periods of time. This delays and reduces heat transfer through the building (Neville, 1995).

This is of primary importance as temperature spikes are smoothed out and reduced as the slow release regulates the fluctuations. From this, energy savings can be made internally as less control is required to sustain a comfortable temperature. Further, this can shift energy demands to off-peak time periods when utility rates are lower. For example, power plants are designed to provide power at peak loads so shifting the peak load can reduce the number of power plants required.

For maximum efficiency from a thermal mass element, the appropriate thickness must be used to stabilise the temperature. Where the element is too thin, heat will penetrate through during the day and there will be little left to release at night. Where the wall is too thick the heat may take too long to penetrate and may be released once there is no need for extra heat. Buildings with suitable thermal mass feel cooler in summer and warmer in winter so less energy is needed for comfortable living and working conditions.

Materials with the greatest factor of specific heat and density will exercise the greatest thermal mass potential, which is measured in terms of volumetric heat capacity as shown in Equation 2.2.

$$\rho C_P = C_P * k \qquad \textbf{(Eq 2.2)}$$

Where: ρC_P = Volumetric heat capacity (J/m^3K)

C_P = Specific heat (J/kgK)

k = Density (kg/m^3)

Comparisons can be made between the effectiveness of concrete and timber as thermal storage materials. Although timber has a greater specific heat capacity per kilogram, once the density of the two materials is considered, concrete has nearly twice the volumetric heat capacity at $2.0x10^6$ J/m^3K to the $1.1x10^6$ J/m^3K of timber (Bellamy, 2010).

This concept can then be extended to thermal effusivity. This accounts for the characteristics of the volumetric heat capacity and the thermal conductivity by taking the square root of their product. This property is loosely comparable to admittance and provides a measure of how quickly the building material will absorb heat from the room. The internal heavyweight layer of SCP provides high effusivity which draws heat out of the room relatively quickly. The external lightweight insulating layer, with low effusivity, then holds the heat to be released at a later time when the internal temperature drops. Table 2-1 below shows these properties of normal weight concrete with a comparison to timber for reference.

Table 2-1: Thermal properties of normal weight concrete and timber (Bellamy, 2010)

	Specific heat, C_p (J/kgK)	Density, ρ (kg/m^3)	Thermal conductivity, k (W/mK)	Volumetric heat capacity, ρC_p (J/m^{3}K)	Thermal effusivity, $(\rho C_p k)^{1/2}$
Concrete	880	2300	1.6	2.0×10^6	1800
Timber	2100	500	0.12	1.1×10^6	350

The most ideal materials to provide thermal mass have low but not excessively low thermal conductivity. This is to say that materials with high thermal conductivity will release absorbed heat too quickly where materials with extremely low thermal conductivity will take too long to absorb the heat in the first place and have limited storage capacity. SCP provides a mechanism for achieving the best results from two materials with different properties such that the heat is absorbed comparatively quickly, then held and released slowly.

2.5.4 Total Thermal Resistance

Total thermal resistance is an overall measurement of insulation effectiveness which, in its most basic sense, is defined as the thickness divided by the thermal conductivity of the material. This is known as the static *R-value* and is expressed in units of m^{2}K/W. For example; a 200 mm thick wall with thermal conductivity of 0.2 W/mK, would have an R-value of 1 m^{2}K/W. The higher the R-value of a product/material, the better thermal resistance it possesses. This means it is more energy efficient as a building material. Some typical static R-values for concrete wall systems are shown in Table 2-2 below (CCANZ, 2007a):

Table 2-2: R-values for some typical concrete wall systems

System	R-value (°C/W)
Strapped (25mm) & lined 150mm concrete masonry (with reflective foil)	0.85
Strapped (25mm) & lined 150mm concrete masonry (pumice aggregate)	0.63
Strapped & lined 150mm concrete masonry (with 25mm polystyrene insulation)	1.00
200mm cavity insulated concrete masonry block (Partially filled)	0.73
250mm cavity insulated concrete masonry block (Partially filled)	1.00
150mm concrete masonry block with 50mm expanded polystyrene exterior	1.70
Precast panel with polystyrene (50mm polystyrene) cast in	1.61
200mm insulated concrete formwork block	2.98

SCP theory suggests it can be created to perform with high R-values. At this stage, early testing has seen SCP provide moderate R-values of 0.8-1.0 m^{2}K/W (Mackechnie and Bellamy, 2011). Longer term tests and adjustments to the development process may however, see these values improve.

This static R-value however, does not provide complete information for how panels may act in service. As well as simply dividing the thickness of each layer by the thermal conductivity, consideration must be given to the characteristics of the interfaces between the different strata. Further thermal resistance can result from heat entering and leaving the panel, hitting the surface and from wavelength changes as the heat passes through mediums of differing density. Here extra

exterior and interior surface resistances of 0.03 and 0.09 m^2K/W respectively, can be added (Mackechnie and Bellamy, 2011). Figure 2.10 shows the interfaces within the panel; between the lightweight, transition, and heavyweight phases, each with different thermal properties.

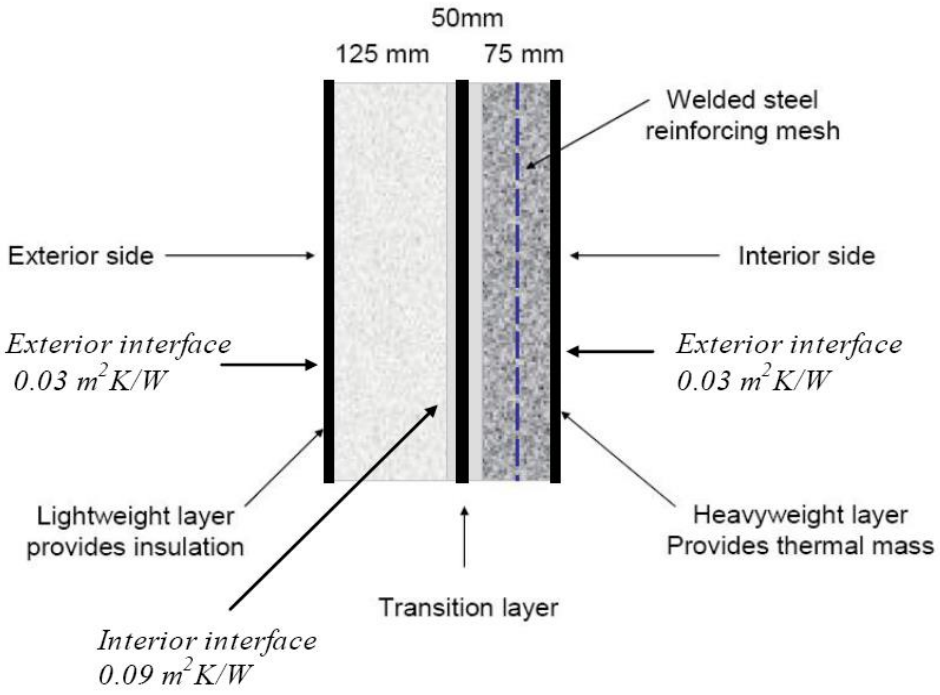

Figure 2.10: Schematic diagram of thermal interfaces within SCP (Mackechnie and Bellamy, 2011)

Static R-values do not model real environmental conditions, which change continuously thereby activating thermal mass of concrete. To address this, further testing has been carried out on SCP to measure the thermal performance as would be observed in service; dynamic R-value measurements. This test used stratified panels made with both Portland cement blends and inorganic polymer blends. Large panels, of 250 mm nominal thickness, were placed in a north-facing wall of a solar laboratory at the University of Canterbury (43.5°S). These panels were exposed to ambient conditions on the exterior face while the interior face was kept at a controlled indoor room temperature of 20°C. Two lightweight polystyrene panels of roughly the same static R-value were used as control panels. With no windows in the laboratory, there was no opportunity for any solar gain on the exterior surfaces. The exterior façade was directly exposed to the sun and painted grey. Conduction heat flows were measured at the interior surfaces of the panels using thermal sensors. Solar radiation on the exterior surface was monitored as well as the indoor and outdoor temperatures (Bellamy and Mackechnie, 2010).

The results of this dynamic thermal analysis showed that where steady-state R-values for SCP were only moderate (typically 0.8-1.0 m^2K/W), the dynamic thermal performance was considerably better with values reaching up to 2.55 m^2K/W (Bellamy and Mackechnie, 2010). This also showed that, under steady indoor conditions, 250 mm thick SCP panels demonstrated superior annual heating and cooling performance over polystyrene panels. These results indicate that the panels perform particularly well in buildings that need both heating and mechanical cooling.

2.6 Lightweight Concrete

Lightweight concrete can be produced either by using lightweight aggregates or by entraining air into the concrete. This can be adjusted to varying degrees such that a range of concrete properties and strengths can be produced. Lightweight concrete is often classified by the relationship between its cement content, compressive strength and unit weight. Table 2-3 below shows how these are grouped into three main categories; insulating, structural insulating and structural (Bobrowski, 1978) (Mindess et al., 2003).

Table 2-3: Classification of lightweight concrete aggregate

Lightweight aggregate concrete	Dry density [kg/m^3]	Strength range [MPa]	Main use
Low density concrete: (Insulating concrete) No fines concrete, porous, cement paste does not fill all the volume between aggregate particles	300-800	0.7 - 2	Cast in situ insulation Insulating layer in the prefabricated elements
Moderate strength concrete: (Structural insulating concrete) Low porosity between aggregate particles	600-1300	7 - 14	Load-bearing and insulating constructions Lightweight blocks and bricks
Structural concrete Dense concrete	1300-2000	17 - 63	Structures where strength is required and thermal insulation may not be so important, reducing total cost

As little strength is provided by most lightweight aggregates, the water/cement ratio in lightweight concretes is often lower than that of normal weight concretes of similar strengths. Despite the contribution of this increased density, it is the strength of the aggregates that ultimately determines the compressive strength of the concrete.

As the density of the aggregates is increased to enhance the compressive strength, thermal bridging becomes more prominent and the thermal conductivity increases. This reduces the ability of the concrete to provide thermal insulation. Figure 2.11 shows the correlation between concrete density and compressive strength for a range of lightweight aggregates. Beneath this, Figure 2.12 shows the thermal conductivity of inorganic polymer and Portland cement mixes against the density.

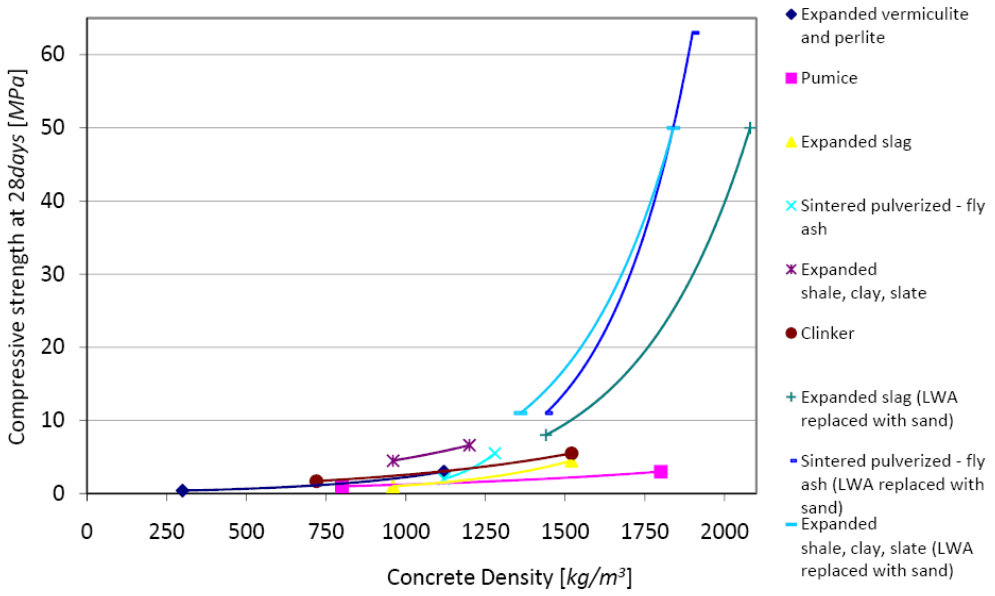

Figure 2.11: Density versus strength of concrete using different lightweight aggregates (Mindess et al., 2003)

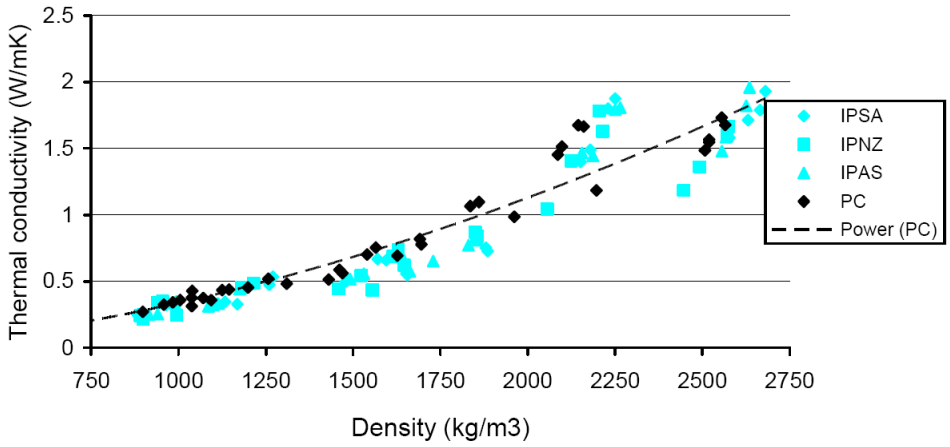

Figure 2.12: Thermal conductivity vs. density (Mackechnie and Bellamy, 2011)

For the purpose of SCP, insulating properties are of primary importance for the lightweight layer so expanded glass beads (EGB) are used. These provide maximum insulation due to their very low density made up of a closed cell structure that consists essentially of 98 percent air (Poraver, 2006). Concrete made with EGB does not absorb moisture to the same degree as concrete made with gassing agents and lightweight mineral aggregates which can absorb up to 20 to 50 percent of the concrete dry weight. This means EGB concrete is lighter and can be designed to float on water.

Lightweight concrete has been proven to have sufficient strength, durability, fire resistance and heat and sound insulation for most building applications. Design advantages are also apparent with smaller gravity and seismic loads resultant from lighter sections. Work on the materials and mixing has shown that lightweight concrete exhibits less tendency to segregate than normal weight concrete as the aggregates are inclined to float rather than sink to the bottom of the mix (Asgeirsson, 1994). Despite the benefits shown by research so far, further work is required before lightweight concrete becomes more widely used in the construction industry.

3 MATERIALS

Several different combinations of materials have been tested for the production of SCP. Park compared a wide range of mix designs with various quantities of water and different binders and aggregates (Park, 2006). The tests incorporated fly ash and slag as supplementary cementitious materials and slag, perlite, expanded glass beads (E.G.B.) and pumice as the lightweight aggregate options. These are shown in Table 3-1 with reference to different series; E-economic, M-moderate, C-cheap and highly viscous mixes. Tests were carried out for density, thermal conductivity, R-value and compressive strength in both the lightweight and heavyweight layers. The main focus of this research however, was to study the rheological ranges for stratification and associated thermal properties.

Table 3-1: Mix designs of optimal insulated lightweight stratified concrete mixes (Park, 2006)

No.	Binder (kg/m^3)			Water (kg/m^3)	Sp (%xB)	Fine Agg. (kg/m^3)				Coarse Agg.
	PC	F/A	Slag			Slag	Perlite	E.G.B.	Pumice	
E-O-N	425	-	-	335	-	100	80	50	-	350
M-O-N	425	-	-	307	-	150	30	50	150	300
C-O-N	425	-	-	285	-	-	-	90	170	300
FC-0.4	250	250	-	270	0.4	100	80	50	-	300
FC-0.8	350	250	-	270	0.8	100	80	50	-	300
SC-0.4	350	-	150	280	0.4	100	80	50	-	300
SC-0.8	350	-	150	280	0.8	100	80	50	-	300

The slump flow and rheological properties of each mix were recorded before the 'Washing Out' test was used to determine the segregation coefficient of each mix (Park, 2006). This test accounted for the weight of the coarse aggregates relative to the weight of the concrete to gauge the degree of stratification. A greater segregation coefficient indicates more significant stratification. Readings for vibration after 0, 15 seconds and 30 seconds are given, with the rheological properties in Table 3-2.

Table 3-2: Rheology and segregation comparison between the different mixes

No.	Rheology		Consistence		Segregation coefficient		
	τ_0 (Pa)	μ (Pas)	Slump (mm)	Flow (mm)	0 s	15 s	30 s
E-O-N	33	11.5	235	430	0.05	0.38	0.58
M-O-N	63	16.5	205	390	0.05	0.26	0.50
C-O-N	61	14.6	200	455	0.03	0.21	0.46
FC-0.4	276	43.4	NA	380	-	-	0.28
FC-0.8	30	25.2	NA	530	-	-	0.39
SC-0.4	85	54.2	NA	410	-	-	0.27
SC-0.8	4	30.9	NA	560	-	-	0.39

These results suggest that the wetter mixes yield better stratification. The mixes with more superplasticiser also benefit from greater stratification and have notably higher flow values. Other observations imply that pumice tends to resist segregation. The fly ash and slag mixes are not as well stratified as the mixes containing only Portland cement as binder.

This research gives further evidence that the segregation tendency is most closely related to the viscosity of the concrete. That is the resistance to flow is much greater in the case of high viscosity concrete. The coarse aggregates are therefore kept in position with minimal movement during vibration. Although flowability is not necessarily directly related to the stratification potential of the mix, it gives a good indication (Park, 2006).

Continuing from Park's research, Saevarsdottir looked at different material combinations to produce SCP in the controlled laboratory setting (Saevarsdottir, 2008). This was initiated with two combinations of aggregates:

- Pumice and perlite as lightweight materials and greywacke chips (greywacke sandstone) as heavyweight material, designed to utilise local New Zealand materials. This mix is designated as PUM.
- Expanded glass beads (2-4 mm) and perlite as lightweight materials and slag as heavyweight material. Easily sourced in Europe, these products are recycled materials so add a sustainable aspect. This mix is designated as GB.

After extensive testing of these mixes, the pumice-perlite combination was not consistent enough to guarantee quality of mix and stratification. In response, an extra mix was developed:

- Two grades of expanded glass beads (2-4 mm and 0.5-1 mm) as lightweight material and slag as heavyweight material. This mix is designated BB.

In conjunction with these aggregate combinations, two binder systems were used:

- Portland cement, a general purpose cement from Westport
- Inorganic polymers, made with fly ash and/or slag, activated with alkali and sodium silicate solutions and thermal curing

A linear relationship was found between the yield shear stress and the plastic viscosity for the GB mix and the BB mix. This relationship indicated that in order to achieve satisfactory stratification:

- The lower the plastic viscosity, the higher the yield shear stress can be
- The lower the yield shear stress, the higher the plastic viscosity can be

A relationship was not found for the pumice-perlite mix, most likely due to variability in the aggregate material properties.

Using the same notation as Saevarsdottir, stratification coefficients were calculated for each mix. This is defined by taking a ratio between the centre of mass and centre of area of the hardened concrete; this is elaborated on in chapter 4, section 4.3.1. The stratification coefficient gives an indication as to the level of stratification relative to an upper and lower critical value (CV_1 and CV_2 respectively). That is whether the sample is:

- Poorly stratified ($SC < CV_2$)
- Moderately stratified ($CV_2 < SC < CV_1$) or
- Well stratified ($SC > CV_1$)

Indicative values are $CV_1 = 21$ and $CV_2 = 12$.

A comparison can be made between the three aggregate combinations by taking averages of the stratification coefficients for each as shown in Table 3-3.

Table 3-3: Stratification of the different aggregate combinations

Aggregate Mix	Stratification Coefficient (%)	Stratification Rating
PUM	11.1	Moderate
GB	21.9	Moderate/Good
BB	26.5	Good

It is also notable that the yield shear strength and plastic viscosity readings were less than 100 Pa and 40 Pa.s. as required for nearly all mixes but some of the PUM mixes. These results suggest that the combination of two grades of EGB as the lightweight material and the slag as the heavyweight material was the best of these. The ideal composition of SCP is shown in Figure 3.1.

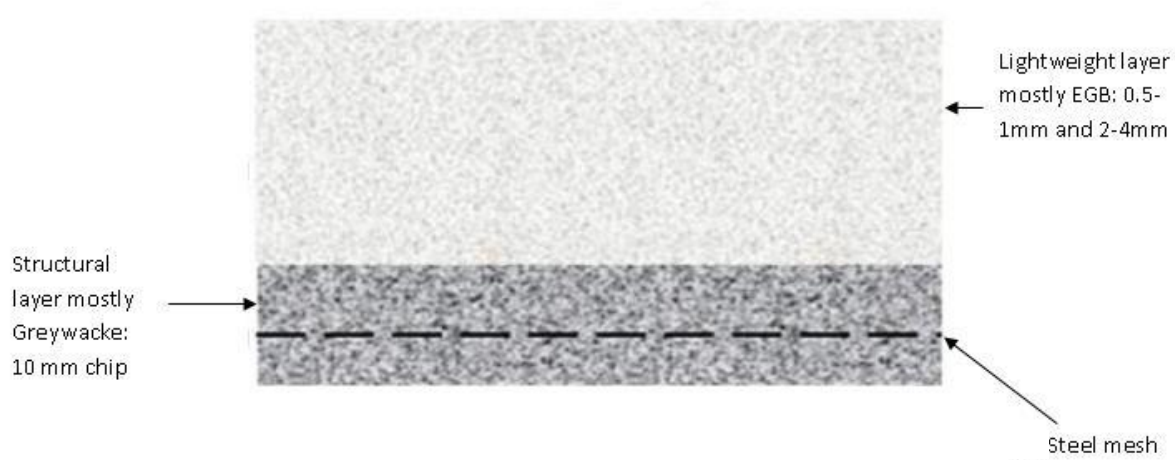

Figure 3.1: SCP ideal composition

Drawing from the experimental work of these past projects, the materials for this project were chosen to ensure both the quality of the finished SCP product and to meet the workability requirements of the fresh concrete. As the focus for this project was to produce SCP in an industrial setting, the materials were chosen with consideration for pragmatic constraints. As this included the challenges of large scale mixing in the industrial setting, it was important to choose materials that could be easily sourced locally and materials that the operators were familiar with.

The materials outlined in this chapter were deemed most appropriate to produce the most consistent results in terms of production quality and stratification of the panels.

3.1 Aggregates

Aggregates make up the bulk of concrete and provide a cheap way to greatly improve the stiffness and dimensional stability of the concrete. The elastic modulus of the concrete can be a function of the aggregate where marginal aggregate sources are used. This is often the case in New Zealand due to the variable geomorphology. Where harder stiffer aggregates are used, the elastic modulus of the concrete is usually not a function of the aggregates as they are stiffer than the paste.

Aggregate choice can be subject to availability based on geography as it is cheaper to use aggregates sourced locally.

The performance of any given type of aggregate is a function of its size, shape, texture and strength; all of which contribute to the overall dimensional stability of the concrete. These characteristics are often associated with geological conditions. New Zealand geology is variable due to volcanic activity and tectonic plate movement in recent geological time. This produces significant differences in aggregate properties within a relatively small geographical area.

Since aggregates make up over 70 percent of the concrete by mass, they can also provide hygrometric stability to the concrete which can reduce the sensitivity of the mix to moisture fluctuations (Alexander and Mindess, 2005). This is particularly pertinent for self-compacting mixes where the water content can be as high as 200 L/m^3 or above. The aggregates for this project were both lightweight and heavyweight, each of which included both coarse and fine components.

3.1.1 Lightweight Aggregates: Expanded Glass Beads

Lightweight aggregates, in the form of expanded glass beads (EGB), were used to create an aerated layer for the exterior face of the panel for maximum insulation. EGB are created from recycled glass that cannot be further used by the glass industry for new products. These beads are prepared by grinding raw glass to a fine powder and combining with some water, binding agents and expanding agents. Then, in a granular dish, rotating about a furnace at approximately 900°C, the beads are produced. The resulting product entraps a minute chamber of air inside each creamy round granulate. After cooling, the spherical beads are sorted by size.

There are several benefits for concrete production wit EGB (Poraver, 2006). The amorphous glass structure of the beads means they are:

- Very light yet pressure resistant
- Highly heat-insulating
- User friendly due to spherical grain structure
- Alkali resistant so suitable for use with cement
- Non-flammable
- Purely mineral
- Suitable for sound absorption

However some disadvantages arise from the use of EGB:

- Energy intensive to produce
- Alkali silica reactive
- Low strength capacity

This project employs the use of two different bead sizes with properties as shown in Table 3-4.

Table 3-4: EGB basic properties

Bead Diameter (mm)	Granular Density (kg/m^3)	Compressive Strength (MPa)
0.5 - 1.0	470 ± 50	2.0
2.0 - 4.0	320 ± 40	1.4

3.1.2 Heavyweight Aggregate Materials: Greywacke

Heavyweight aggregates are used to create the dense structural layer on the interior face of the panel providing thermal mass. Greywacke sandstone was used in this research.

Greywacke is a dull grey stone that consists of alternating layers of hard muddy grey, slightly metamorphosed sandstone and darker mudstone (argillite). This means it is often found in thick or thin beds with slates and limestone. New Zealand greywacke was formed in crumbled, folded layers as marine sediments were scraped off the ocean floor by the toe of an overriding plate (Thornton, 2003). It can be found in most places around New Zealand including on mountains, in rivers and on beaches. As it forms a large percentage of the basement rock for the country, it has been subject to significant tectonic movement over the last 300 million years, though most of it is less than 250 million years old.

The clastic texture of greywacke explains why it is often very deformed, fractured and can be veined with quartz. It is a hard rock with grain sizes of 0.06 – 2 mm, typically with angular clasts visible to the naked eye (Smith, 2005).

As Table 3-5 shows, greywacke is relatively heavy aggregate choice, compared with some other commonly used aggregates, which gives it both the ability to stratify through a fresh mix and to provide substantial fabric energy storage capacity. Due to its medium quartz content and the presence of pores, greywacke presents a nice compromise as it provides thermal mass but is not too highly conductive as to draw and release heat too quickly.

Table 3-5: Basic properties of some standard aggregate types (Alexander and Mindess, 2005, Neville, 1995)

	Limestone	Quartzite	Basalt	Dolomite	Greywacke
Relative density	2.5-2.8	2.6-2.7	2.6-3.0	2.7	2.7-3.0
Thermal conductivity (W/mK)	1.5	3.5	2.0	3.3	2.9

For concrete application, the usability and quality of Greywacke depends on many criteria, the most pertinent of which are (Mackechnie, 2006):

- The age of the material; stability considered to be proportional to age.
- The specific source of the rock, therefore exact composition.
- The degree of lithification or induration of the sediment as stability and hardness are attributed to pressure and heat from greater depth of burial.
- The shape of the particle; crushed (angular), semi-crushed or rounded.

Greywacke sandstone and gravels are the most commonly used concrete aggregates. In major regions, as for most of New Zealand, it is sourced as quarried rock where in smaller centres, such as some South Island centres, it is taken from alluvial gravels. Due to the variety of sourcing means and geographical areas, there is a range in quality from the strong, stable highly indurated sandstones to the marginal gravels containing some inclusions which can cause weakness and chemical instability in some cases.

For the purpose of this project, the greywacke used was 8-10 mm chip with a specific gravity of 2.65, considered to be non-alkali-silica reactive. Southern greywacke is particularly useful as it

displays absorption of below 0.8 percent (Alexander and Mindess, 2005). Greywacke sand was used as a fine aggregate for this SCP production.

A grading sample was taken of both the 8-10 mm chip and the sand from Stahlton precast yard. These sample tests were carried out in accordance with ASTM C 136 "Sieve Analysis of Fine and Coarse Aggregates" (ASTM, 2006). The resulting grading of the coarse and fine grained aggregates is shown in Table 3-6 and Table 3-7 where a mass of 500 grams was used for the coarse sample and 200 grams for the fine aggregate.

Table 3-6: Grading of the coarse greywacke aggregate

Sieve size	Individual % retained	Cumulative % retained	% passing
13.2 mm	0.00	0.00	100.00
9.5 mm	0.80	0.80	99.20
No. 4 (4.75 mm)	89.11	89.91	10.09
No.8 (2.38 mm)	10.09	100.00	0.00
No. 16 (1.18 mm)	-		-
No. 30 (600 µm)	-		-
No. 50 (300 µm)	-		-
No. 100 (150 µm)	-		-
Pan	-		-
Total	100.00		

Table 3-7: Grading of the fine greywacke aggregate

Sieve size	Individual % retained	Cumulative % retained	% passing
9.5 mm	0.00	0.00	100.00
No. 4 (4.75 mm)	2.07	2.07	97.93
No.8 (2.38 mm)	21.16	23.23	76.77
No. 16 (1.18 mm)	13.08	36.31	63.69
No. 30 (600 µm)	9.18	45.49	54.51
No. 50 (300 µm)	22.39	67.88	32.12
No. 100 (150 µm)	26.03	93.91	6.09
Pan	6.09	100.00	0.00
Total	100.00		

From this sample the fineness moduli are 5.91 and 2.69 for the coarse and fine aggregates respectively.

This shows that the coarse aggregate is almost completely within the range of 4.76 mm to 9.5 mm. This uniformity is important for the strength of the hardened concrete. The fine aggregate is well graded and fits the ASTM guideline that stipulates that the fine aggregate should not have more than 45 percent passing any sieve and retained on the next consecutive sieve (ACI, 2007).

3.2 Binders

Binders make up the matrix within the concrete that holds the aggregates together and provides strength. The most common binder is Portland cement; it is often the only binder used. As both technical and environmental demands increase, using Portland cement as the only binder is becoming less feasible.

Supplementary cementitious materials (SCM) contribute to the properties of hardened concrete through hydraulic or pozzolonic activity. Natural pozzolans can be used individually with Portland or blended cement or in different combinations. These materials encourage further production of cement compounds by reacting chemically with calcium hydroxide. They are often added to reduce permeability, increase strength, or influence other concrete properties. As SCM are recycled waste products, their use in concrete is not only economical but also addresses the issue of sustainability.

3.2.1 Portland Cement

Portland cement (PC) is created by burning ground calcined limestone and clay together. The burning process changes the chemical properties of the materials and creates stronger cement than using just plain crushed limestone.

A typical analysis of a general purpose Portland cement, with density of 3100kg/m^3 and fineness of 350-360m^2/kg, is shown in Table 3-8 (Holcim, 2006). Table 3-9 shows the compound composition of the major clinker constituents.

Table 3-8: Typical analysis of Ultracem (GP PC) from Holcim, Westport

SiO_2	20.7%	Na_2O	0.2%
Al_2O_3	4.1%	TiO_2	0.2%
Fe_2O_3	2.0%	Mn_2O_3	0.2%
CaO	66.1%	P_2O_5	0.1%
MgO	0.9%	Cl	0.01%
SO_3	2.5%	LOl	2.7%
K_2O	0.5%	Na Eq	0.5%

Table 3-9: Typical analysis of Ultracem Clinker

Tri-calcium Silicate (C_3S)	65%
Di-calcium Silicate (C_2S	20%
Tri-calcium Aluminate (C_3A)	8%
Tetra-calcium Aluminoferrite (C_4AF)	7%

Cement can be produced in two ways, one of which is termed ‘wet process technology’, used in the Holcim Westport cement works. This begins with the grinding of limestone and clay in a ratio of approximately four parts limestone to one part clay. The chemical composition of the fine thin slurry produced is carefully controlled with adjustments to the amounts of limestone and clay. This slurry is then fed into the upper end of a rotary kiln while an intense flame in maintained at the bottom by blowing in finely ground coal. The slurry moves slowly down the kiln producing ‘clinker’ as it is dried and heated to almost 1500 degrees Celsius. This reaction changes the chemical properties of the material such that it reacts with water to form a binder. To regulate the early setting characteristic of cement, the clinker is finely ground with about 5 percent gypsum (Holcim, 2010).

Cement can also be produced using 'dry process technology', used in the Golden Bay Cement Whangarei system. No water is added during this process and moisture levels are kept to below one percent. This more modern technique is considered to be significantly more energy efficient, but it is claimed that wet process technology produces a better level of mixing of raw materials. Embodied energy for these processes are relatively high and range from 1110 to 1470 kWhr/tonne. As a result of this, cement production is responsible for 7 to 10 percent of the total CO_2 emissions worldwide. Due to this high CO_2 output, research is currently being undertaken into ways to reduce the energy requirement for cement production (McLeod, 2005).

Inorganic polymer cement (IPC) is made from fly ash and blast furnace slag activated with alkali solutions that polymerise forming chains of aluminium, silicon and oxygen. This type of cement, being created completely from waste materials, is more sustainable due to relatively low embodied energy (Basalo et al., 2010). IPC SCP (Stratified Concrete Panels) can have advantages in terms of thermal performance as IPC mixes have lower thermal conductivity than PC mixes; higher density concrete has greater thermal conductivity so lower thermal resistance. Thermal conductivity in the insulating top layer was measured at between 0.2 and 0.3 W/mK for PC concrete with IP concrete tending to have slightly lower results. SCP created with PC has been shown to reach R-values of to 0.6-0.8 m^2K/W where IPC mixes have reached up to 1.0 m^2K/W.

IPC is however, not as predictable and consistent as PC so is not as feasible for the commercialisation of SCP at this stage. Also, as IPC is more expensive than PC and is not locally available, it is not an economically viable option at present in New Zealand.

A blend of Portland cement and SCM can be used to benefit from the technical advantages of SCM while retaining the economic advantages and consistent, well understood properties of using a Portland cement mix. This fairly carbon intensive approach can be justified by allowing for the ability of SCP to reclaim significant amounts of CO_2 when in service. As the exterior face of SCP in service is the lightweight layer, maximum re-absorption rates of CO_2 can be achieved.

3.2.2 Microsilica

Microsilica 600 is a highly reactive pozzolan. This means when it is combined with calcium hydroxide, cementitious properties are produced, often referred to as a cement extender (Malhotra and Mehta, 1996). It is processed from natural, white silica deposit found in New Zealand. Like silica fume, it is a very fine amorphous silica and falls into the microsilica family of products (NZS3122, 1995). It is classed as a "silica fume" in the NZ Standard 3122:1995 – Specification for Portland and Blended Cements. When added with Portland cement, microsilica facilitates high performance concrete by promoting the following benefits:

- Increased compressive strength
- Improved abrasion resistance
- Reduced water permeability
- Improved resistance to chemical attack
- Very low chloride ion diffusion
- Improved sulphate resistance
- Reduced efflorescence
- Improved stability in geothermal environments

The fine grained nature of microsilica can however provide some technical difficulties. Microsilica mixes use low replacement levels of cement. This means that only about 8 percent of the cement is

replaced by the microsilica, low in comparison to fly ash which can replace over 30 percent of the cement. Also, as microsilica is so fine, excellent particle dispersion is required to achieve the benefits of a densified microstructure and so that the material does not clump together causing weak areas. Microsilica is also relatively expensive compared to cement since it must be finely ground, which is an energy intensive process.

In New Zealand and parts of Asia, microsilica is used in infrastructure projects, ports and harbour development, commercial and industrial floors and the construction of buildings and structures located in aggressive environments (Microsilica New Zealand, 2009).

The high performance of concrete produced using microsilica is achieved through three principal mechanisms:

- The very fine particles of microsilica are able to fill the microscopic voids between the cement particles, creating a less permeable concrete microstructure. The manufacturing process ensures the optimisation of particle size and distribution.
- The pozzolanic reaction occurring when the free calcium hydroxides are liberated in the cement hydration process reacts with the microsilica to produce additional calcium silicates.
- The fine particle size reduces concrete bleed and improves the aggregate cement paste interface.

The selective quarrying operation and blending process ensures that the variation in chemical composition of the finished product is minimal. The fineness of the product is achieved through grinding. Continuous monitoring of the grinding process produces a product that has a particle size distribution which consistently lies within a pre-determined envelope. The chemical and physical properties of microsilica are outlined in Table 3-10 and Table 3-11 (GoldenBay, 2009).

Table 3-10: Typical chemical properties of Microsilica 600 by percentage mass

SiO_2	Al_2O_3	SO_3	Fe_2o_3	MnO	TiO_2	CaO	K_2O	P_2O_2	MgO	Na_2O	LOI
87.89	4.31	0.13	0.59	0.03	1.16	0.32	0.49	0.05	<0.02	0.14	5.01

Table 3-11: Particle size analysis micron percentage passing

Microns	100	50	20	10	5	2	1	0.4
% pass	100	99.6	97.9	94.5	84.6	55.6	35.0	12.2

Microsilica is particularly useful for SCP as it reduces the threat of alkali silica reaction posed by the EGB. Microsilica increases the density and impermeability of the cement matrix which helps to inhibit water movement. This effectively binds free alkalis in calcium silica hydrates and reduces the hydroxyl ion concentration of the pore solution. The reaction between the glass beads and the cement paste is therefore reduced to a level such that insufficient gel is formed and cracking by expansion is avoided.

3.3 Chemical Admixtures

Admixtures are added to concrete to optimise required characteristics. Often these characteristics make the fresh concrete easier to work with so that it is appropriate for the specific application. This can be in the form of controlling the setting speed, increasing spread without significantly

increasing the water content, or a range of other benefits that ultimately improve the performance of concrete.

3.3.1 Superplasticiser: Polycarboxylate Ether (PCE) Based

Superplasticiser is used to simulate the effect of adding water but without the detrimental side effects such as reduced strength and potential segregation. Also known as high range water reducers, these polymers are used as dispersants to avoid particle aggregation and improve flow characteristics by use of polarity. This means cement particles are well dispersed throughout the mix.

Sika ViscoCrete-5-555 is a light blue aqueous solution of modified polycaboxylate, a mixture of two ploycarboxylate ethers, with approximate density of 1.10 kg/L. It is a third generation polymer-based ultra high range superplasticiser for ready mix and precast concrete. Unlike more common, traditional admixtures that employ electrostatic repulsion to distribute cement particles, third generation products use steric stabilisation throughout the substrate. Molecules that carry $–CO_2Na$ groups which, in water, dissociate into $–CO_2$ (and Na^+) ions cause a slight negative charge that attaches the admixture to the cement. The long polyether chains then resist entanglement with each other and keep adjacent cement grains apart (Newman and Choo, 2003). This effect is more effective than electrostatic repulsion in the sense that improved workability is retained in the mix. This increases the tolerance such that the mix can be more easily tailored to the specific purpose.

ViscoCrete-5-555 is a suitable superplasticiser for production of concrete that requires extreme water reduction, excellent flowability and optimal cohesion. This makes it particularly useful for self-compacting concretes. Some benefits of ViscoCrete-5-555 are (Sika-Construction, 2003):

- Extremely high water reduction – up to 40 percent
- High early strength development
- High density and high ultimate strengths
- Extended slump life of up to 60 minutes
- Excellent cohesion without segregation

This last point here is of specific interest for the creation of SCP in reducing the sensitivity to early segregation of the mix. It is important for the mix to stay homogenous throughout the mixing, handling and pouring stages so that the aggregate does not separate from the paste.

4 METHODOLOGY AND TEST PROCEDURES

4.1 Fresh Properties and Mix Design

Initial mix design trials were carried out in the university laboratory in 20 litre batches using a high shear pan mixer of 100 L capacity. Firstly, all the constituents were batched out into buckets in the required quantities. The dry ingredients, as outlined in chapter 3, were then poured into the pan mixer and mixed for approximately 30 seconds to encourage an even distribution of dry particles. Water and superplasticiser were then gradually added with frequent visual checks to avoid over saturating the mix leading to early and uncontrolled segregation. When the mix looked to be of appropriate consistency, a spread test was carried out as explained below. This process was repeated until the flow of the mix was considered satisfactory. A note of the final water content used was taken at this point.

The mix was then distributed into test cylinders, slightly overfilling them to allow for settlement under vibration. The cylinders were then subjected to vibration at 3000-3500 rpm for varying lengths of time. The different lengths of time of vibration produced a continuum of stratification levels. The degree of stratification for each test was observed after cutting the cylinders in half with the diamond saw two days after casting.

Several trials were conducted to optimise both the mix design and the time of vibration so that a satisfactory degree of stratification could be consistently produced without early segregation of the mix.

4.1.1 Consistence and Rheology

Several rheological targets had to be met for satisfactory performance of the mix. This meant that constituents were altered in a controlled fashion after each trial to fine tune the design and meet the required targets. Simple control tests were undertaken to measure the rheological properties as outlined below.

The consistence of the high flow concrete mix was assessed using the spread test (NZS3112, 1986a). This test was carried out with a standard cone of height 300 mm (major diameter of 200 mm and minor diameter of 100 mm), a flat, smooth surfaced, non-absorbent 800 x 800 mm level tray as the base, and a measuring tape. With the cone placed upside down on the tray, the concrete was poured into the cone until level with the top. Then, without tilting, the cone was lifted up to about 50 mm above the tray over a two second interval letting the concrete flow outwards as shown in Figure 4.1. Once the concrete had stopped flowing (or after about ten seconds), two perpendicular diameter measurements were then taken. The average of the two, to the nearest 10 mm, was considered to be the spread (NZS3112, 1986a). The target for this test was a spread measurement of 500-520 mm. Anything less than this would be likely to hold the stones up in the paste while much more could lead to segregation during handling.

Figure 4.1: Spread test at 500 mm

The specific rheology targets required to meet this were (Mackechnie, 2010c):

- Yield shear stress of less than 100 Pa
- Plastic viscosity of less than 40 Pa.s

These were tested using the BML-Viscometer, shown in Figure 4.2, a coaxial cylinder viscometer for coarse particle suspensions. This measures the rheological properties of cement paste, mortar and concrete with 80 mm slump or higher. The BML-Viscometer is able to measure a shear stress between 0.5 and 2000 Pa; that is from a highly flowable mortar to a low workable concrete (ConTec, 2003). The BML process is fully automated to minimise operator influence.

The bucket was filled with the concrete mix up to approximately 30 mm from the top then the coaxial cylinders were lowered into the mix. The standard test was used which begins at the highest speed and is gradually reduced stepwise to the lowest required speed for the mix. For a normal testing time of three to four minutes, the concrete is only subject to movement for about 75 seconds.

Figure 4.2: BML Viscometer

The rheological properties are measured here, using Equation 4.1, considering the fundamental parameters of the Bingham model:

$$\tau = G + H \times v \qquad \text{(Eq 4.1)}$$

Where: G represents the flow resistance which is a measure of the force required to move the concrete

H is the viscosity factor, measuring the resistance with increasing rotational speed

v is the rotational velocity (controlled variable)

As the outer cylinder rotates, torque is applied to the stationary inner cylinder. During this process, a torque-speed diagram is plotted from which a linear regression is used to calculate G and H (with 90 percent confidence intervals).

The change in viscosity during this test is then used to provide a segregation factor (Seg) for the mix. This is defined as the relative change in viscosity (slope) during the test, modelled by Equation 4.2. This is demonstrated in Figure 4.3a, where the yield shear stress is found when the rotational speed is zero (shown with the arrow). The ideal rheological zone for SCP shown in Figure 4.3b:

$$Seg = \frac{H - H'}{H} \qquad \text{(Eq 4.2)}$$

From this information, values can be attained for the:

- Yield value (τ_o): caused by inter-particle forces within the concrete, such that the material appears stiff until these bonds are broken in shear.
- Plastic viscosity (μ): resistance to flow once the yield stress has been exceeded

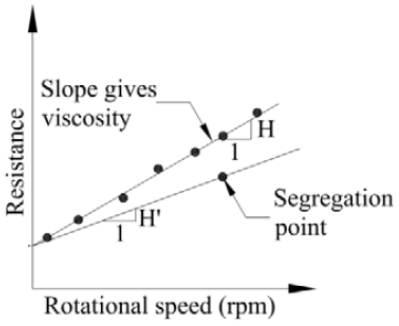

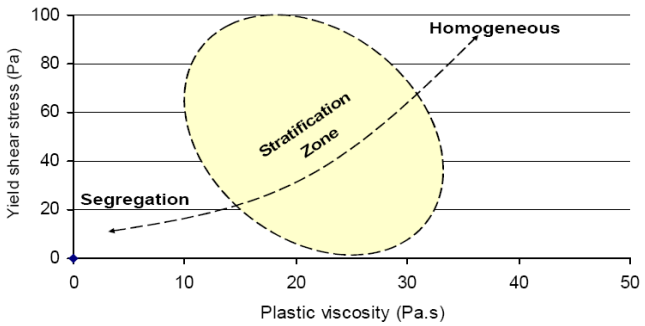

Figure 4.3a (left): Typical torque-speed diagram from BML-Viscometer (ConTec, 2003)
Figure 4.3b (right): Ideal rheological zone for stratification (Mackechnie et al., 2009)

An initial mix was suggested based on previous work by Saevarsdottir and Mackechnie as shown in Table 4-1 below.

Table 4-1: Initial mix design

Material	Weight (kg)	SG	Volume (L)
GP Cement	400	3.14	127.3
Microsilica	30	2.2	13.6
Batch Water	160	1.00	160.0
Sand	250	2.63	95.1
8-14 mm agg.	350	2.63	133.1
Coarse EGB	85	0.30	283.3
Fine EGB	75	0.46	163.0
Visco 555	(1000 mL)	1.1	1.0
Trim Water	40	1.00	40.0

Iterations were then performed on the mix to best meet the explained rheological targets. These are explained in detail in chapter 5.

4.1.2 Vibration Time and Energy

As well as rheological targets, these test cylinders were also used to obtain the ideal length of vibration time with several attempts given for different mix design trials. This was carried out by splitting the eight cylinders for each mix into four groups of two and giving each group a different length of vibration time. As explained below, these trials were all carried out with a vibration input of approximately 3500 rpm. After each trial, corrective action was taken to find the optimum and most consistent time of vibration.

It was acknowledged that the vibrating action of the laboratory table was not completely representative of that of the large factory vibrating table. This was due to the different sizes and masses of the tables, with the university laboratory table measuring 2000 mm x 750 mm and the factory table at 2000 mm x 4000 mm. Some initial tests were carried out however, using a G-force meter which suggested that the overall G-force provided by each table was in a similar range when the university table was set at 3500 rpm. As the exact motion of both the tables was difficult to quantify in a short time frame, it was acknowledged that the vibration times deduced from the laboratory cylinder trials may be subject to some variation for the large scale panel casting. The vibration time adjustment was based on observation during the vibration of each panel.

Later tests were conducted with a greater emphasis on frequency. This meant that more attention was paid to the exact vibrating frequency of the table such that changes to this could be made for a more stratified finished product. This is elaborated on in Chapter 6.

4.1.3 Rod Penetration Test

In order to better estimate the level of stratification at any given time during vibration, a test was carried out that was designed to assess the accuracy of using each of five different tamping rods, described in Table 4-2. These were dropped into the vibrated concrete panel straight after vibration, as an external measure of the degree of stratification of the panels. These were cast in four 150 mm x 150 mm x 500 mm beams to avoid any edge effects that may result from cylinder usage.

The concrete was mixed as usual but with slightly more water in an attempt to increase stratification. Due to a resulting spread of around 570 mm, the mix was on the verge of being too wet and in some instances may have segregated under conveyance. Despite this being unfavourable for a large scale panel, this effect was useful for this test; each beam had a different quantity of aggregates for the structural layer due to the incomplete uniformity of the mix.

The initial plan was to vibrate the beams for 15, 30, 60 and 90 seconds. This was then updated after the first trial at 60 seconds left the top 40 mm almost completely void of paste. This was attributed to the combination of a wet mix and a very dynamic table, relative to the industry tables. The remaining vibration times were changed to 15 s, 25 s and 40 s. As the point of this experiment was to test the accuracy of the rods, it was important to get a range of stratification levels so the specifics of vibration times were not important, especially considering the differences between the tables.

Table 4-2: Physical properties of the five rods

Rod	**#1**	**#2**	**#3**	**#4**	**#5**
Weight (g)	183	342	623	747	690
Length (mm)	305	560	405	475	285
Diameter(mm)	10	10	15	15	20

The five rods were then each dropped into the mix in different points along the beam. In most cases an initial twist was required to break through the surface layer as little paste was left on the top. The rods were each then left to fall under their own weight. A ‘structural layer’ reading was then taken for each rod.

The beams were then cut into several segments where the rods had been dropped so that an exact measurement could be taken at each point.

4.2 Site Panel Tests

4.2.1 Panel Casting

To test the practicality of creating large scale SCP in an industrial setting, a trial casting process was carried out at Stahlton precast yard in Hornby, Christchurch. This was started by casting a panel using the same mix design as used at the university laboratory. For each of the trial panels, the concrete was mixed in the large pan mixer with high shear mixing action. The mixer, with maximum capacity of 1.0 m^3, was suitable for the 0.6 m^3 mix used. The process was carried out by adding the full extent of the normal weight dry ingredients; cement, aggregates, sand and microsilica, with a small amount of water. The EGB was added last to minimise the crushing of the air pockets within the beads. Finally, the super-plasticiser was poured in with some water (as not to add neat) before the final amount of water was added incrementally until the desired spread of 500 mm was reached. To fine tune this during some of the trials, multiple spread tests were carried out during mixing as not to overshoot the required spread value by adding too much water.

Once the mix was deemed satisfactory, it was poured into a skip that was carried across to the large vibrating table as shown in Figure 4.4. Care was taken during this transporting process to minimise bouncing that could encourage early segregation of the mix. A small amount of the mix was poured into the formwork to allow for a quick visual check to make sure that early segregation between the aggregates and the paste had not occurred. The full mix was then poured into the formwork on the vibrating table and vibrated to promote stratification.

Figure 4.4: Large vibrating table at Stahlton precast yard

After each attempt at producing a successfully stratified panel, slight changes to the process were made to improve the final product. These changes were based mostly around the length, intensity and style of vibration as elaborated on in chapter 6. Two successfully stratified one-storey height panels (2500-3000 mm x 800-1000 mm x 250 mm) were to be cast to proceed with the following tests.

4.2.2 Warping Tests

A significant potential issue for the SCP is differential shrinkage between the two strata causing warping. This could be an effect of environmental variations such as temperature or humidity, or the different concrete properties, especially elastic modulus and strength. As Figure 4.5 shows, it could be expected that the lightweight layer shrinks relative to the structural layer due to its weaker properties, a phenomenon that may only be exacerbated further during service conditions as the structural layer is exposed to more severe drying on the interior face.

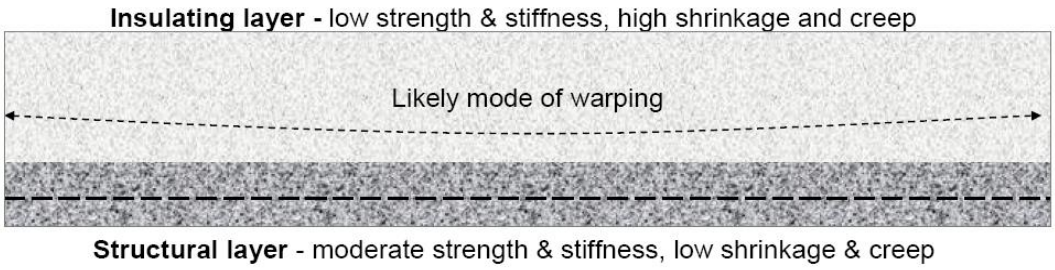

Figure 4.5: Potential warping of stratified concrete (Mackechnie et al., 2007)

To measure the potential effects of warping across the panels, the two satisfactorily stratified panels were erected as if in service, for an extended period. The panels were orientated to face north as to generate the maximum range of environmental exposure and create the 'worst case' scenario for warping. The panels were bolted at the bottom, as shown in Figure 4.6, such that they had minimal restraint to warping so maximum credible out-of-plane deformations would result.

The panels were left for two months with weekly measurements taken for any significant warping deformations. This was carried out by fixing a straight edge to the back of each panel and measuring any curvature (in excess of 0.5 mm) between the square and the panel. This was measured either as a deflection at the top of the panel where it showed convex curvature, or at the centre, assuming a parabolic curve, for concave bending. The test setup is shown in Figure 4.7 with exaggerated deformations for clarity of explanation. The measured deflections were then compared against the ACI acceptable level for warping (as discussed in literature review section 2.3.1). The results were also checked against the common guideline for sufficient serviceability of a 0.2 percent limit for bending deflections (less than 1 mm of deflection per 500 mm height) (Saevarsdottir, 2008).

Figure 4.6: Front face of the standing stratified panels

The initial reading for panel warping was taken on July 22nd and the final on September 23rd. During this two month time period, a combination of warm clear days and snow fall led to a range of temperatures from -6.3°C (Jul 26th) to 20.8°C (Aug 24th) (Metservice, 2011). A full list of the temperatures over the testing period is provided in Appendix 1.

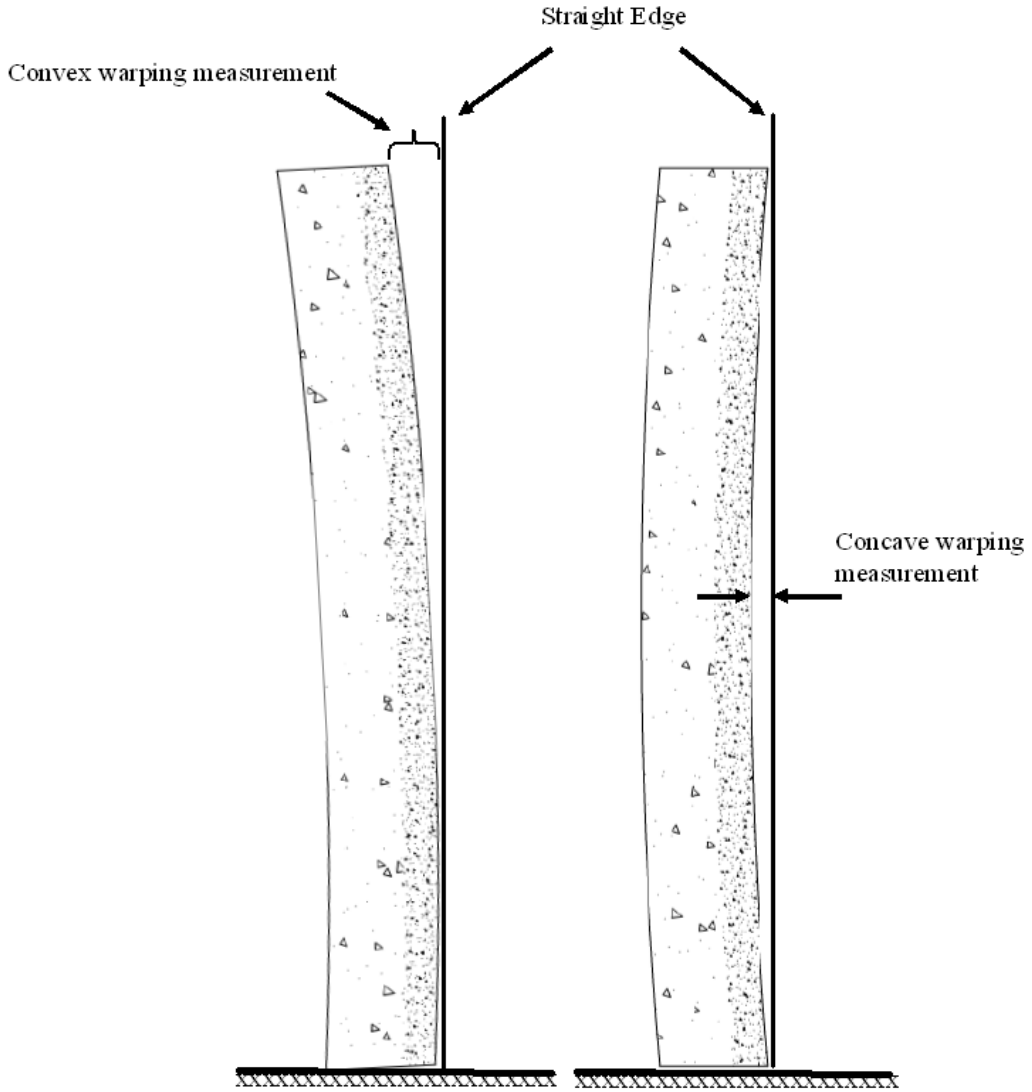

Figure 4.7: Out-of-plane warping convex and concave measurements

A reading was taken from the left, centre and right sides of each of the panels from which an average was taken to assess the cumulative deformation over the trial period. The results of this test were then compared against warping considerations of 0.2 percent, as used by Saevarsdottir (Saevarsdottir, 2008), and the maximum out-of-plane bowing value of ±0.5 in. (±13 mm) used by PCI (Sorenson et al., 2000).

After two months, each of these panels was cut in half vertically leaving one half in place for continued warping monitoring (beyond the scope of this project), now as a worst case scenario with a 'thin' panel, while the other half was used for the laboratory tests outlined in the hardened properties section below.

Warping readings were also taken from four panels after four years of exposure to the elements to gauge any extended movement that may occur in the medium term.

4.2.3 Monitoring of Panel Condition

During the two months of warping monitoring, visual inspections of the panels were also made to assess the degree of surface quality in terms of efflorescence and discolouration and also cracking at the interface or transversely across panel. This was a purely qualitative assessment.

4.3 Hardened Properties

Tests were carried out after successful creation the stratified concrete panels. Where cores were required from the panels, they were extracted using a 90 mm core drill. The following stratification, structural, thermal and durability tests were then carried out on samples taken from three sets of panels:

- O1; 3-4 year old panels from previous work by Mackechnie (2007-08)
- S3; an earlier panel from this work that is reasonably well stratified but with no mesh (refer to section 6.1.3)
- U1, U2 and U3; new panels produced at Stahlton

4.3.1 Degree of Stratification/Centre of Mass

Initial indications of the degree of stratification were given by cutting each panel into smaller pieces for various tests (~150 mm wide strips) to visually assess the degree and uniformity of the stratification process along the length of the panel.

The stratification coefficient was measured by taking the distance between the centre of gravity and centre of area of cylinders to give a further indication of the level of stratification. This technique is demonstrated in Figure 4.8 below.

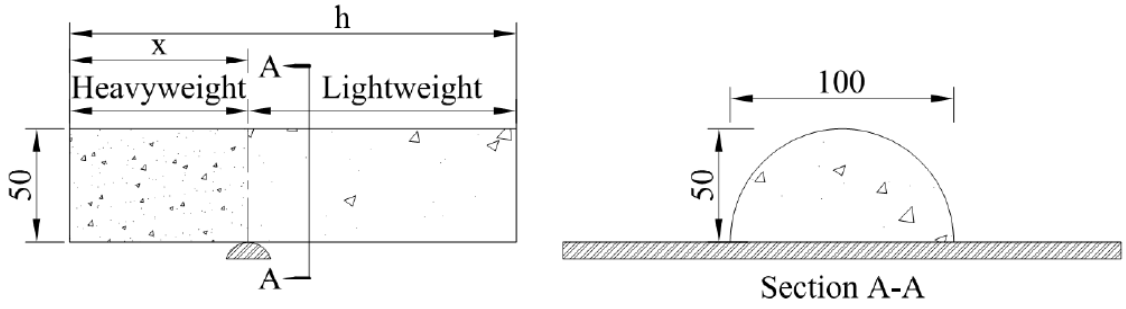

Figure 4.8: Apparatus used to find the centre of mass of the cylinders (Saevarsdottir, 2008)

The stratification coefficient was then found using Equation 4.3:

$$SC\ [\%] = \frac{h/2 - x}{h/2} \times 100 \qquad \text{(Eq 4.3)}$$

Where h is the height of the cylinder (200 ± 5 mm) and x is the distance to the centre of gravity measured from the bottom of the structural layer.

Once the specific characteristics of the materials used have been determined, the stratification coefficient gives an indication as to the level of stratification relative to an upper and lower critical value (CV_1 and CV_2 respectively). That is whether the sample is:

- Poorly stratified ($SC < CV_2$)
- Moderately stratified ($CV_2 < SC < CV_1$) or
- Well stratified ($SC > CV_1$)

Indicative values are $CV_1 = 21$ and $CV_2 = 12$.

4.3.2 Density and Compressive Strength Test

To ascertain the density in each of the two strata, small 60 mm cubes were extracted from both layers of the various samples, using the diamond saw. These cubes were then vacuum saturated and weighed. The weight of each was then divided by the volume to deduce the hardened density.

These cubes were then tested in compression to determine indicative values of the compressive strength in each of the two layers. This quantity is useful as it is the most universally understood; concrete is often described in terms of its compressive strength. This value also provides extra evidence for the likely expected structural performance. The cubes were compressed to ultimate failure using a loading cell with loading capacity of 400 kN. A lightweight cube in compression is shown in Figure 4.9.

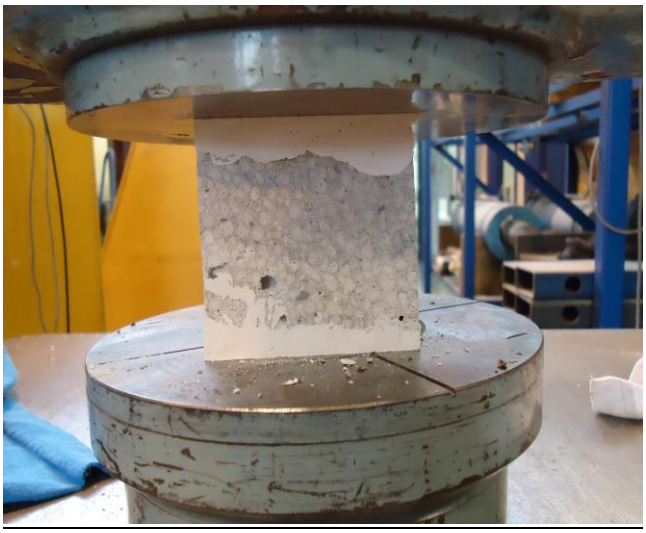

Figure 4.9: 60 mm lightweight concrete cube in compression

4.3.3 Axial Compressive Strength

The compression test was carried out on strips of approximately 150 mm wide by 950 mm long from each of the panels to be tested.

In accordance with NZS 3112, specification tests for determining concrete strength (NZS3112, 1986b), the ends of the strips were first levelled as to not deviate more than 0.5° from square or be concave or convex by more than 0.05 mm. Where ends were not quite level, 12 – 18 mm plywood was placed at the ends to evenly distribute the load over the cross-section. The specimens were

then placed in the Avery Model 7104 DCJ machine with 1000 kN capacity and aligned vertically as columns as shown in Figure 4.10.

Figure 4.10: Axial compression test set up in 1000 kN capacity Avery machine

Gradual loading at a constant rate of 30 kN/min was then applied until failure, avoiding any shock loading. The maximum load for each strip was recorded and the compressive strength calculated as follows:

$$\sigma[MPa] = {}^{F_{max[N]}}/_{A[mm^2]} \qquad \text{(Eq 4.4)}$$

Where σ is the axial compressive strength of the specimen, F_{max} is the maximum load and A is the cross-sectional area.

Details of the modes of failure were taken to deduce the weak areas or potential reasons for failure.

4.3.4 Flexural Tensile Strength and Displacement

The flexural strength of the panels was assessed using 950 mm x 150 mm strips. A reaction frame was used with a four point loading setup as shown in Figure 4.11.

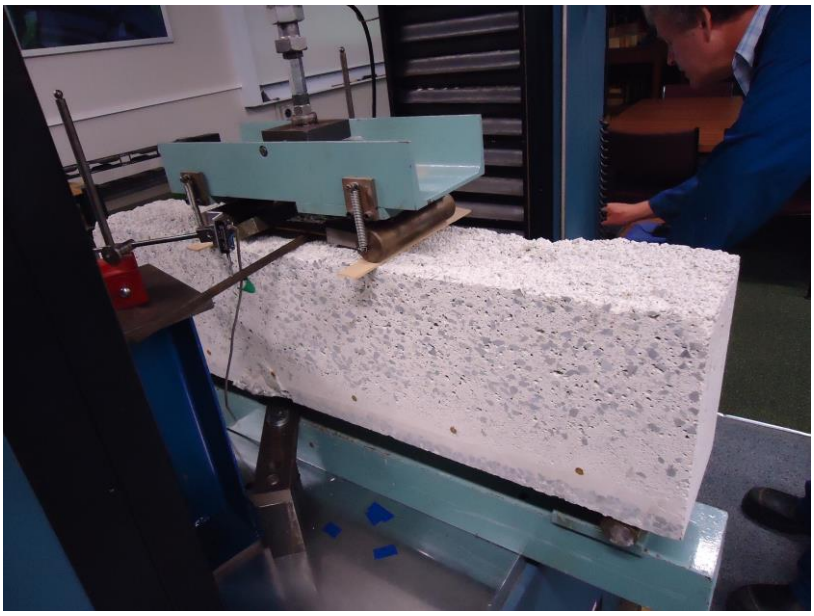

Figure 4.11: Flexural test setup

For a fair and valid test, the forces had to be applied vertically, avoiding any eccentricity. Following NZS 3112 (NZS3112, 1986b), the length of the strips was to be between three and four times the depth of the section. At a depth of 270 mm on average, the strips at approximately 950 mm long fit into this category. The strips were centred on the bearing blocks with the lightweight surface facing upwards to the load applying blocks. The loading blocks were applied at third marks along the beam as shown in Figure 4.12.

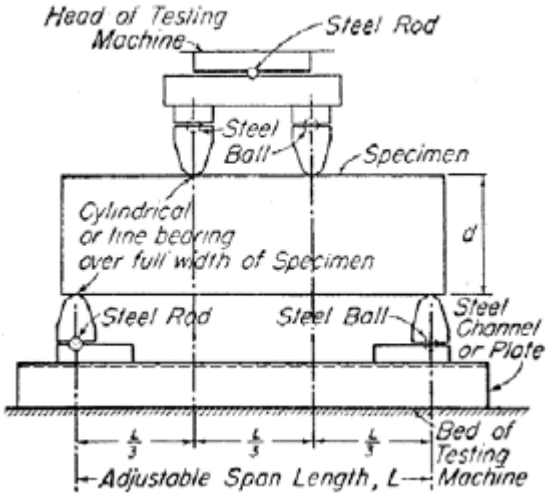

Figure 4.12: Four point loading test setup (NZS3112, 1986b)

Constant load was then applied without any shocks, at a constant rate of 1 to 2 MPa/min until specimen failure. From the recorded maximum load, the flexural capacity was calculated. The average width and depth along the failed sections were measured.

When the fracture occurred in the middle third of the span length, the flexural tensile strength was calculated to the nearest 0.2 MPa using Equation 4.5:

$$T_f[MPa] = \frac{PL}{bd^2} \quad \text{(Eq 4.5)}$$

When the fracture occurred more than 5 percent of the span length outside the middle third, the flexural tensile strength was calculated to the nearest 0.2 MPa using Equation 4.6:

$$T_f[MPa] = \frac{3Pa}{bd^2} \quad \text{(Eq 4.6)}$$

Where:

- T_f is the flexural tensile strength
- P is the maximum load [N]
- L is the span length [mm]
- b is the average width [mm]
- d is the average depth [mm]
- a is the distance between the line of fracture and the nearest support

To measure the displacement, a small metal bar was setup across the centre of the beam as shown in Figure 4.13 and a displacement reading was taken 7 times/second. Using one reading from each side of the beam, an average was taken to minimise reading error.

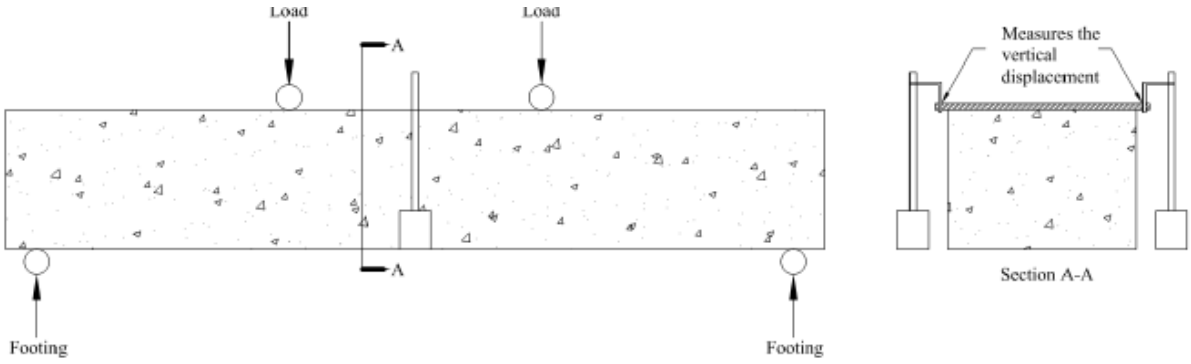

Figure 4.13: Displacement measurement apparatus during flexural test (Saevarsdottir, 2008)

4.3.5 Direct Tension (Pull apart) Test

To test the potential weakness along the interfacial layer between the two strata, the direct tension test was used by testing cores in axial tension. This was setup by attaching 25 mm steel plates to each end of the cylinder cores with epoxy (Sikadur-31) and threading a loop hook to the other side of the plate. Using the Avery machine; model 7109 DCJ, with maximum loading of 100 kN, tension was then applied at a slow rate of about 2 kN/min until the point of failure. The load was applied uniformly across the section of the cylinder. A schematic of the effective load application is provided in Figure 4.14. The full test setup is shown in Figure 4.15.

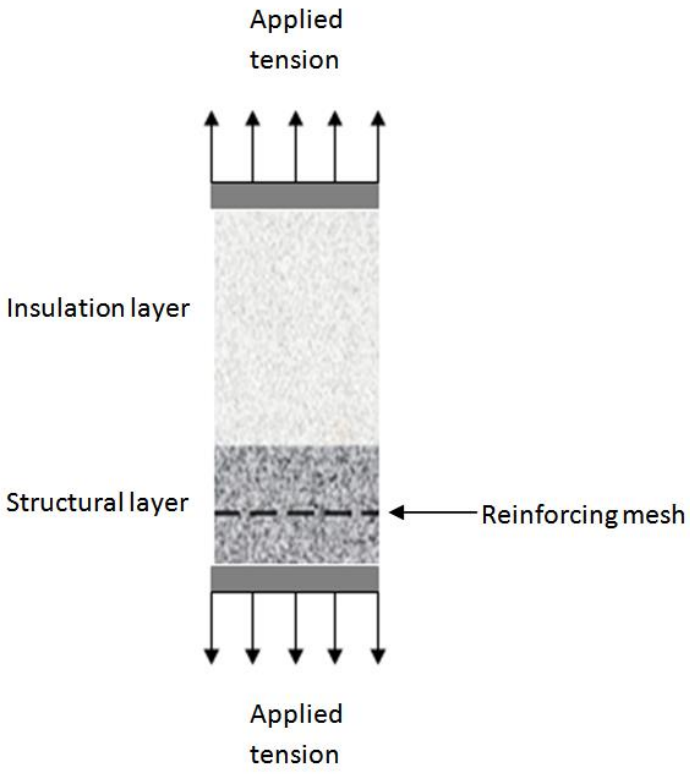

Figure 4.14: Schematic of direct tension application

This is the standard procedure for testing the tensile strength concrete and overlay materials as stated in ASTM C1583 / C1583M which is suitable for both field and laboratory use to determine any of the following (ASTM, 2004):

- The near-surface tensile strength of the substrate as an indicator of the adequacy of surface preparation before application of a repair or overlay material
- The bond strength of a repair or overlay material to the substrate
- The tensile strength of a repair or overlay material

Although this standard refers to concrete repairs or overlays specifically, the method is appropriate to use for delamination testing of SCP due to the potentially weak transition layer between the two strata which may be considered analogous to an overlay joint.

Figure 4.15: Concrete cylinder in place for axial tension test

The failure load was recorded from which an average maximum tensile stress was deduced. Observations of the failure plane were made to assess the most significant point(s) of weakness.

4.3.6 Thermal Properties

A non-steady state method of thermal analysis transient plane source (TPS) was used to provide rapid measurements of the thermal performance. It is a modern technique that gives information about the thermal conductivity, thermal diffusivity and specific heat per volume of the material under study (Gustavsson, 2005).

The Hot Disk Thermal Constants Analyser is a heat source and a dynamic temperature sensor that uses a transiently heated plane sensor in the form of an electrically conducting double spiral (nickel foil) which is sandwiched between two sheets of an insulating material. This was placed between the two plane surfaces of the cores to be tested before an electrical current was passed through. This current provided is high enough that the temperature of the insulating material is increased by several degrees. The resistance (temperature increase) was recorded as a function of time. Figure 4.16 diagramatically shows the setup for the thermal analyser test with current source, I, and the resistance/temperature sensor between the tested material, in this case the two half core cylinders.

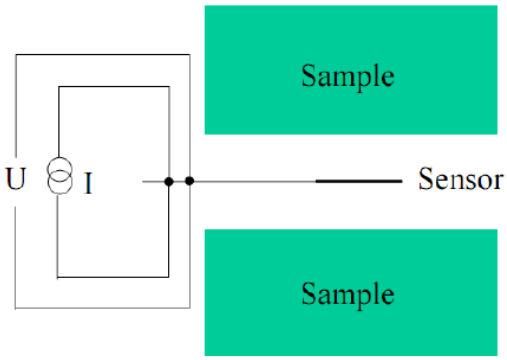

Figure 4.16: Hotdisk setup (Gustavsson, 2005)

The initial resistance, R, was then calculated from Equation 4.7 as a ratio of the voltage and current:

$$R_0 = {}^{V}/_{I_0} \quad \text{(Eq 4.7)}$$

From Equation 4.8, the sensor effect P_0 was calculated:

$$P_0 = R_0 \times I^2 \quad \text{(Eq 4.8)}$$

The thermal parameters were then found using Equations 4.9 and 4.10:

$$R = R_0(1 + \alpha \Delta T) \quad \text{(Eq 4.9)}$$

$$\Delta T = {}^{\alpha P_0}/_{\alpha \lambda} \times F(\tau) \quad \text{(Eq 4.10)}$$

Where:

- R is the probe resistance [Ω]
- R_0 is the initial resistance [Ω]
- α is the temperature coefficient [K^{-1}]
- T is the temperature [K]
- P_0 is the sensor effect
- a is the sensor area [mm]
- λ is the thermal conductivity
- F(τ) is information about κ
- κ is the diffusivity

When ΔT is plotted against F(τ), the best fit curve gives the diffusivity and the slope gives the conductivity. The specific heat is found by using Equation 4.11:

$$C_p = {}^{\lambda}/_{\kappa} \quad \text{(Eq 4.11)}$$

The thermal conductivity measures the ability of a material to conduct heat, and is defined as the ratio of heat flux to temperature gradient, whereas the specific heat is the amount of heat per unit mass required to change the temperature of a material by one degree.

The samples used for testing were 90 mm diameter cores from each of the SCP samples cut lengthways down the middle to provide the plane surfaces. These samples, shown by Figure 4.17, were left to reach ambient room condition for 7 days after cutting, and then tested for thermal properties.

Figure 4.17: a) Hotdisk filament in place

Figure 1.16: b) Material seal around filament

The R-value (total thermal resistance) was calculated (m^2K/W) with Equation 4.12:

$$R - value = {}^{thickness}/_{thermal\ conductivity} \qquad \text{(Eq 4.12)}$$

This value however, underestimates the full R-value as extra thermal resistance of up to 0.12 m^2K/W is provided by the surface contact resistance between both the exterior faces and the interior interface between the two strata. This test therefore produces a conservative R-value, above which the results in service can be expected to exceed. It also does not measure the dynamic responses and thus thermal mass does not contribute.

4.3.7 Water Sorptivity Test

Absorption is the process whereby fluid is drawn into a porous, unsaturated material under the action of capillary forces. Sorptivity on the other hand, is defined as the rate of movement of a wetting front through a porous material under the action of capillary forces. Several general absorption tests have been developed where a concrete sample is immersed in water and the total mass absorbed used as a measure of the absorption. These tests do not quantify the rate of absorption and do not distinguish between surface and bulk effects but measure the porosity of the concrete. Porosity is a percentage measure of the void spaces in a material; space within that can be occupied by water or other fluids. This can therefore be measured by taking the volume of the water filled space and dividing it by the total volume.

Due to the nature of SCP concrete, the sorptivity itself is not a very useful measurement. It may be expected that the more porous lightweight concrete would absorb water much faster than the heavyweight concrete; as the voids in the lightweight concrete are relatively large however, the wetting front travels slowly as there is great space to fill and capillary action is weaker. This means the structural layer, with porosity of 10-15 percent, tends to absorb water faster than the insulating layer, with porosity of around 30 percent. The resulting porosity, or void percentage, from this test is therefore a much more useful measurement as it can be used to find the density and strength of the concrete.

In preparation for the water sorptivity test, 90 mm cores were taken and cut into approximately 25 mm thick slices which were then oven dried at 50°C for 7 days to leave uniform moisture content across the samples. As slices were taken from the whole core, slices had either purely structural/heavyweight properties, purely insulation/lightweight properties or a combination of both. Six different samples were taken from each cylinder to give an indication of the changing porosity properties throughout the depth of the stratified concrete.

A modified version of Kelhan's sorptivity test was used here (Kelham, 1988). The circular edges of the sample were sealed using tape to ensure unidirectional absorption and the samples were then placed on wet paper towels to expose them to a few millimetres of water as shown below in Figure 4.18.

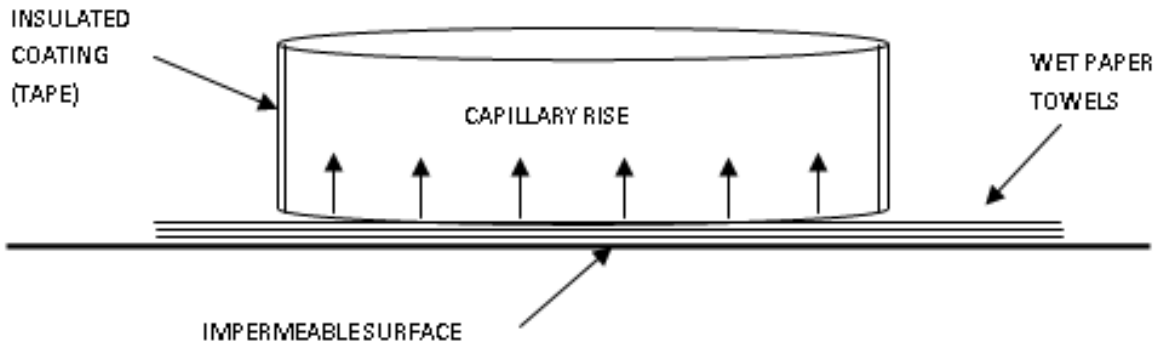

Figure 4.18: Water sorptivity test setup using core slice

The tape was only applied around the sides leaving both ends fully exposed as is shown by Figure 4.19a. Readings were taken at the time intervals 0, 1, 2, 4, 8, 16, 32 and 64 minutes by weighing the sample (mass of water absorbed) with an electronic balance. The samples were finally vacuum-saturated to determine the effective porosity as shown in Figure 4.19b.

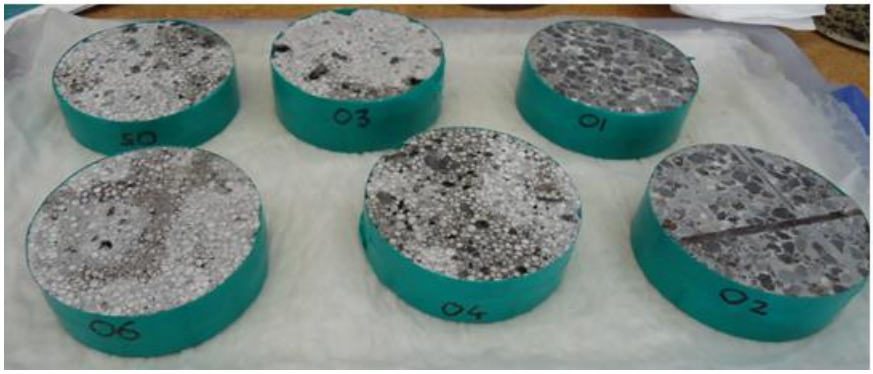

Figure 4.19: a) Water sorptivity sealed samples **Figure 4.19: b) Vacuum saturating samples**

The mass of water absorbed was then plotted against the square root of time with the slope representing the sorptivity (S) shown in Figure 4.13:

$$S = \frac{\Delta M_t}{t^{1/2}} \times \frac{d}{M_{sat} - M_0} \qquad \text{(Eq 4.13)}$$

Where:

- ΔM_t is the change of mass with respect to the dry mass [g]
- M_{sat} is the saturated mass of concrete [g]
- M_0 is the dry mass of concrete [g]
- d is the sample thickness [mm]
- t is the period of absorption [hr]

5 FRESH PROPERTIES AND MIX DESIGN TRIALS

An iterative process was used to find the optimum SCP mix design and slight modifications were made after each trial in an attempt to best meet the required rheological targets as explained in chapter 4. This was yield shear stress of less than 100 Pa and plastic viscosity of less than 40Pa.s. The requirement was to provide a robust mix design, with tolerance for minor variations in batching, by consistently meeting these targets.

This is reported chronologically below explaining the results of each mix with the corrective action taken shown in bold. Mix designs were batched in 20 L lots but are shown per cubic metre for clarity. Each mix is designed to slightly over yield as some crushing of the EGB is expected.

A stratification coefficient is given where photographs are provided for a quantifiable comparison of the level of stratification.

5.1 First trial mix

The first mix, shown in Table 5-1 was suggested by Mackechnie based on previous work with Saevarsdottir (Saevarsdottir, 2008). As the quantity of large particles in this mix design was relatively high, it was expected that the mix would resist spreading to the target level as some aggregates would be unable to sink through the paste and may therefore reduce the flow.

Table 5-1: First trial mix proportions (per cubic metre)

Material	Weight (kg)	SG	Volume (L)
GP Cement	400	3.14	127.3
Microsilica	30	2.20	13.6
Batch Water	160	1.00	160.0
Sand	250	2.63	95.1
8-14 mm agg.	350	2.63	133.1
Coarse EGB	85	0.30	283.3
Fine EGB	75	0.46	163.0
ViscoCrete 555	1000 mL	1.10	1.0
Trim Water	40	1.00	40.0

As expected, this mix did not flow well enough and despite adding 15 L/m^3 (300 mL) of extra water, the mix still refused to spread beyond 380 mm. The yield shear stress reached 117 Pa which is close to but slightly outside the intended range, with a plastic viscosity of 40 Pa.s just scraping inside the target range.

After 60 seconds of vibration, the stratification of this sample was fairly poor.

5.2 Second trial mix

In an effort to increase the spread of the mix and draw the rheological property values down slightly, 25 percent more ViscoCrete 555 was added to the mix. This is shown in

Table 5-2.

Table 5-2: Second trial mix proportions (per cubic metre)

Material	Weight (kg)	SG	Volume (L)
GP Cement	400	3.14	127.3
Microsilica	30	2.20	13.6
Batch Water	160	1.00	160.0
Sand	250	2.63	95.1
8-14 mm agg.	350	2.63	133.1
Coarse EGB	85	0.30	283.3
Fine EGB	75	0.46	163.0
ViscoCrete 555	**1250 mL**	**1.10**	**1.25**
Trim Water	40	1.00	40.0

This mix flowed much more easily and a spread of 510 mm was achieved without the need for any extra water. The yield shear stress and plastic viscosity at 74 Pa and 29.2 Pa.s respectively were well within the required zones.

The stratification of this trial however, was less than satisfactory even though it was vibrated for 60 seconds; the majority of the heavyweight aggregates had not dropped through the paste, leaving the end result very close to homogenous with no indication towards a forming structural layer.

5.3 Third trial mix

Mix 3 was a replica of mix 2 as the rheology had been deemed suitable. Here different lengths of vibration time were applied to the mix in an attempt to achieve an acceptable level of stratification.

Despite using the same mix as above, the spread only reached 400 mm for this trial. It appeared as though the mix was free flowing from one side of the cone and comfortably reached the 500 mm mark, whereas from the other side of the cone, the mix did not flow to a desirable degree leaving an uneven oval shaped spread. This suggested that a longer mixing time was required for a more uniform end product.

Despite the unsatisfactory spread result, the mix was vibrated as planned to get an idea of appropriate vibration times. Vibration times of 30, 45, 60 and 90 seconds were trialled in an attempt to get a range of results from ‘poorly stratified’ to ‘over vibrated - nearly segregated’. Pictures of 30 seconds and 45 seconds of vibration are shown in Figure 5.1 and 60 and 90 seconds in Figure 5.2.

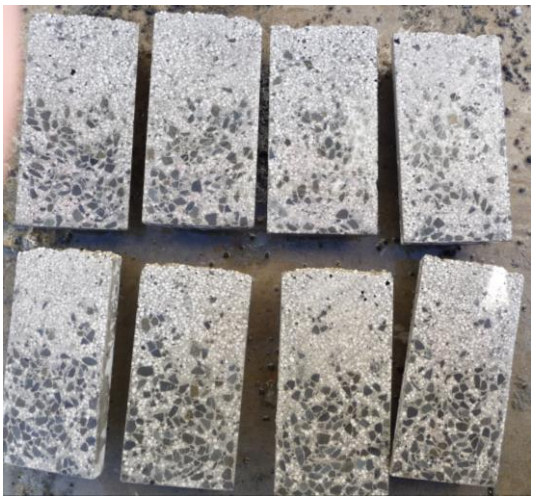

Figure 5.1: Vibration on third trial mix of 30 seconds (top) and 45 seconds (bottom)

As expected, the 30 second mixing time trial was not stratified enough. The 45 second cylinder, though still far from perfect, was at least demonstrating some incipient layering.

Figure 5.2: Vibration on third trial mix of 60 seconds (top) and 90 seconds (bottom)

The 60 second mix came close to the desired end product with only a few stones holding up in the lightweight layer. The 90 second trial appeared to have been vibrated for too long with a thin layer forming between the two distinct strata, hinting at a possible delamination plane in service. Stratification coefficients for each time trial are shown in Table 5-3.

Table 5-3: Stratification coefficients for third trial mix

Time (s)	Stratification coefficient
30	0.14
45	0.17
60	0.21
90	0.25

5.4 Fourth trial mix

To further increase the spread of the mix again, a small amount of sand and fine EGB were removed and another slight increase in Visco 555 was adopted. This update is shown below in Table 5-4.

Table 5-4: Fourth trial mix proportions (per cubic metre)

Material	Weight (kg)	SG	Volume (L)
GP Cement	400	3.14	127.3
Microsilica	30	2.20	13.6
Batch Water	160	1.00	160.0
Sand	**225**	**2.63**	**95.1**
8-14 mm agg.	350	2.63	133.1
Coarse EGB	85	0.30	283.3
Fine EGB	**70**	**0.46**	**163.0**
Visco 555	**1400 mL**	**1.10**	**1.4**
Trim Water	40	1.00	40.0

Again the mix struggled to flow sufficiently to a spread of even 400 mm so another 5L/m^3 (100 mL) of water was added but to no great benefit. The yield shear stress at 62 Pa and plastic viscosity at 9.2 Pa.s were both very low, suggesting that the mix should stratify well. Being such low values however, this could increase the risk of segregation.

Though a longer mixing time was implemented, again the mix showed some variability across the diameter with the mix spreading unevenly from each side of the cone resulting in an oval shape, showing signs of inconsistency. No signs of early segregation were observed during this testing.

Again some different lengths of vibration were given with times of 45, 60 (Figure 5.3) and 75 seconds (Figure 5.4) used in response to the results of the last attempt.

Figure 5.3: Vibration on fourth trial mix of 45 seconds (top) and 60 seconds (bottom)

These results were very similar to those above with 60 seconds still not quite long enough for optimum stratification.

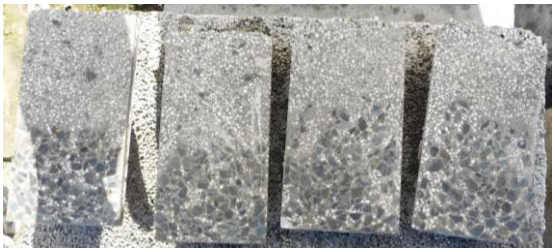

Figure 5.4: Vibration on fourth trial mix of 75 seconds

Here still, the stratification was not as clear as it should have been so a further adjustment to the mix was required as this length of vibration time should have yielded more stratified results. Stratification coefficients are shown in Table 5-5.

Table 5-5: Stratification coefficients for fourth trial mix

Time	Stratification coefficient
45	0.17
60	0.19
75	0.21

5.5 Fifth trial mix

Despite reluctance to exceed 200 L/m^3 of water for this mix, a slight increase in water was used here to increase the flow and reduce the resistance to flow that had resulted from the last few mixes. This was in the form of 5 extra L/m^3 of batch water with another 5 L/m^3 extra usable as trim water if required. An increase in Visco 555 was also added to help with this by potentially increasing the dispersion to develop a more uniform nature across the mix (this is still within a safe level to avoid unwanted segregation) (Sika-Construction, 2003). These changes are shown in Table 5.6. For this trial, mixing was carried out for a longer time including mixing of the dry materials before water addition.

Table 5-6: Fifth trial mix proportions (per cubic metre)

Material	Weight (kg)	SG	Volume (L)
GP Cement	400	3.14	127.3
Microsilica	30	2.2	13.6
Batch Water	**165**	**1.00**	**165.0**
Sand	225	2.63	95.1
8-14 mm agg.	350	2.63	133.1
Coarse EGB	85	0.30	283.3
Fine EGB	70	0.46	163.0
Visco 555	**1800**	**1.10**	**1.8**
Trim Water	**40/45**	**1.00**	**40.0/45.0**

Here a more desirable spread of 520 mm resulted with very low yield shear stress and plastic viscosity values at 8 Pa and 25 Pa.s respectively, sitting low within the target range.

This mix was initially intended to be vibrated for 60, 75 and 90 seconds but due to the observation of some bead bouncing due to lacking surface paste, this was adjusted to 45, 60 and 75 with a 30 second trial added as well to gauge the lower bound of this more flowing mix. Vibration times of 30 and 45 seconds are shown in Figure 5.5 and vibration of 60 and 75 seconds shown in Figure 5.6.

Figure 5.5: Vibration on fifth trial mix of 30 seconds (top) and 45 seconds (bottom)

The extra workability of this mix demonstrated an increase in stratification for these lengths of time of vibration time. 45 seconds of vibration was very close to the optimum target result.

Figure 5.6: Vibration on fifth trial mix of 60 seconds (top) and 75 seconds (bottom)

Here a third layer started to form at the interface which indicated excessive vibration time. (It was notable here that the cylinders did not have equal amounts of heavyweight and lightweight aggregates, these varying quantities of components were not a factor on the larger scale panel).

Table 5-7: Stratification coefficients for fifth trial mix

Time (s)	Stratification coefficient
30	0.17
45	0.20
60	0.24
75	0.26

The stratification coefficients here are comparable to those found by Saevarsdottir, where only 2 out of 25 of these previous results were better than the best value here of 0.26. On average, these sets of results are very similar but the range here of 0.17-0.26 compares to a much wider previous range of 0.07-0.28, developed through using a wide range of materials. From the GB (EGB, perlite and slag) and BB (2 grades of EGB and slag) mixes from this previous work however, nearly all stratification coefficients are over 0.20 (Saevarsdottir, 2008).

5.6 Final mix design and vibration time

The best mix design for this work was the fifth trial mix. This included the extra water and super-plasticiser for enough flow to make most effective use of the vibration. Based on this, vibration for the first full scale casting, was to be carried out for 40 seconds initially, unless excessive bouncing of beads occurred on the surface before this time. The panel was then to be tamped to gauge the stratification with the option of a further ten to fifteen seconds if required.

This mix design, created in controlled lab conditions, was potentially subject to some slight water content adjustment when produced on the larger scale. This was controlled so that the required rheological properties were met for best stratifying performance.

5.7 Rod Penetration Test Results

Two days after the rod penetration test was completed; the beams were cut into sections to assess the accuracy of the rod readings from the earlier measurements as shown in Figure 5.7.

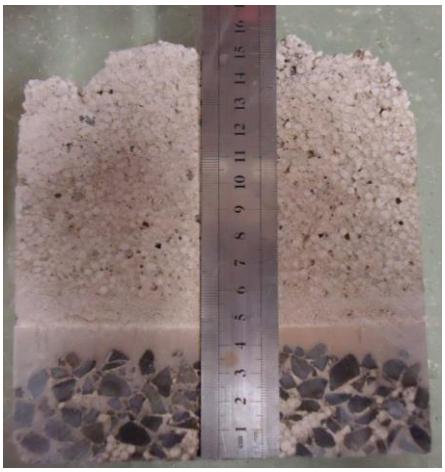

Figure 5.7: Measuring the structural layer

The results of this are presented and explained in Table 5-8 and Table 5-9 for each of the different vibration times. From this, a conclusion about which rod is most appropriate for the structural layer testing was deduced. Due to the poor distribution of materials as a result of the overly wet mix, it was concluded that a wetter mix is not the answer in encouraging greater stratification.

Table 5-8: Tests for 15, 25 and 40 seconds of vibration

15 seconds of vibration			
	Rod Reading (mm)	Measured Reading	Absolute Difference
Rod 1	25	30	5
Rod 2	15	28	13
Rod 3	13	26	13
Rod 4	20	25	5
Rod 5	30	24	6
25 seconds of vibration			
	Rod Reading (mm)	Measured Reading	Absolute Difference
Rod 1	75	75	0
Rod 2	80	77	3
Rod 3	70	79	9
Rod 4	67	80	13
Rod 5	85	80	5
40 seconds of vibration			
	Rod Reading (mm)	Measured Reading	Absolute Difference
Rod 1	40	48	8
Rod 2	30	47	17
Rod 3	27	47	20
Rod 4	30	45	15
Rod 5	35	43	8

The 25 second test was carried out last so contained significantly more aggregates due to the early segregation of the mix. Also, a noticeable paste layer developed here which may explain why Rod 5 predicted a thicker layer despite being heavier, as it may have been held up in the paste due to its greater width and inability to penetrate effectively.

The test for 60 seconds of vibration was unusable except for further demonstration of the effects of over-vibrating and an over-wet mix. The rods struggled to even break the surface of the beads as there was little to no fluid content present.

Table 5-9: Total difference in measurement between each rod and the structural layers

Rod Number	**Total Difference (mm)**
Rod 1	13
Rod 2	33
Rod 3	42
Rod 4	33
Rod 5	19

Rod 1 (the lightest) was best overall, shown graphically in Figure 5.8. Despite this, all rods gave a fairly good indication of at least acknowledging a forming structural layer, once more than 30 or 40 mm of aggregate had begun to collect at the bottom.

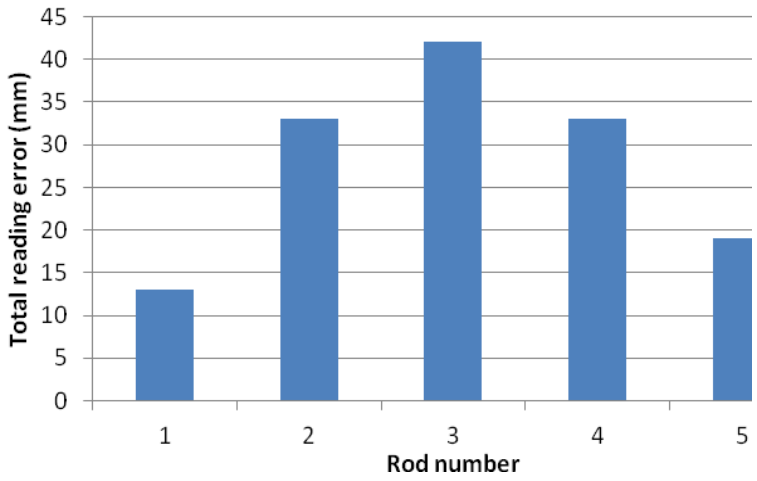

Figure 5.8: Total error for rod test

This work on developing an appropriate mix design was then taken to the industrial setting at Stahlton precast concrete yard to test it on a larger scale. Here the insensitivity to minor variations in batching was tested. This process is discussed in Chapter 6.

6 SITE PANEL TESTS

6.1 Trial Panel Casting at Stahlton Precasting Yard

Once a suitable mix design was developed, casting commenced at Stahlton precast yard in an attempt to recreate the laboratory controlled results on the larger scale. The available material allowed for the casting of several panels so that the production technique could be streamlined and the quality of the final product optimised. In response to the outcome from each trial panel, changes were made to fine tune the process for the next effort as explained in detail below.

6.1.1 Trial Panel 1

The first step for this trial was to recreate the same fresh properties of the mix with a 600 litre mix rather than the 20 litres used in the lab. The pan mixer at Stahlton with maximum capacity of 1 m^3 or comfortable capacity of 0.8 m^3 was easily sufficient for this panel casting. Despite only requiring 500 litres to fill the panel formwork, a 600 litre mix was used to account for spillage and crushing of some of the glass beads under the weight of the larger mix. Due to the potentially unpredictable nature of the large scale mixing at this stage, the water was added last at a slow rate as not to over saturate the mix and cause premature segregation. Despite the water requirements of 205 L/m^3, (123 L for the 0.6 m^3 mix) as specified by the lab trials, only 167 L/m^3 was used (100 L) including the moisture content of the sand. Even so, this was added incrementally until visual inspection suggested that the right consistency had been reached before a spread test was used as a final check.

Following this, when the mix was deemed to be at the target consistency of 500 mm spread, the fresh concrete was poured into a skip that was carried to the vibration table. A last minute visual segregation test was employed after the transportation before the 2 m x 1 m x 250 mm formwork box was filled and vibration was applied.

After the nominated 45 seconds of vibration as designated by the lab trials, it was apparent that stratification was not taking place, at least not on the top surface where stones were trapped. A further minute of vibration was applied to the panel but with no improvement. Continued vibration was used until five minutes were up and little to no paste was left on the surface.

On inspection two days later when the panel was cut in half, as expected; no stratification had occurred suggesting this particular test setup to be insufficient for commercial production.

6.1.2 Trial Panel 2

In discussion with regards to the reasons for failure to cast a successful first panel, it was suggested that the vibrating table had only had 60 percent of its maximum weight directed to the vibration. This meant that an increase to the action of the vibration could be implemented by changing the position of the throwing weights. This action was taken for the second attempt at casting.

The mix was then created in the same fashion as the first attempt by adding some of the water at the end to fine tune the spread to the required 500 mm. After several attempts to reach the required rheology at similar water content, the final amount added was 225 L/m^3 (135 L) which did not correlate at all with past work. It was later discovered that the cement scales had been incorrectly calibrated such that 40 percent extra cement had been added to the mix.

The extra weight added to the vibration did not change the energy output of the table to any noticeable level. Even though the mix had been batched incorrectly, the spread was still close to the required level and it was clear that no stratification was going to occur with the lacking energy provided.

6.1.3 Trial Panel 3

In response to these failures, it was suggested that the specific characteristics of the vibration were not suitable for the desired response. As the action of the table was very quick and the weight of such a large plate of steel is great, the table surface was not given enough chance to travel vertically. This meant a large percentage of the motion transferred to the mix was delivered in a horizontal direction as opposed to the necessary vertical motion.

To address this, a frequency control system was purchased in an effort to slow the vibration speed to attain a greater displacement and increase the dynamic action of the table throw. From visual inspection it was clear that some frequency settings drove a much greater response out of the table than others. Frequencies of 34.7 Hz and 45 Hz were particularly noticeable as providing a much stronger vertical response than the original 50 Hz setting. This was quickly tested by placing a bucket of water on the table and watching the response at the different frequencies to visually judge the optimum vibration energy.

The concrete was mixed as before and the correct spread was achieved with a much more comparable 183 L/m^3 (110 L) of water. The vibration was then increased progressively to the nominated 34.7 Hz and vibrated for one minute after which it appeared as if nothing was happening once again. Another minute of vibration was applied before paste was starting to leave the surface again.

On inspection the next day, the results were surprising with a distinct structural layer of around 70 mm forming at the bottom. A small layer of stones had been caught on the top surface as they had not been able to break through the slightly crustier top layer, this giving the impression of lacking stratification at the time. A few stones were bridging the lightweight layer down each side due to the rotation caused by the style of vibration. A very small layer of paste had begun to accumulate between the structural and insulating layers, as can be seen on Figure 6.1, but this was not considered a significant delamination threat.

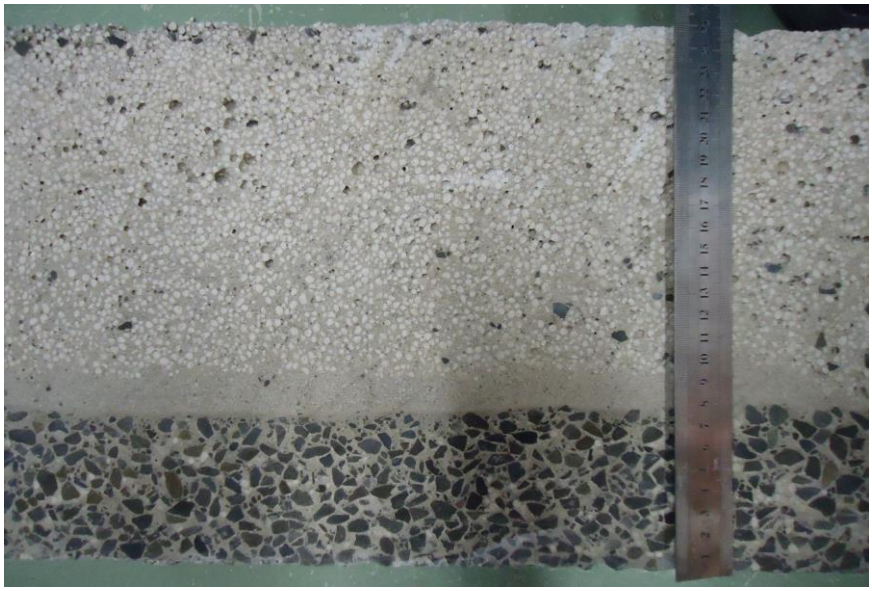

Figure 6.1: Trial panel 3 - reasonably well stratified (Stahlton table)

Though this attempt was not considered perfectly stratified, it was a very positive step in the right direction with a stratification coefficient of 0.23. From this, any reproducible results could be considered satisfactory.

6.1.4 Trial Panel 4

Based on the success of trial panel 3, a bigger panel at 3 m x 0.8 m x 250 mm was cast to model the height of a single storey. In an attempt to slightly improve trial panel 3, the vibration time for panel 4 was cut down to one minute to hold more paste at the surface for a better surface finish and to reduce the presence of the intermediate layer. In an effort to remove the trapped stones off the surface, the formwork was overfilled before vibration so that the top layer could be smoothed off after vibration, leaving only glass beads on the surface. Further, this meant that the finished surface was likely to be flatter than that of panel 3 which incorporated some undulations.

As with the other panels, the top surface during vibration did not appear to be affected by the vibration but the experience from the last panel had suggested this was not a concern and stratification may still have been occurring.

Unfortunately, this was an incorrect assumption and there was no evidence of stratification when the hardened panel was sectioned.

6.1.5 Trial Panel 5

For this panel, more emphasis was put on the reading of the penetration rod as it was clear that the surface effects were not indicative of the level of stratification below. Using evidence from the last two panels, it was predicted that the optimum vibration time was between 90 and 100 seconds.

Carrying out the process as for the other panels, the required 500 mm spread was met. Vibration was then applied for one minute when a penetration rod check was carried out indicating no stratification. This continued to be the case after another minute of vibration was applied. On later inspection, the results agreed with the rod as no stratification had resulted as shown below in Figure 6.2.

Figure 6.2: Trial panel 5 - poorly stratified (Stahlton table)

6.1.6 Industrial Setting Review

After five attempts at creating a panel in the industrial setting there was little evidence to suggest that it is a plausible venture with the current setup. Despite the third panel providing some promising results, no consistency was attained so the process had to be altered.

There are some potential reasons why the third panel was very close working while none of the others showed any signs of vibration at all. These potential reasons could include:

- During the third panel vibration, the frequency was increased progressively from zero to 34.7 Hz, where it was set at 34.7 Hz over the whole period for the following two panels.
- The presence of people on the table for some of the trials may have changed the weight of the system by enough to alter the results.
- The extra weight of the slightly bigger panels 4 and 5 may have again decreased the displacement.

However, none of these reasons seem significant enough to cause such a change between the results of the panels and it remained too difficult and expensive to quantify this further. As such, a change of direction was implemented with the acceptance that this table, designed simply to remove the air from a mix, could not consistently provide enough energy for satisfactory stratification.

6.2 Revisited Vibration Assessment and Vibrating Table

Due to the inability to continue the satisfactory result of the third panel, a new approach was required. Based on the knowledge that the university laboratory vibrating table could provide the required energy for the stratification of the panels, the next panels were cast on this table but at Stahlton yard using the industrial setting. Due to the smaller size of the table, the panel could only be cast at 2500 mm x 800 mm x 250 mm. This was still close enough to a full storey height for the warping test to follow.

6.2.1 Panel 1 – University Vibrating Table

For this attempt, the same design was mixed as per the other trials and the 500 mm spread achieved. Due to malfunctioning of the university vibrating table caused by slipping of the turning belt, this panel received little vibration energy. Although there was some indication of stratification after 30 seconds, it was deemed unsafe to run the table for any longer as it began to emit smoke. The resulting panel was not satisfactory as shown in Figure 6.3.

Figure 6.3: Trial panel 1 for warping tests – poorly stratified (university lab table)

After this trial, some repair and maintenance work was carried out on the vibrating table to ensure that it could run smoothly under the weight of the panel before the next trial.

6.2.2 Panel 2 – University Vibrating Table

Following the same mixing process, the mix was created again. As the sand was at a moisture content of 9 percent, 80 L of water was enough to push the spread of the mix out to 650 mm. This was rectified by adding an extra 2 kg of microsilica, rounding this up to 20 kg for the 0.6 m^3 mix. This was enough to hold the mix from segregating prematurely.

Vibration was applied gradually from 2500 rpm through to 3500 rpm over a 45 second interval. The stratification was then checked with the penetration rod showing that between only 30 and 40 mm of structural layer had formed with some irregularity so another 15 seconds of vibration was given as the indication was. The indication after this extra 15 seconds of vibration was that a more consistent layer of over 50 mm in places had formed. Vibration was stopped here to evade voiding the surface of paste. The final outcome of this panel, with a stratification coefficient of 0.21 is shown in Figure 6.4.

Figure 6.4: Trial panel 2 for warping tests – reasonably well stratified (uni lab table)

Despite plenty of paste being left on the surface, this panel was very difficult to finish smoothly. Using a screed, the mix was worked down to the level of the formwork, and then a trowel was used at regular intervals in an attempt to pull the paste to a smooth finish.

6.2.3 Panel 3 – University Vibrating Table

The third attempt at a panel to be used for the warping test was created in similar fashion but with a closer eye on the spread before two much water was added. With the intention of a very slight increase to the spread, it reached 530 mm and no signs of any early segregation were present.

Vibration was applied for 45 seconds as for the last panel and again the structural layer was too thin so another 15 seconds was given. Still only about 40 mm had accumulated so a final 15 seconds of vibration was provided. This was further justified by the heavy presence of paste remaining on the surface. After this, a 60 mm structural layer was indicated by the penetration rod so vibration was stopped.

This panel was more difficult again to finish as the surface had become quite sticky and resistant to finishing. The cross-section of the satisfactorily stratified panel with stratification coefficient of 25 is shown in Figure 6.5.

Figure 6.5: Trial panel 3 for warping tests – satisfactorily stratified (uni lab table)

A comparison between the inputs and outputs of the attempted panels is shown in Table 6-1 with the panels chosen for further testing highlighted.

Table 6-1: Stratification comparison of the panels

Vibrating Table	Panel number	Frequency (rpm)	Vibration time (s)	Stratification coefficient
Stahlton	S1	3000	300	0.03
Stahlton	S2	3000	240	0.03
Stahlton	**S3**	**0-2245**	**120**	**0.23**
Stahlton	S4	2245	60	0.05
Stahlton	S5	2245	90	0.07
University	**U1**	**<2000**	**30**	**0.08**
University	**U2**	**2500-3500**	**75**	**0.18**
University	**U3**	**2500-3500**	**90**	**0.21**

6.2.4 Sensitivity Testing Using a Range of Stratified Panels

With a range of stratification levels over these three panels, poor to satisfactory, a sensitivity test was deemed appropriate. By testing five panels with increasing stratification coefficients (U1, U2, U3, S3 and O1) the properties of each could be compared to find a critical level of stratification for satisfactory thermal performance. A brief description and visual assessment (long section) of each panel to be tested is given with the results of the hardened property tests in Chapter 7.

6.3 Site Monitoring

6.3.1 Warping

Figure 6.6 shows the initial reading for the beginning of the test. From this initial reading of the profile of the erected panels, each had a very minor concavity of 1-2 mm. The weekly readings are presented in Table 6-2 and Table 6-3. During this two month time period, a range of weather conditions including warm sunny days and two significant snow fall events contributed to a temperature range hitting a maximum of 20.8°C (Aug 24th) and a of low of -6.3°C (Jul 26th) as recorded at Christchurch airport (Metservice, 2011). A full list of temperatures over the trial period is given in Appendix 1.

Figure 6.6: Taking the initial warping reading at Stahlton precast yard

Table 6-2: Warping measurements for moderately stratified panel, U2 (mm)

	Wk 0	Wk 1	Wk 2	Wk 3	Wk 4	Wk 5	Wk 6	Wk 7	Wk 8	Wk 9
Left	1.5	1.5	1.5	1.5	1.5	1.5	1.5	1.5	1.5	1.5
Mid	1.5	1.5	1.5	1.5	1.5	1.5	1.5	1.5	1.5	1.5
Right	2.0	2.0	2.0	2.0	2.0	2.0	2.0	2.0	2.0	2.0
Avrg	1.7	1.7	1.7	1.7	1.7	1.7	1.7	1.7	1.7	1.7

Table 6-3: Warping measurements for well stratified panel, U3 (mm)

	Wk 0	Wk 1	Wk 2	Wk 3	Wk 4	Wk 5	Wk 6	Wk 7	Wk 8	Wk 9
Left	1.5	1.5	1.5	1.5	1.5	1.5	1.5	1.5	1.5	1.5
Mid	1.5	1.5	1.5	1.5	1.5	1.5	1.5	1.5	1.5	1.5
Right	2.0	2.0	2.0	2.0	2.0	2.0	2.0	2.0	2.0	2.0
Avrg	1.7	1.7	1.7	1.7	1.7	1.7	1.7	1.7	1.7	1.7

These results show that neither panel experienced any significant deformation from the initial shape of the formwork during this period. It is fair to assume that if these panels were to experience any warping out of plane then the majority of this would have occurred in the initial stages of placement. This test will continue to run however, beyond the completion of this thesis.

The results from this warping test concur with the results from the more accurate past testing (Saevarsdottir, 2008). This work by Saevarsdottir showed some very minimal warping of the panels, but all of which were within the recommended 0.2% (1/500). These combined results give strong evidence for dimensional stability in terms of out-of-plane warping of SCP.

Measurements carried out on the four year old laboratory cast panels also showed no measurable warping (less than 1 mm out of plane). This gives validation to extrapolate the results from this work to suggest that warping is not a problem for SCP in the medium term.

6.3.2 Condition

Visual inspection of panels over the two month time period did not give rise to any examples of efflorescence, discolouration or cracking at the interface. This is consistent with long term observations on older panels; SCP made with inorganic polymer have shown some efflorescence on the exterior surfaces but panels made with Portland cement have been free from deterioration.

6.3.3 Further Testing

After this satisfactory performance of the two panels in the warping and condition tests, these two panels were cut in half down the long axis. While half was left in place to continue the warping testing into the long term future, the other half of each was taken down to begin the hardened property testing as chapter 7 explains. Along with these, the poorly stratified panel, U1, was also used to complete the sensitivity testing with the range of three panels with varying degrees of stratification.

7 HARDENED PROPERTIES TESTS RESULTS

7.1 Degree of Stratification/Centre of Mass

7.1.1 University Panel 1 (U1)

This panel received inconsistent vibration due to the mechanical faults of the University table. Full vibration was not provided by the table due to poor connections between the motor and vibrating surface as some bolts were loose after transportation to the precast yard. This meant that the end result was not only unsatisfactory, but also rather irregular. Though most of the panel showed no evidence of stratification, a few aggregate clusters of up to 30 mm depth had formed. Some localised areas were almost completely void of aggregates, of either kind, leaving bands of paste. Figure 7.1 shows part of a long section of this panel with stratification coefficient of 0.07.

Figure 7.1: Vertical cross-section of panel U1

7.1.2 University Panel 2 (U2)

Stratification of panel U2 was an improvement on U1 showing some tendency towards forming a stratified structural layer. Though not as irregular as U1, this panel did have some variation across the length as Figure 7.2 shows. The structural layer was 45 mm deep in several areas but this was often contaminated with lightweight aggregate. Though the majority of the greywacke had left the top 50 mm of the section, some of it was still caught high up in the insulating layer; a stratification coefficient of 0.12 resulted.

Figure 7.2: Vertical cross-section of panel U2

7.1.3 University Panel 3 (U3)

Panel U3 had a more defined structural layer than panel U2 with a 60 mm structural layer forming across nearly the whole section as shown in Figure 7.3. This was the result of both a slightly greater spread and slightly longer vibration time than the last panel, both as a response as to how well Panel U2 stratified. Some areas in the insulating layer were left almost completely free of greywacke aggregates resulting in a stratification coefficient of 0.15.

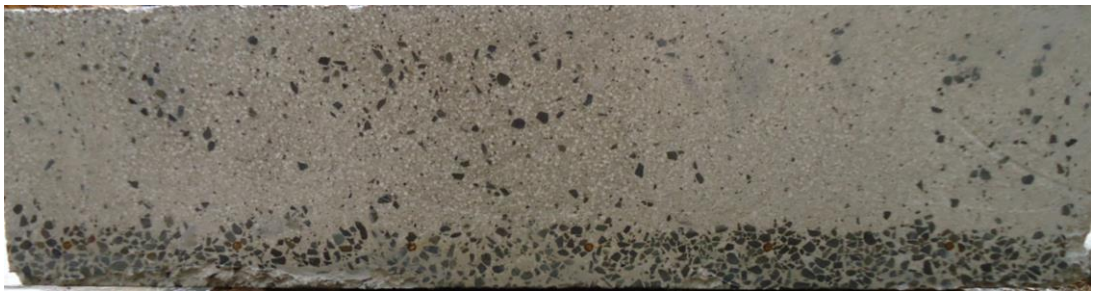

Figure 7.3: Vertical cross-section of panel U3

7.1.4 Stahlton Panel 3 (S3)

Panel S3, created on the Stahlton vibrating table, had a fairly well consolidated 65 - 70 mm structural layer with very few greywacke aggregates left floating in the insulating layer. A transition layer of paste begun to form between the two layers as can be seen in Figure 7.4. The relative clarity of the two strata here meant that the stratification coefficient was much improved at 0.22. As this panel was cast in the preliminary trial stages of production, no reinforcing mesh was used here.

Figure 7.4: Vertical cross-section of panel S3

7.1.5 Old Panel 1 (O1)

This panel, created four years ago by Mackechnie and Bateman in the university laboratory, had better stratification than any of the panels cast in the industrial setting. A solid structural layer averaging 75 mm deep sat beneath an insulating layer almost completely void of heavyweight aggregates. Panel O1 was created using slightly different materials to the other panels tested here, most notably slag in place of greywacke as the heavyweight aggregate. The stratification coefficient of this panel was 0.24.

Figure 7.5: Vertical cross-section of panel O1

7.1.6 Stratification Coefficients

The stratification coefficient measured from samples taken of each of the panels is given in Table 7-1.

Table 7-1: Stratification coefficients for the SCP samples

Panel	Stratification Coefficient	Stratification Level
U1	0.07	Poor
U2	0.12	Poor - moderate
U3	0.15	Moderate
S3	0.22	Moderate – good
O1	0.24	Good

The different levels of stratification from this sample encompass the full spectrum of quality from poor to good. This confirms the measured panels were sufficiently different for the sensitivity testing of the SCP performance based on the degree of stratification.

7.2 Density and Compressive Strength Test

The hardened density and compressive strength of each of the samples was tested using 60 mm cubes. The results are shown in Table 7-2.

Table 7-2: Density and compressive strength of the SCP samples

Panel	Hardened density (kg/m^3)		Average compressive strength (MPa)	
	Heavyweight	Lightweight	Heavyweight	Lightweight
U1	1382	1371	8.9	7.4
U2	1808	1169	12.4	7.3
U3	1882	1036	9.4	5.5
S3	2319	1138	57.4	10.7
O1	2562	1386	39.8	3.2

These results show density difference increasing between the heavyweight and lightweight layers as the level of stratification increased. Generally the density of the lightweight layer decreased slightly with stratification as fewer heavyweight aggregate particles were caught in the lightweight strata. Panel O1 included the use of some different materials so to make direct comparison with the other panels is difficult. The strength of the structural layer greatly increased with stratification as the structural strata became better consolidated. Figure 7.6 shows the increasing density difference between the two layers with increased stratification. Past work, during which panel O1 was cast, showed an average lightweight density of 1400 kg/m^3 and heavyweight density of 2245 kg/m^3 (Saevarsdottir, 2008).

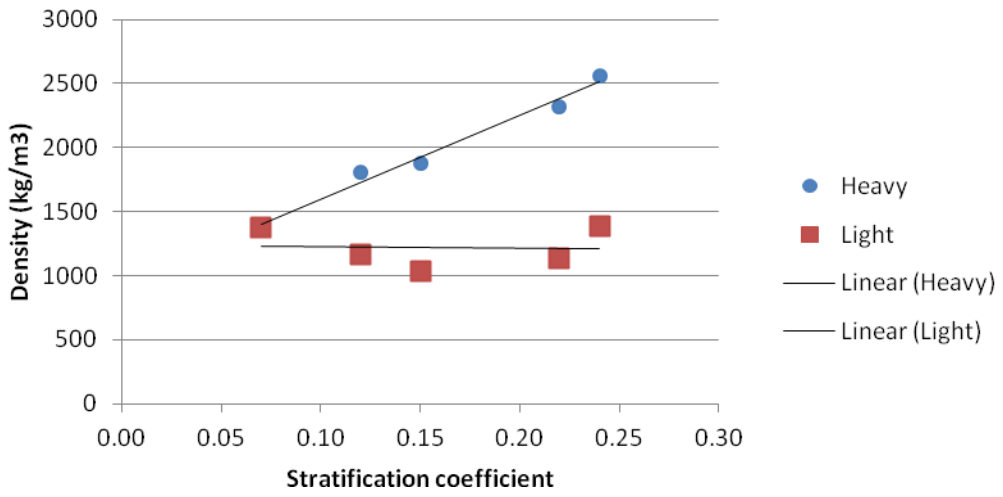

Figure 7.6: Density versus stratification coefficient

A similar trend was found when comparing the compressive strengths of the stratified concrete panels. Here the difference became more noticeable with increased stratification. These results suggest that there may be a stratification level, around 0.20, above which the properties greatly improve. The university panels all showed a very minor difference between the compressive strengths of the heavyweight and lightweight layers where the S3 and O1 panels showed a dramatic difference as the strength of the structural layer increased to a remarkable level, particularly for panel S3. This is shown in Figure 7.7.

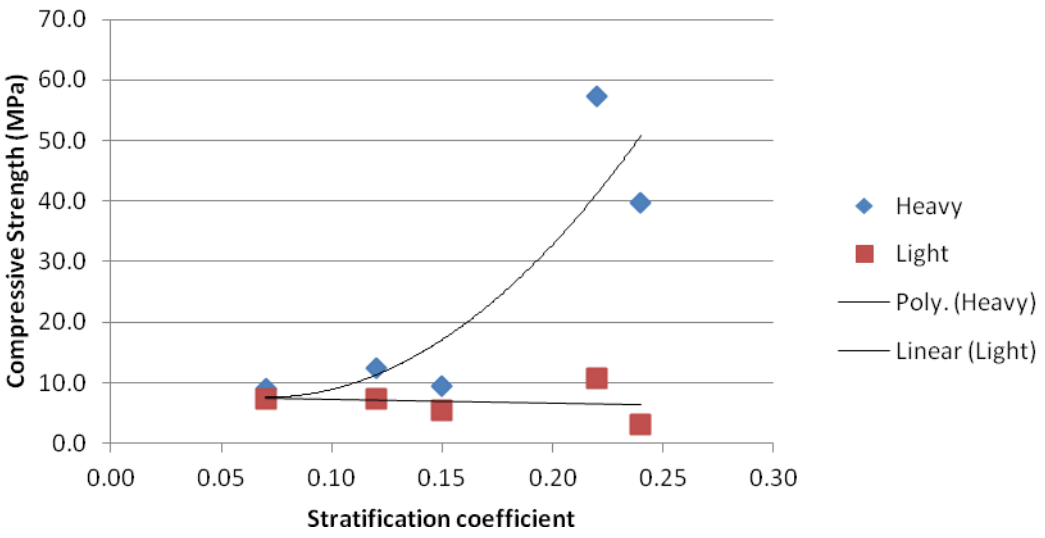

Figure 7.7: Compressive strength versus stratification coefficient

These compressive strength values are more extreme in both directions than previous findings from SCP samples. Earlier research found compressive strengths for Portland cement panels of 9 MPa and 30 MPa, for the lightweight and heavyweight layers respectively, and 12 MPa and 25 MPa for inorganic polymer samples (Mackechnie et al., 2009). Other research on PC SCP showed an average strength for the lightweight layer of just less than 10 MPa and 22.5 MPa for the heavyweight layer. IPC mixes fared worse with 8.5 MPa and 14.5 MPa but this mix design was not ideal (Saevarsdottir, 2008).

The lightweight strengths from previous results compare fairly closely to, although slightly higher than, the values found from this research. The main reason for the relatively low structural strength of the U series panels from this research is the EGB contamination within the structural layer. After the test cubes had been crushed, it was clear that connected paths of lightweight aggregate had initiated the failure in every case before the heavyweight aggregates were even tested, even in panel U3 where relatively small amount of EGB was present. The higher strength of the structural layer in the S3 panel may be attributed to the slightly larger chip used within the well consolidated structural stratum.

When comparing these results with the warping test results (Chapter 6), it was notable that warping did not appear to depend on compressive strength or density in each layer; no curling occurred in any of the panels. For a SCP panel with good stratification, the lightweight layer had very low stiffness relative to the structural layer. This meant that it had the ability to deform in response to any movement that may have resulted from the differential between the two material bands, with no warping occurring overall. Following this logic, it might be expected that a lightweight layer contaminated with heavyweight aggregate, as in a poorly stratified sample, may provide some resistance to bending movement from the structural layer or transition zone resulting in curling of the section. It is clear however, that where stratification was poor, neither layer developed significant strength or stiffness. This meant that there was high creep potential across the section so no great resistance was provided either side of the transition boundary, so stresses that might have caused curling were relieved.

7.3 Axial Compressive Strength

The different samples were tested as columns in axial compression using the Avery model 7104 DCJ machine with 1000 kN capacity. An explanation of each test is given below with experimental results to follow.

7.3.1 U1 Axial Compression Results

Since panel U1 had little stratification, there was no obvious weak point for likely axial load failure. The two tests carried out failed in a similar fashion to each other. The first test sample experienced crushing at the top causing a diagonal strut to form and a large section to fall off as shown in Figure 7.8. The second test failure begun with crushing at the bottom before the same mode of failure occurred. The two test samples reached ultimate strengths of 8.2 and 6.4 MPa respectively.

Figure 7.8: Axial compression failure of panel U1 – test 1

7.3.2 U2 Axial Compression Results

The two tested samples from panel U2 reached different ultimate strengths when tested. During the first test, some cracking occurred at 185 kN. From this point the section gradually deformed as the lightweight layer began to crush and eventually reached an ultimate load of 282 kN (7.4 MPa). The second test specimen reached 130 kN before some cracking occurred. Load was carried however, up to 411 kN (10.8 MPa) before a crack, starting at the transition layer, ripped diagonally through the lightweight layer dislodging a significant section of the panel strip, shown in Figure 7.9.

Figure 7.9: Axial compression failure of panel U2 – test 2

7.3.3 U3 Axial Compression Results

The first U3 test sample failed with a section breaking off after cracks forming at the bottom of the strip traversed to the top of the lightweight layer. After some extensive cracking at 140 kN, this strip eventually failed under 345 kN (9.2 MPa). The second test strip, as shown in Figure 7.10, failed after a crack spanned the height of the column near the top of the lightweight layer. The ultimate load for this strip was one of the lowest at 246 kN (6.6 MPa).

Figure 7.10: Axial compression failure of panel U3 – test2

7.3.4 S3 Axial Compression Results

Two tests were carried on this SCP strip which produced remarkably similar results. Both strips began to lose a small amount of load carrying capacity at around 100 kN as the lightweight layer began to crush progressively. From this point on the lightweight layer continued to gradually deform with small cracks forming and growing. In both cases however, the load was still applied up until around 300 kN (8.2 MPa) before a significant section of the lightweight layer broke off and ripped through the heavyweight layer as shown in Figure 7.11. This value may have been slightly improved with the inclusion of reinforcing mesh, as was used in all other panels and would be used in construction.

Figure 7.11: Axial compression failure of panel S3

7.3.5 O1 Axial Compression Results

Only one strip from this panel was available for testing due to limited material. As this sample had been exposed to the elements for four years, some minor damage was evident before this test was carried out in the form of small hairline cracks across the top of the lightweight layer. This may have been a factor in the relatively low ultimate load of 158 kN (4.2 MPa) under which this strip failed, though the eventual failure mode did not appear to stem from any existing fault. This capacity is notably lower than previously tested laboratory cast panels that reached axial compressive strengths of between 5 and 20 MPa (averaging 9.8 MPa) (Saevarsdottir, 2008). This panel, with the greatest stratification of the tested samples, experienced delamination along the interface between the two strata. As Figure 7.12 shows, a major crack developed from the base and travelled upwards along the boundary while some crushing occurred at the top of the lightweight layer.

Figure 7.12: Axial compression failure of panel O1

7.3.6 Axial Compression Comparisons and Discussion

The values and averages from the axial compressive testing are shown in Table 7-3.

Table 7-3: Axial compressive test results

Panel/test	U1-1	U1-2	U2-1	U2-2	U3-1	U3-2	S3	O1
Depth (mm)	237	181	255	254	252	253	250	240
Breadth (mm)	157	234	150	150	153	147	150	154
Ultimate load (kN)	306	273	282	411	345	246	307	158
Ultimate strength	**8.2**	**6.4**	**7.4**	**10.8**	**9.2**	**6.6**	**8.2**	**4.2**
Average (MPa)	**7.3**		**9.1**		**7.9**		**8.2**	**4.2**

The average axial compressive strengths of each of the tested panels were comparable and within range of each other. The particularly low result from the O1 test may suggest that better stratification can lead to lower axial compressive strength; as there was only one sample available for testing here, this result is not absolutely conclusive, by any means. Furthermore, no such trend continues through the other samples with varying stratification. This can be seen in Figure 7.13 where the panels are in order of increasing stratification. A linear trend line is shown.

The axial strength may be most accurately correlated with the compressive strength of the lightweight layer as this tended to be the critical factor of failure during this test. These values are noted next to the respective axial compressive strength on Figure 7.13 to show how axial strength can be loosely expected to decrease with weaker compressive strength in the lightweight layer.

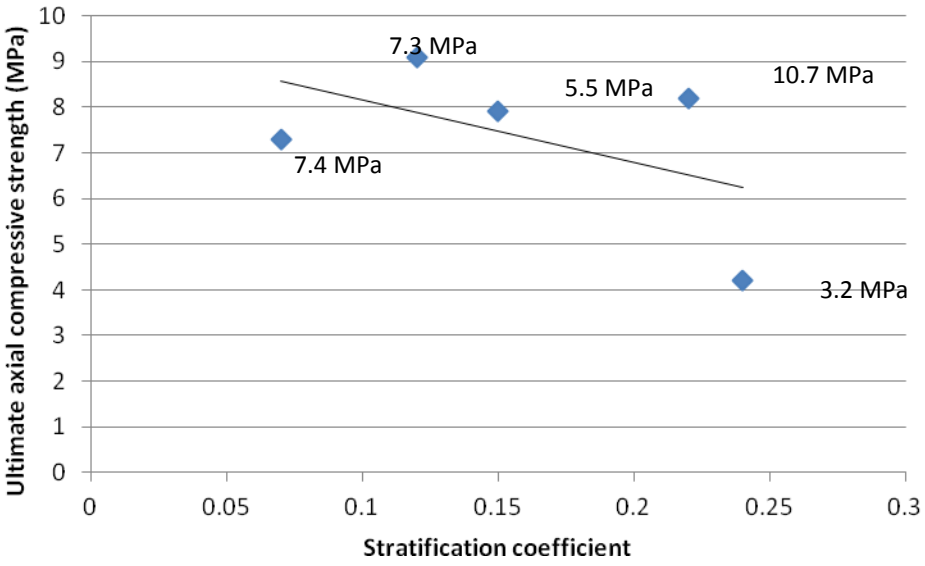

Figure 7.13: Ultimate axial compressive strength for each panel versus stratification coefficient

In all cases, failure resulted from crushing of the lightweight layer which generally occurred in a gradual fashion. The air filled expanded glass beads tended to crush and deform slowly, redistributing the load until such a point when the developing cracks caused a significant loss of cross-section. The only test which included any damage at all to the structural layer was that of the S3 panel; in which there was no reinforcing mesh. Apart from the low result of the O1 panel, a fairly consistent compressive strength of about 8 MPa was achieved. This is lower than results from this test on similar panels in the past that have yielded values ranging from 5.0 MPa up to 19.3 MPa, averaging at 9.8 MPa. This is equivalent to a wall of 144 mm thick for the required 17 MPa for residential building (Saevarsdottir, 2008). The results from this research, with an average axial compressive strength of 8.1 MPa (excluding the outlying low result of O1), equate to a wall of 119 mm thick at 17 MPa.

7.4 Flexural Tensile Strength and Displacement

7.4.1 U1 Flexural Results

Test beam 1 failed gradually and demonstrated an unzipping phenomenon along a paste layer above the beginnings of a small structural layer. The stiffness of the beam decreased steadily from the initial cracking at 0.37 mm deflection under a load of 13.3 kN, up to ultimate failure at 1.73 mm under 30.9 kN (2.6 MPa) as shown in Figure 7.15. The steel yielded so failure was ductile. Eventually unzipping along the paste interface caused a section to delaminate as shown in Figure 7.14.

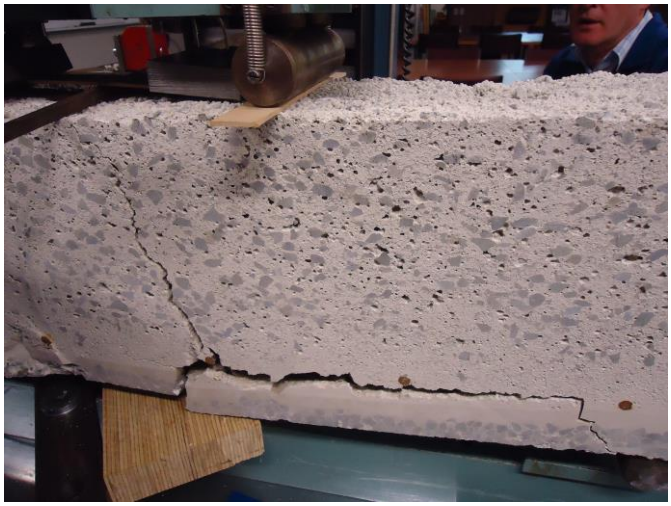

Figure 7.14: Beam U1 flexural failure - test 1

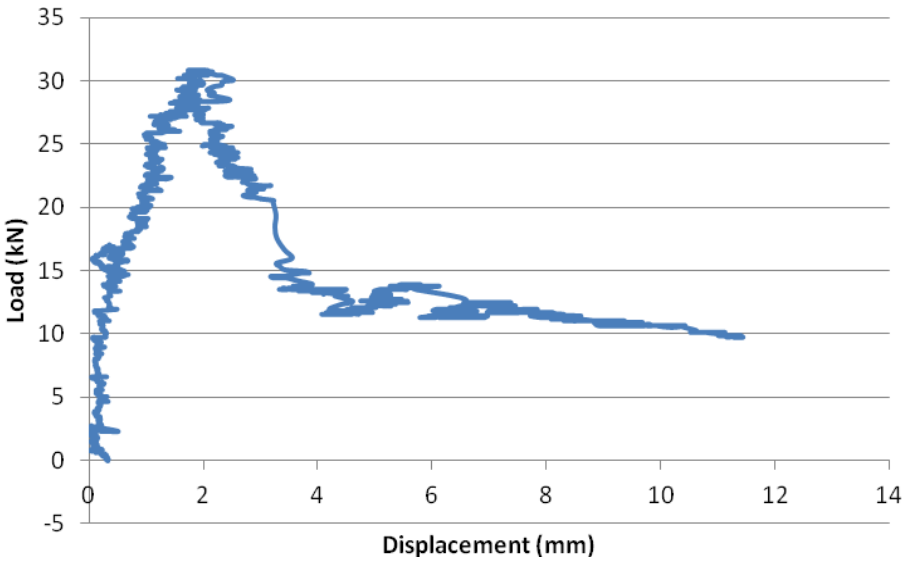

Figure 7.15: Load versus displacement from flexural test for U1 beam - test 1

The second U1 flexural test demonstrated a similar load-displacement shape as the first test, although both first crack and ultimate loads were found to be greater in this test. Gradual stiffness reduction was measured after first cracking at 0.55 mm under a load of 17.7 kN. The ultimate load of 42.0 kN was reached at 2.79 mm giving an ultimate strength of 3.6 MPa. The crack shown in Figure 7.16 occurred slightly to one side of the centre of the beam. A fine crack of similar angle had begun to form in the opposite direction as may be expected from this loading procedure. This was the first flexural test carried out during which fine tuning of the measurement technique was made. As the balance between the two potentiometers was extremely inconsistent, the load-displacement plot was consequently unsteady leading to a irregular load-displacement curve. This problem was fixed before any other tests were carried out.

As shown in Figure 7.16, this beam included an extra half bar of mesh on the side meaning that the effective contribution of the steel in this section was greater than that of the other beams which only had one piece of longitudinal reinforcement. This would partly explain the greater strength achieved in this test.

Figure 7.16: Beam U1 flexural failure – test 2

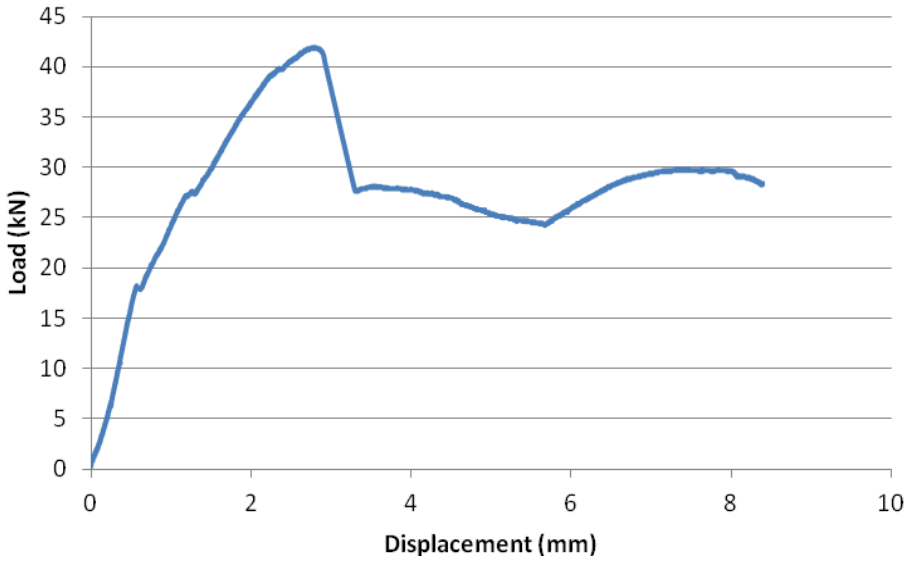

Figure 7.17: Load versus displacement from flexural test for U1 beam - test 2

7.4.2 U2 Flexural Results

The first test of the U2 beams displayed some ongoing stiffness adjustments as the lightweight material began to crush and deform, whilst maintaining some structural integrity. After cracking under a load of 13.0 kN at a displacement of 0.48 mm, the beam eventually reached an ultimate strength of 2.8 MPa from a load of 32.8 kN at a deflection of 3.19 mm. At this point, sudden brittle failure occurred as the steel fractured resulting in a large chunk of concrete spalling off the beam along an angled crack under the loading foot as shown in Figure 7.18. Figure 7.19 shows the changing stiffness and brittle failure.

Figure 7.18: Beam U2 flexural failure – test 1

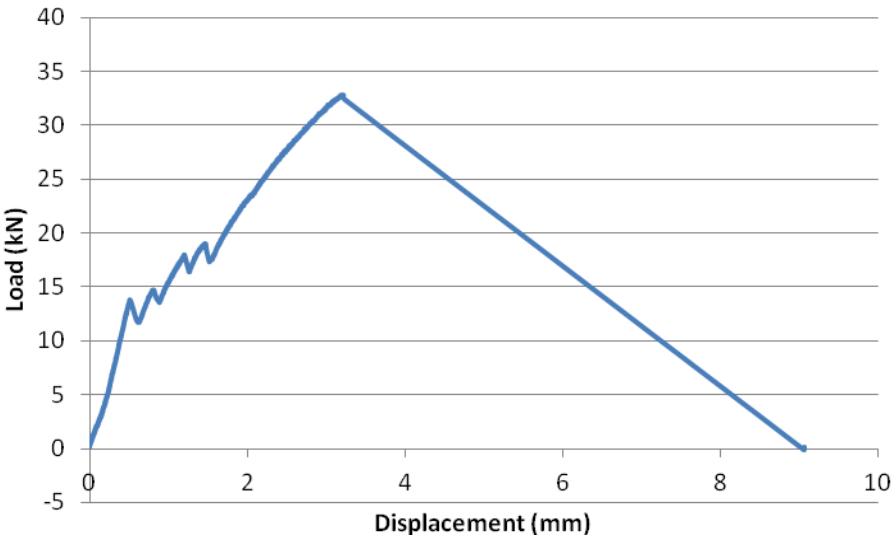

Figure 7.19: Load versus displacement from flexural test for U2 beam - test1

The second U2 flexural test displayed very gradual stiffness reduction. The relatively low first cracking load of 8.6 kN, at a displacement of 0.38 mm, was followed by several small slips where

the lightweight material deformed, shown in Figure 7.21. Eventually, at 7.0 mm under a load of 28.0 kN, the beam reached its ultimate strength of 2.4 MPa before the steel yielded and the member failed in a ductile manner. Two major cracks formed under one of the load footings, one almost vertical while the more critical one was down towards the base footing as can seen in Figure 7.20.

As the steel yielded during this second test, the performance of this beam was much more ductile than in test 1 during which the steel snapped causing brittle failure. This could be due the specific placement of the steel within the section such that bond slippage could occur allowing the steel to yield over a greater length with less concentrated stresses than in test 1.

Figure 7.20: Beam U2 flexural failure – test2

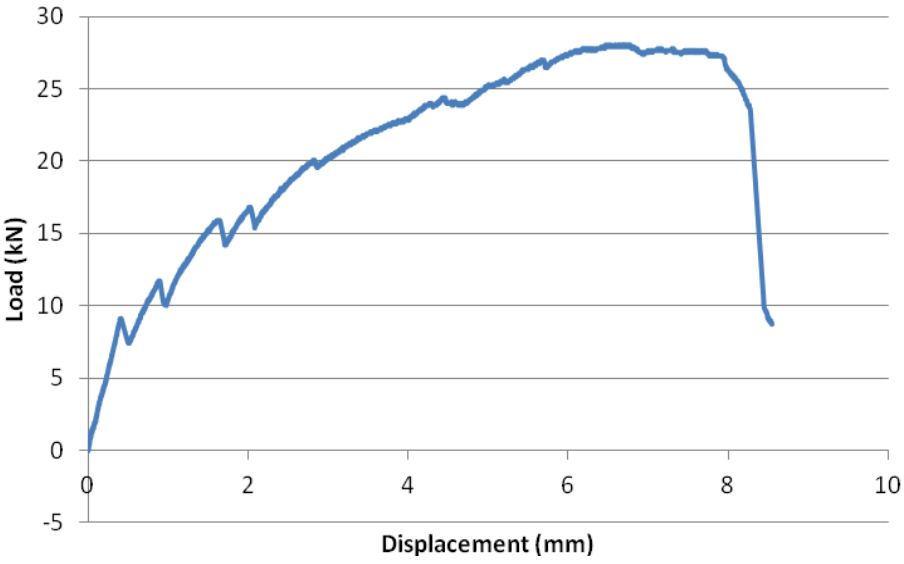

Figure 7.21: Load versus displacement from flexural test for U2 beam - test 2

7.4.3 U3 Flexural Results

The first test for the U3 panel also showed signs of lightweight material crushing as the stiffness began to drop after the first cracking point at 0.47 mm under a load of 9.9 kN. As shown in Figure 7.23, this beam reached a relatively large displacement, demonstrating ductility, until sudden failure when the steel fractured at 7.58 mm under loading of 25.8 kN. Figure 7.22 shows the major crack which was almost directly vertical down from the footing where some concrete spalled as the steel fractured.

Figure 7.22: Beam U3 flexural failure – test 1

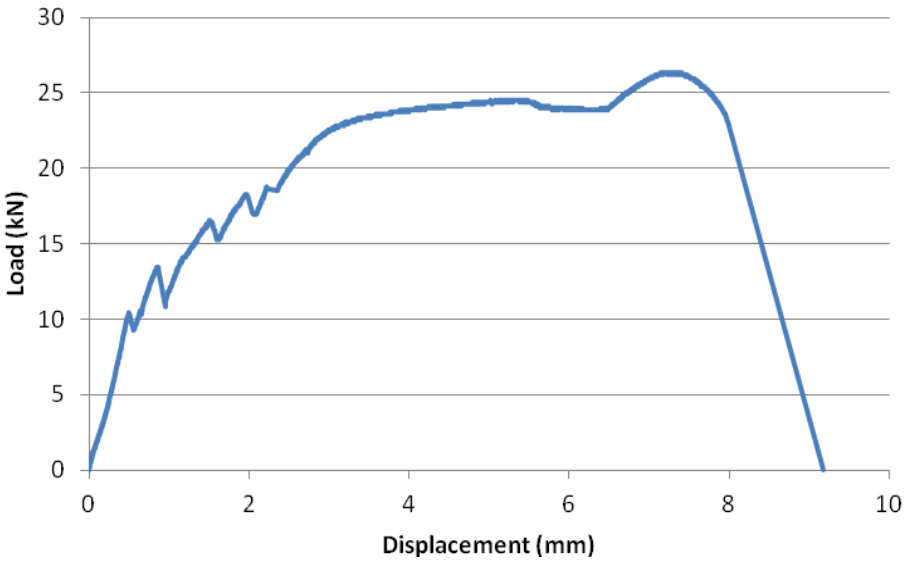

Figure 7.23: Load versus displacement from flexural test for U3 beam - test 1

The second U3 test displayed similar performance to the first with gradual stiffness reduction and some ductility before failure, as Figure 7.25 displays. The failure mode itself was again a result of a near vertical crack under the footing, although as Figure 7.24 shows, another crack closer to the centre had also formed and had begun to open up. This beam reached first cracking at 0.45 mm under a 10.9 kN load and ultimate strength of 2.4 MPa after displacement of 5.47 mm and loading of 30.2 kN.

Figure 7.24: Beam U3 flexural failure – test 2

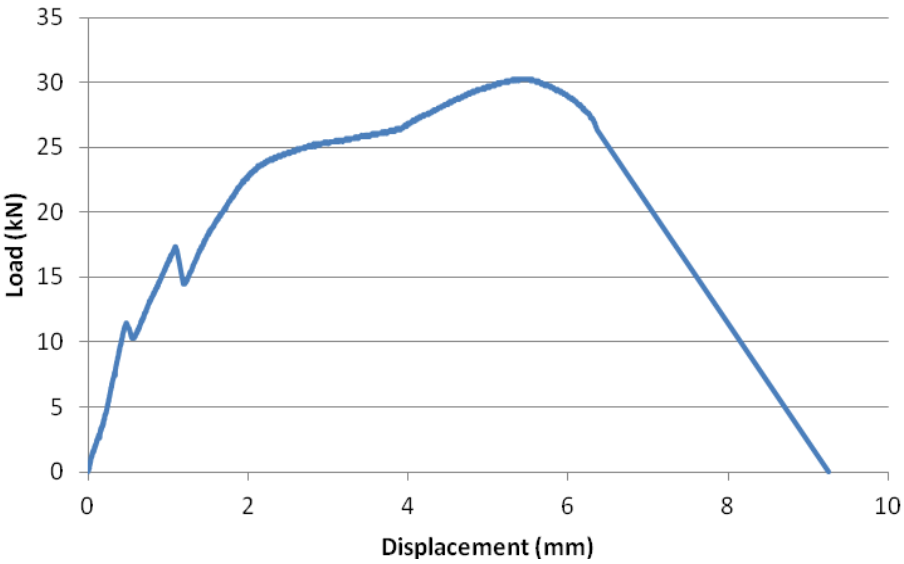

Figure 7.25: Load versus displacement from flexural test for U3 beam - test 2

7.4.4 S3 Flexural Results

S3 was created early in the development process and therefore had no mesh. A flexural test was therefore not possible for this panel.

7.4.5 O1 Flexural Results

Panel O1 demonstrated a relatively stiff elastic modulus. Although some very small cracks developed under a load of about 15 kN (1.4 MPa), the stiffness deterioration was minimal before the ultimate capacity of 3.4 MPa was reached. The concrete then cracked suddenly under the 36 kN load at a displacement of 1.6 mm, shown in Figure 7.27. Some further load was carried by the steel after the initial significant cracking, before strain softening and then sudden brittle failure. As Figure 7.26 shows, the line of failure angled down from one of the top loading points outwards.

Figure 7.26: Beam O1 flexural failure - test 1

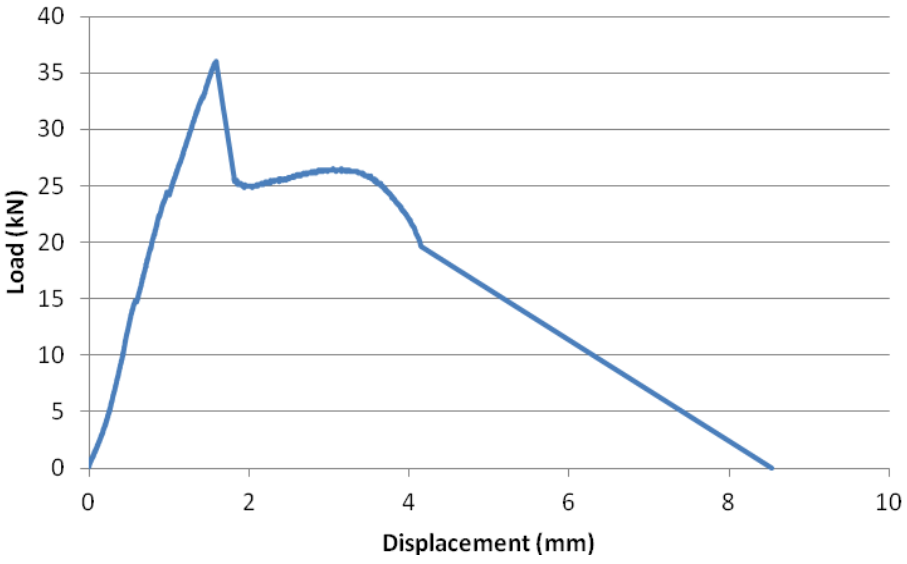

Figure 7.27: Load versus displacement from flexural test for O1 beam

7.4.6 Flexural Comparisons and Discussion

The values and averages from the flexural tests are shown in Table 7-4.

Table 7-4: Flexural test resutls and averages

Panel/test	U1-1	U1-2	U2-1	U2-2	U3-1	U3-2	O1
Depth (mm)	238	243	251	250	255	255	246
Breadth (mm)	171	163	152	152	160	157	159
First crack load (kN)	13.3	17.7	13.0	8.6	9.9	10.9	14.5
First crack displacement (mm)	0.37	0.55	0.48	0.38	0.47	0.45	0.56
Ultimate load (kN)	30.9	42.0	32.8	28.0	26.3	30.2	36.1
Ultimate displacement (mm)	1.73	2.79	3.19	6.52	7.27	5.47	1.59
First crack strength (MPa)	1.2	1.6	1.2	0.8	0.8	1.0	1.2
Ultimate strength (MPa)	**2.6**	**3.6**	**2.8**	**2.4**	**2.2**	**2.4**	**3.2**
Average (MPa)	**3.1**		**2.6**		**2.3**		**3.2**

Figure 7.28 compares the first cracking and ultimate strengths of the tested panels. Both series show the same trend with decreasing strength with improved stratification for the university panels, but a stronger performance from the older panel bucked the trend. The relatively good flexural performance of the O1 panel may have been as a result of the more densified structural layer; fewer expanded glass beads amongst the heavyweight aggregates results in minimal weak failure regions. It is worth considering that the compressive strength of the O1 structural layer was significantly greater than any of the U panels. This may have also been influenced by the slightly different materials used in the O1 panel.

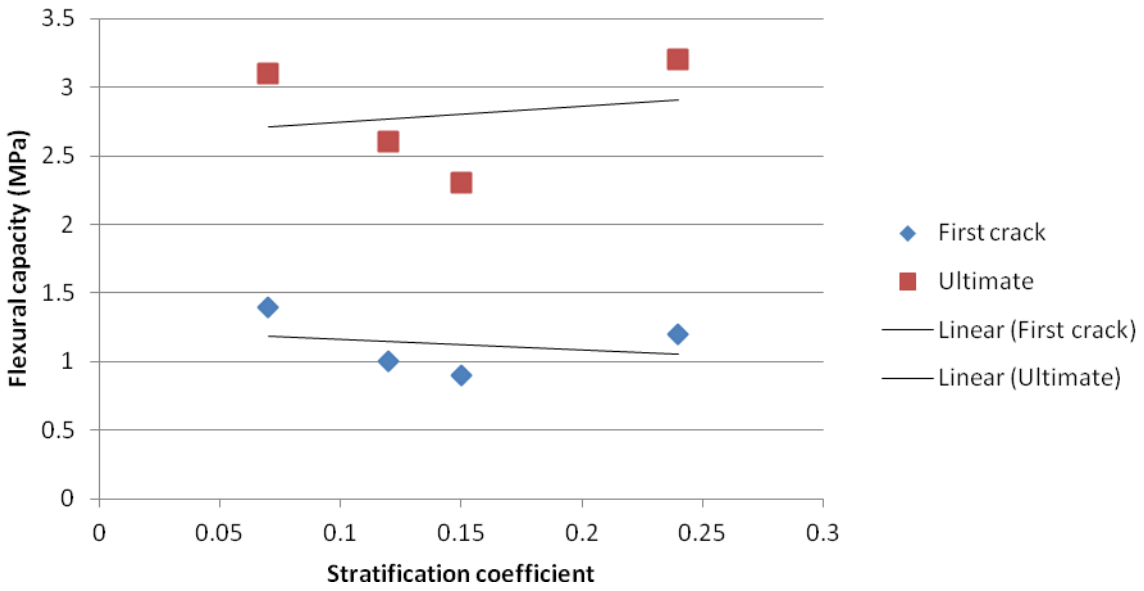

Figure 7.28: First cracking and ultimate flexural strength versus stratification coefficient

Most beams, when tested in flexure, exhibited a crack developing under the top loading foot and travelling diagonally outwards in the rough direction of the bottom support. Against expectation, very little crushing of the soft top layer occurred. In some cases this was due to some extra strength

provided by the greywacke aggregate caught on the top surface increasing the resistance to cracking.

The performance here was weaker than past results where an average first crack flexural strength of 2.3 MPa was measured and an ultimate flexural capacity of 4.3 MPa (Saevarsdottir, 2008). Observations from this work suggest that most strips failed in the middle but there were some exceptions where shear cracking occurred close to the supports. Tests carried out by Bateman show that all flexural tests ended with shear failure (Bateman, 2008).

7.5 Direct Tension (Pull Apart) Test

Each of the samples was tested in axial tension using the Avery 7109 DCJ machine. Three tests were completed for each of the different panels, the results of which are outlined below.

7.5.1 U1 Direct Tension Results

These three cores all failed under fairly similar tensile forces. As there was no distinct transition for this panel, no obvious likely point of failure existed so eventual failure could feasibly occur at any point as can be seen in Figure 7.29 where there is no concordance between failure planes. However, as the degree of stratification was so irregular through this panel, a paste layer had formed in parts. This is particularly noticeable in sample b here, where a paste layer of approximately 15 mm was responsible for the slightly lower tensile failure of this core. Though this layer could certainly not be described as a boundary between two different strata, the lack of aggregate in this region encouraged weaker performance.

3.85 kN 3.00 kN 4.10 kN

Figure 7.29: Tension failure of the three U1 panel core samples; a, b and c

7.5.2 U2 Direct Tension Results

Though this panel was more stratified than the previous, there was no significant transition layer forming between the two forming strata. As Figure 7.30 shows, none of the samples failed in between the two layers, but higher up in the lightweight phase. It is perhaps for this reason that the tensile failure loads for this sample were consistently greater than all the other tested panels.

6.55 kN 6.20 kN 6.10 kN

Figure 7.30: Tension failure of the three U2 panel core samples a, b and c

7.5.3 U3 Direct Tension Results

Stratified further still than the last panel, the tensile capacity of the samples from the U3 panel were still not governed by a transition layer. As Figure 7.31 shows, again all the samples failed in the upper part of the core. The tensile capacity of each of these cores was consistently high in comparison to most samples, slightly lower only than the U2 panel.

5.55 kN 5.00 kN 5.90 kN

Figure 7.31: Tension failure of the three U3 panel core samples a, b and c

7.5.4 S3 Direct Tension Results

Two of these samples, b and c, were consistent with each other showing resistance to tensile failure in the same range as the U series panels. As Figure 7.32 shows, this did not necessarily occur exactly at the interface but higher up in the lightweight layer. The other test, a, broke under a very low loading seemingly against the trend for this panel, so could be considered an outlier for this sample.

1.00 kN 5.08 kN 5.81 kN

Figure 7.32: Tension failure of the three S3 panel core samples; a, b and c

7.5.5 O1 Direct Tension Results

The three different results for this test were reasonably consistent with all samples delaminating under relatively low tensile loads. Figure 7.33 shows how two samples, b and c, broke in the middle of the lightweight layer, not necessarily therefore governed by the interface between the two strata as might have been expected. Sample a however, did fail in the transition phase though not at a lower load than the other samples.

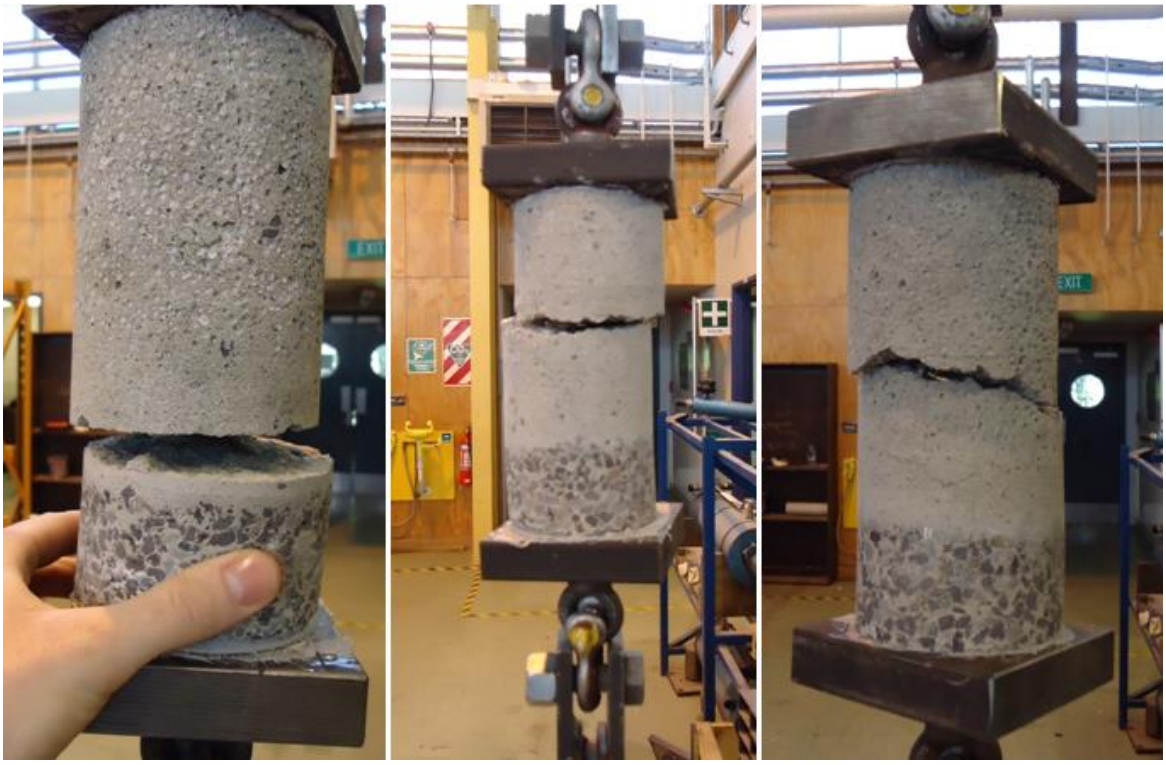

1.15 kN 1.46 kN 0.50 kN

Figure 7.33: Tension failure of the three O1 core samples; a, b and c

7.5.6 Direct Tensile Comparisons and Discussion

The values and averages from the direct tension testing are shown in Table 7-5.

Table 7-5: Direct tension test results

Panel	Test 1		Test 2		Test 3		Average	
	Load	Strength	Load	Strength	Load	Strength	Load	Strength
U1	*3.85*	0.61	*3.00*	0.47	*4.10*	0.64	*3.65*	0.57
U2	*6.55*	1.03	*6.20*	0.97	*6.10*	0.96	*6.28*	0.99
U3	*5.55*	0.87	*5.00*	0.79	*5.90*	0.93	*5.48*	0.86
S3	*1.00*	0.16	*5.08*	0.80	*5.81*	0.91	*3.96*	0.62
O1	*1.15*	0.18	*1.46*	0.23	*0.50*	0.08	*1.04*	0.16

As expected, the tensile strength was very small for all samples, with a maximum value from all the tests of just over 1 MPa. The linear trend line shown in Figure 7.34 does not suggest that any direct correlation exist, but when the result from the almost completely non-stratified panel U1 is excluded, there is a correlation between the degree stratification and the tensile capacity of the panel. As Figure 7.34 shows, the load carried during the direct tension test dropped off considerably as the stratification was increased. This suggests that the tensile capacity is a function of the stratification.

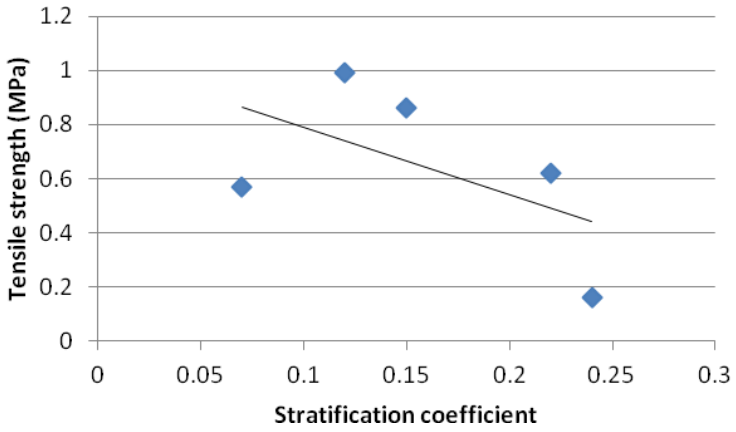

Figure 7.34: Ultimate tensile capacity for each panel from direct tension testing versus stratification coefficient

Of particular interest from this test was the role of the transition phase between the lightweight and heavyweight layers. As predicted, the tensile failures of the samples with minimal to moderate stratification were not governed by this boundary. This though, was also true of the more stratified samples with only one core from the O1 panel breaking in the transition region. This provides evidence to suggest that the transition layer does not play a role unless stratification is well defined, and even then it is certainly not the overriding critical aspect. Bateman found a similar trend with all samples failing in the mid to high lightweight layer, not in the transition phase (Bateman, 2008).

It is again noteworthy that a very approximate correlation exists between the tensile strength from this test and the compressive strength of the lightweight layer. Though this correlation is not as strong as for the axial compression results, there is a tendency towards reduced tensile capacity with a weaker lightweight layer.

Past research using this direct tension test has shown a decline in tensile strength with age. The NZ Inorganic polymer sample dropped from 0.5 MPa at 28 days to 0.3 MPa after 18 months while the IPAS (cast in two separate layers) fell from 0.3 MPa to less than 0.1 MPa. Of greatest interest are the Portland cement samples which dropped from 0.95 MPa down to 0.5 MPa over an 18 month period (Mackechnie et al., 2009). As the samples used in these past tests were from the same batch as the O1 panel used in this research, the results here can be used to further examine the time effects on the tensile capacity. Figure 7.35 shows a notably diminishing trend in tensile strength with time.

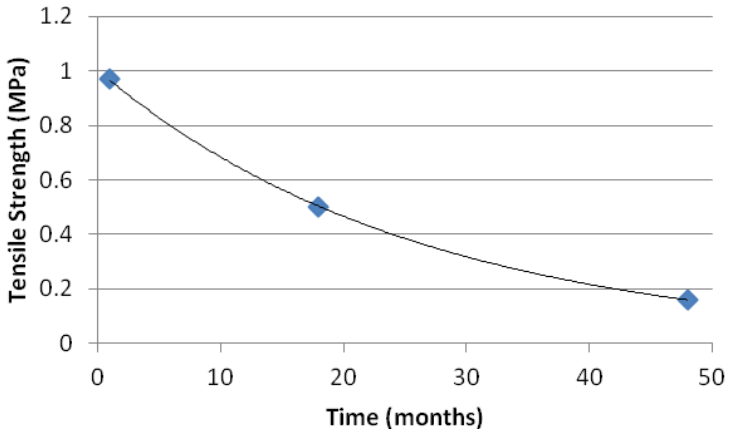

Figure 7.35: Tensile capacity from direct tension test versus time

This tensile strength deterioration with time may be due to several factors. It is possible that the stiffness mismatch between the hardened cement paste and the expanded glass beads that has been exacerbated over time. Though the material has high creep capabilities to redistribute some of the stress caused by this, areas of high stress concentration may provide the basis for micro-cracking, weakening the connection of the paste to the EGB throughout the lightweight section. The bond to the EGB might also have been weakened by alkali-silica reaction. Although this should not occur with fly ash in the concrete, it could occur locally on the EGB surface, further weakening the connection. The broader implications of this may advocate that the section will eventually hold almost no strength such that tensile failure by delamination between the two layers could occur.

It must be clarified however, that these panels, from which the O1 test samples came, were stratified to the maximum tolerable level such that a very clear transition existed between the two aggregate strata. This means the almost over-vibrated panel had an inbuilt defect and very little resistance to tensile stress perpendicular to the layering. This does not necessarily suggest that lesser stratification would improve tensile strength however, as not all the older samples failed in the transition region.

A potential partial solution for this is to more carefully monitor the stratification of the panels during vibration such that a transition layer of such thickness is not able to form so that some aggregate interlock exists between the layers. Using fibres within the mix or mechanical inserts such as solar tubes in the panel may also help provide extra tensile strength in the weaker areas.

7.6 Thermal Hotdisk Test

The hotdisk thermal analyser was used to measure the thermal properties of the different SCP samples. For each of the five samples, three 90 mm cores were tested for thermal conductivity, thermal diffusivity and specific heat. Readings were taken from the heavyweight layer, the transition layer and the upper and lower lightweight layers. From this, average results were taken and are shown in Figure 7.36 and Figure 7.37 where 1 represents the heavyweight layer through to 4 as the upper lightweight layer. Further numerical data from this test can be found in Appendix 2.

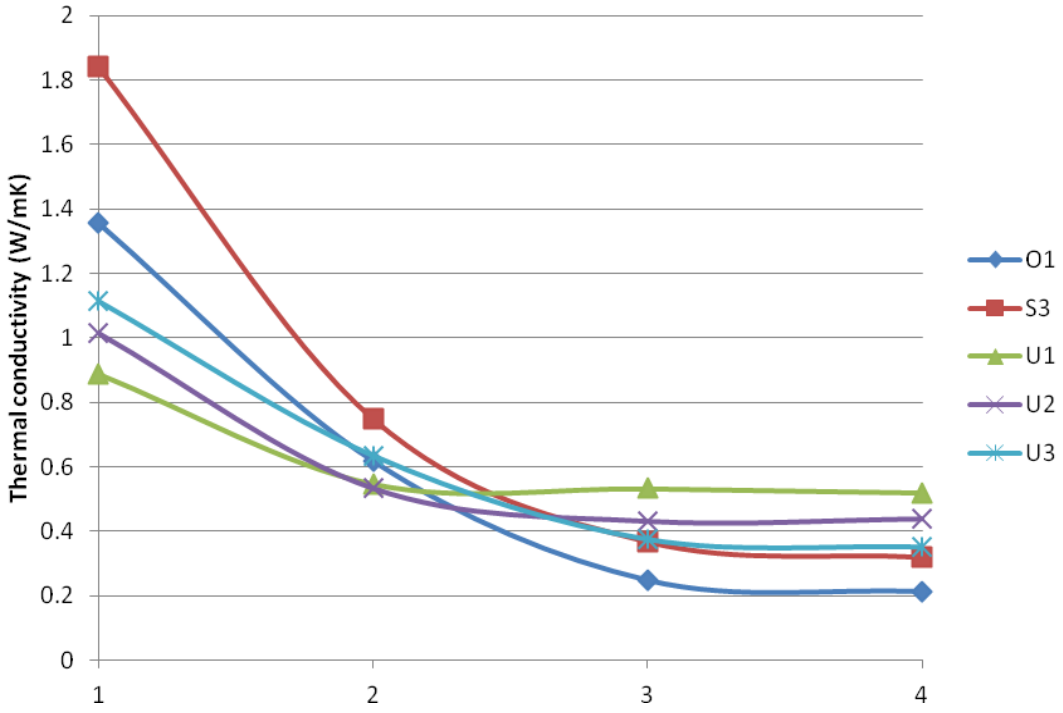

Figure 7.36: Average thermal conductivity for the SCP samples

This figure shows that the thermal conductivity of O1 was significantly lower in the lightweight section compared with the other panels. This was a result of the uncontaminated insulating stratum. As the other panels, in contrast to O1, all demonstrated some degree of thermal bridging through aggregate caught in the insulating layer, their respective insulating abilities were reduced.

As the stratification of S3 was better than that of the U series panels, it demonstrated much greater thermal conductivity in the structural layer. This is because the aggregates were more closely packed so the thermal resistance was much less. By extension, the relatively low heavyweight aggregate content in the insulating layer of S3 explains why it had lower thermal conductivity than the U series panels in the lightweight region.

Each of the U series panels had a smaller range of thermal conductivity over the depth of the panel; less in the structural layer and more in the insulating layer, than both O1 and S3. This was not surprising when considering the lower level of stratification in the U series panels. The more uniform distribution of both heavyweight aggregates and lightweight EGB meant that thermal bridging could occur throughout the depth of the panel while a minimal amount of thermal

resistance was provided in all areas too. This severely reduced the overall thermal performance relative to the more stratified O1 and S3.

Similar observations can be made when comparing the specific heat performances of the panels. As Figure 7.37 shows, the U series panels had flatter specific heat curves, particularly U1 and U2. This meant that, due to the lesser stratification of these panels, the more homogenous material did not exercise much variance throughout the section. Whereas the more stratified panels had more concentrated regions of both heavyweight and lightweight aggregates so the respective higher and lower heat capacities were more evident across the depth of the panel. Where stratification is poor therefore, SCP does not reach the required level of either thermal mass or insulation.

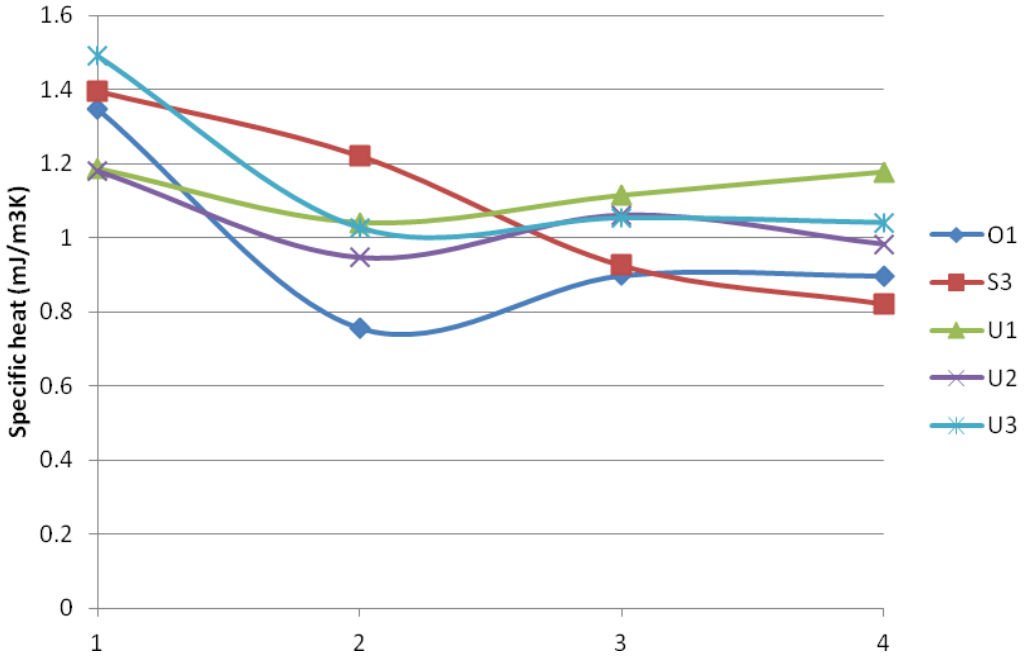

Figure 7.37: Average specific heat for the SCP samples

Table 7-6 shows the calculated R-values using an average of the four readings from each core. These values do not include exterior and interior resistances, of 0.03 and 0.09 m^2K/W respectively, that are usually added. As expected, there is a correlation between stratification coefficient and R-value. This trend appears to be skewed from a linear regression in the higher ranges so a second order polynomial trend line is used as shown graphically in Figure 7.38.

Table 7-6: Calculated R-values for the different SCP panels

Panel	Average Total Thermal Resistance (R-Value) (m^2K/W)
U1	0.36
U2	0.40
U3	0.42
S3	0.55
O1	0.89

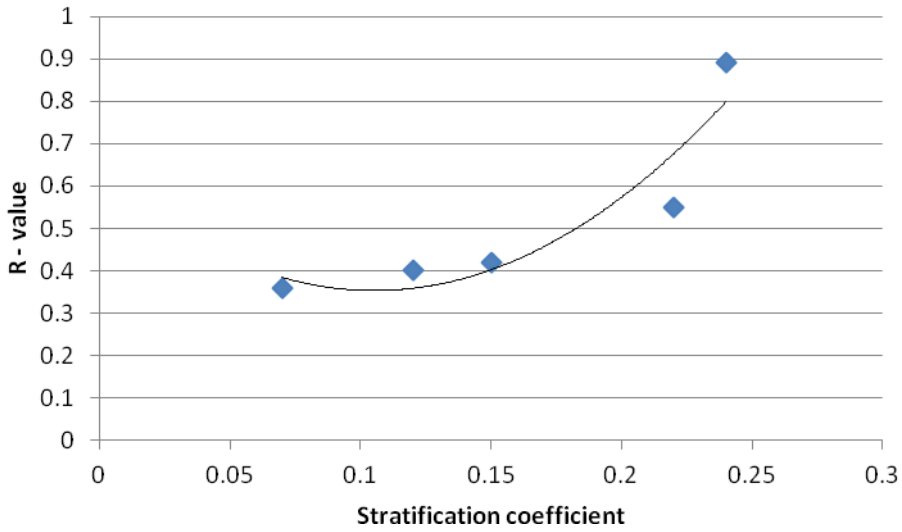

Figure 7.38: Total thermal resistance (R-values) versus stratification coefficient

Generally the SCP thermal targets were not met for these panels. This sensitivity test suggests however, that with a small increase in stratification, beyond a critical point of around 0.2, the R-value should dramatically increase. This means that where stratification is greater, more heavyweight aggregate, with high thermal conductivity, will be concentrated in the structural layer leaving the lightweight layer with little (or no) heavyweight aggregate contamination. A thicker, clearer lightweight layer containing no heavyweight aggregates will have very low thermal conductivity, notably reducing the R-value for the panel. Where sufficient stratification is attained, the required R-values are within reach.

Past work has achieved thermal conductivity values as low as 0.2 in the insulating layer. From this, static R-values of 0.8 – 1.0 m^2K/W were achieved (Mackechnie et al., 2009). Panels tested by Saevarsdottir reached similarly high values (Saevarsdottir, 2008), as is evident with the performance of panel O1 here. These values are close to meeting the requirements for sufficient performance for effective use in buildings. Work by Bellamy and Mackechnie quantified the dynamic R-values for a more realistic measure of service performance. From this research, much greater R-values of up to 2.55 m^2K/W were measured with similar SCP panels exposed to fluctuating external temperature and solar radiation (Bellamy and Mackechnie, 2010).

7.7 Water Sorptivity Test

From each panel, three cores were taken and cut into 6 slices of approximately 25 mm. In the following tables, slice 1 represents the bottom of the core, which is the heavyweight layer, through to slice 6 as the top lightweight layer. The average sorptivity and porosity values from the five panel samples are shown below in Table 7-7 and Table 7-8. All panels showed increasing porosity from the denser layer (slice 1) up to the lighter layers. As expected, this trend was more marked in the panels with greater stratification; panel U1 showed a range of only 14.7 % from slice 1 to slice 6 where panel O1 had a range of 33.8 %.

The sorptivity of the samples did not display any discernible pattern in relation to the level of stratification. This is because the measurement is skewed where large voids are not as absorptive as smaller ones, due to capillary action, so take longer to fill. Further information on water mass accumulation from these tests is given in Appendix 3.

Table 7-7: Average measured sorptivity

	Panel U1	Panel U2	Panel U3	Panel S3	Panel O1
Slice 1	2.60	1.51	0.92	6.51	2.38
Slice 2	4.55	1.26	1.18	5.37	6.58
Slice 3	2.81	1.10	0.90	4.36	4.62
Slice 4	2.73	1.27	1.23	2.23	5.61
Slice 5	2.89	1.23	1.09	1.95	4.17
Slice 6	2.74	1.28	1.14	2.58	4.82

Table 7-8: Average measured porosity

	Panel U1	Panel U2	Panel U3	Panel S3	Panel O1
Slice 1	22.0	28.4	26.9	10.2	17.6
Slice 2	33.7	31.7	28.8	10.7	15.3
Slice 3	41.4	41.6	38.9	18.1	48.3
Slice 4	40.2	48.9	47.1	31.6	50.2
Slice 5	36.3	49.6	48.8	35.4	51.9
Slice 6	36.7	41.1	45.7	35.5	51.4

Figure 7.39 and Figure 7.40 respectively show the average sorptivity and average porosity for the five different samples from the heavyweight layer up to the lightweight layer.

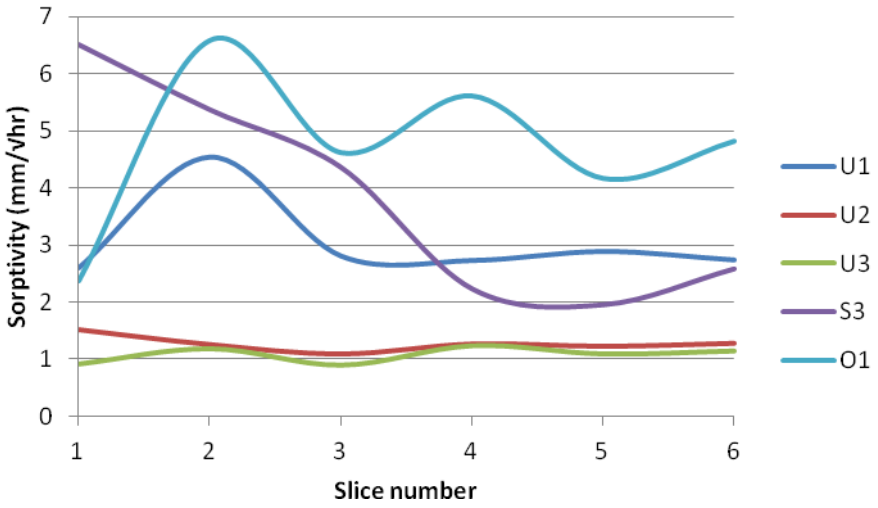

Figure 7.39: Sorptivity versus depth of panel

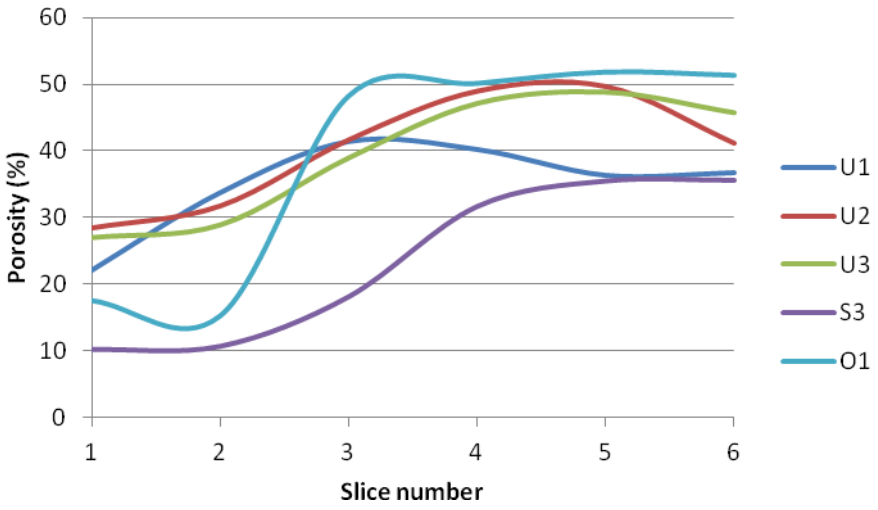

Figure 7.40: Average porosity versus depth of SCP

Figure 7.40 gives a visual representation of the effectiveness of sufficient stratification; the O1 and S3 panels span a wider range between the two extremes of porosity than do the university panels. Improved stratification increases the concentration of heavyweight aggregates in the structural layer, resulting in greater absorption and abrasion resistance. Where stratification was poor here, lightweight aggregates got caught in the structural layer which increased the porosity.

Porosity values of SCP were found to range from 10 – 50 % within the material in the past (Mackechnie et al., 2008) (Saevarsdottir, 2008). This correlates exactly to the range found here. This is considerably higher and more variable than porosity in structural concrete, which generally has values below 15%. Stratified concrete is not intended for structural applications however, since good thermal performance can only be achieved using a high porosity, low density material.

8 CONCLUSIONS AND RECOMMENDATIONS

8.1 SCP Development and Potential Adoption

Stratified concrete was initially conceived as a way of achieving high levels of insulation without unduly compromising the thermal mass of a concrete panel, cast from a single mix. While the concept was developed to optimise processing and thermal performance for residential applications, the added benefits of utilising waste materials were soon realised. Conceptually, the idea of SCP is relatively simple although it does require significant changes in materials, processing and analysis of performance.

Funding and development of a laboratory solution for SCP has been undertaken over the last eight years at the University of Canterbury. Park investigated a wide range of concrete mixes and defined optimum rheological ranges for controlled segregation of concrete (Park, 2006). Further development by Saevarsdottir characterised the properties of SCP produced under laboratory conditions, using mostly waste materials (Saevarsdottir, 2008). Full thickness SCP were then produced in the laboratory and exposed to Christchurch weather conditions for several years in a solar laboratory. This research was able to show the thermal benefits of SCP under fluctuating environmental conditions and the advantage over normal lightweight walls (Mackechnie and Bellamy, 2011).

Research outlined in this thesis focused on the feasibility of reproducing SCP under normal industrial conditions. From this industrial trial, the following limitations of this industrial trial were found:

- Some of the materials selected were mostly sub-optimal and were chosen for local availability and reasonable cost.
- No significant investment in resources was possible by the precast concrete company since this collaboration was undertaken as a free trial.
- Enthusiasm for the project was found to diminish from senior management downwards and interest waned as the trials continued and became more technically challenging.
- Limited time, resources and materials meant that there was pressure to reach an outcome regardless of some technical deficiencies.

With any new technology, market acceptance is always difficult to gain. As this new development is particularly unusual in terms of building materials and processing, it may be met with resistance from the conservative nature of the building and construction industry. Successful innovation is generally a compromise between product effectiveness and ease of adoption. Rogers showed there are five main factors that influence successful adoption of innovations. These are briefly considered within the building and construction fields to illustrate the challenges that would need to be overcome (Rogers, 1995):

- Relative advantage of SCP over other competing systems is difficult to quantify accurately and thermal performance may show little advantage when assessed under steady state conditions.
- Compatibility of SCP with current construction is not high as there would need to be significant changes in materials and processing.
- Complexity is not significantly different in terms of production but would require some training and development of simple control measures.
- Trialability of building products is difficult to undertake since it involves fairly large costs and financial risk.
- Visibility of the results of building product innovation is low unless well marketed.

Adoption of SCP in New Zealand is also dependent on several local factors:

- Public perception about concrete being a cold material in a country exposed to a mostly cold climate.
- Concrete considered to be inherently brittle and heavy in a seismically-active land.
- Statutory changes such as carbon taxation, building insulation and seismic standards are likely to influence the building industry in the future.
- Development of local sources of lightweight aggregates is not well advanced in New Zealand.
- Required shift in focus of precast concrete production from unique engineered products to mass-produced items with dedicated processing equipment.

As Shapira and Rosenfeld discuss, where there is a requirement or 'market-pull', new technology can be created. Establishing a relationship between the university and the industry however, can shift this market-pull to 'technology push'. This means that there is a driving force for industry innovation such that existing technologies readily 'precede the problem' and are ready to implement when so decided by the academia-industry collaboration (Shapira and Rosenfeld, 2011).

8.2 Feasibility of Production Process

The mixing process was carried out using a high shear pan mixer at Stahlton precast concrete yard. The lightweight aggregates and microsilica were added manually with some visual judgement required in the initial stages. Homogenous mixes were consistently created, reaching the required rheological targets with little fine tuning needed. This suggests that the approach to this stage of the SCP casting process is satisfactory using current concrete yard procedure. Most concrete yards are supplied by concrete readymix trucks which was not assessed during this work.

The vibration process was not as successful with several iterations required during these industrial trials. Though in most of the trials there was some indication that stratification was beginning to occur during vibration, acceptable results were difficult to achieve and control in the early trials. The vibrating bed at Stahlton, as for any precast yard, is only designed to lightly compact moderate consistence concrete and certainly not to segregate concrete. With the use of the

vibrating table from the university in the later trials, some consistency was established and moderately well stratified panels could be guaranteed.

The most difficult problem to address before SCP can be consistently and accurately produced is the monitoring of stratification during vibration. The adopted method employed in this work was to use a penetrometer device that would sink into the mix during vibration such that it would rest on the structural layer providing a measure of the depth of this layer. Though this method gave a good estimation of the structural layer depth in most trials, it is rather crude and localised to one particular point. Something more reliable is required for dependable production.

The finish of the panels was poor in most cases as the EGB on the top made it difficult to achieve a smooth surface. Some heavyweight aggregates were left on the surface in the early trials as they got trapped on top of the EGB layer as it began to crust over. In later trials the formwork was slightly overfilled so that the top of heavyweight aggregates could be easily removed leaving a smoother surface. This improved the surface to some degree but not to an acceptable standard for external display in service. This was not a critical consideration or concern for this particular project.

8.3 SCP Properties

Five trials were carried out on the vibrating table at the Stahlton yard during the initial trial process. The resulting stratification from these panels ranged from very poor through to good. Tests were carried out on one of these panels in conjunction with the three panels cast using the university vibrating table and one older panel from previous laboratory production. These tests measured structural, thermal, and durability properties. These panel samples encompassed a range of stratification levels from poor to good so these tests were useful for gauging the sensitivity of these properties to the level of stratification. Table 8-1 shows the worst to best range of values for the properties tested during this project against previously tested laboratory cast panels (Saevarsdottir, 2008, Bateman, 2008, Mackechnie et al., 2009).

Table 8-1: Comparison between laboratory and industry cast SCP panels

Test performed	Laboratory panels [‘07-‘08]	Industry Panels [‘10-‘11]
Axial compressive strength (MPa)	5.4 – 23.5 [11.4]	6.4 – 10.8 [8.1]
Flexural strength (MPa)	1.4 – 4.9 [2.3]	2.2 – 3.6 [2.7]
Tensile strength (MPa)	0.11 – 1.18 [0.57]	0.16 – 1.03 [0.76]
Thermal resistance (R-value)(m^2K/W)	0.4 – 1.0 [0.62]	0.36 – 0.55 [0.43]
Porosity (%) (heavyweight)	10.0 – 29.9 [23.5]	10.2 – 33.7 [24.0]
(lightweight)	23.4 – 53.9 [37.8]	18.1 – 49.6 [40.0]

[ ] indicates average values

These results emphasize the difference between the panels that were well stratified and those that were poorly to moderately stratified. In most cases, as expected, strength was reduced as stratification improved. The axial strength however was greater for the panels with a more concentrated structural layer. The porosity values achieved were similar to those found in past work; that is the structural layer had good absorption resistance but was highly porous due to trapped lightweight material (Saevarsdottir, 2008). The major difference between the laboratory and industry cast panels was in the thermal performance. The total thermal resistance for the well stratified panels was nearly 50 percent better on average with the best performance from the

industry panels only just exceeding some of the worst laboratory results. It was notable that at a stratification coefficient above about 0.20, the thermal properties significantly improved at a non-linear rate. This comes as a result of the contamination of heavyweight aggregates within the insulating layer in the poorly stratified concrete panels; thermal bridging results from this which draws the heat through quicker, significantly reducing thermal resistance.

Some of the performance differences here can be attributed to the larger scale of the industry cast panels with 0.5 m^3 mixes used in this work, up from the 0.4 m^3 of the previous laboratory mix. The 25 percent increase in mass on the vibrating table reduces the vertical travel and therefore the shearing action on the concrete. It is also notable that the materials used in this work were slightly altered from the past laboratory work to represent a more likely industry mix design using materials that are readily available and are well understood by the industry workers.

Another consideration for this project was to assess the potential for larger scale SCP to warp, based on the material differences between the two strata. Past work has suggested that this was unlikely to be a factor (Saevarsdottir, 2008). After two months of exposure to the elements, the full scale SCP panels did not show any signs of warping. This was partially attributed to the ability of the lightweight layer to creep in response to movement from the heavyweight layer, cancelling any bending overall. Where stratification was worse, neither layer possessed any significant stiffness; although each layer could potentially curl in itself, the high creep potential of both layers meant that any overall bending was effectively cancelled out. This dimensional stability was demonstrated to continue into the medium term with measurements from four year old, well stratified panels showing that warping was still not an issue. This suggests that warping is neither a factor of stratification level nor age.

Testing and long-term observations have shown no issues for SCP panels made using Portland cement in terms of efflorescence and discolouration. The long term tests did show that the tensile strength of the well stratified panels diminished with time from the short term to medium term. This will be a concern if the trend continues and the tensile strength eventually tends to zero resulting in imminent delamination in service.

Suitable cover is provided for the reinforcing mesh as it is embedded in the middle of the structural layer; 40 mm of solid cover depth is given on the internal side of the panel with up to 40 mm given on the exterior face plus the remaining 170 mm of insulating layer. Though the structural layer has relatively high porosity for structural concrete, the absorption resistance is sufficient. As the porosity of the exterior layer is also high, environmental factors such as freeze-thaw do not cause concern as expansion within the layer is allowed for.

8.4 Economic Feasibility of SCP

SCP has the potential to be more costly to produce than normal concrete as some of the binders and lightweight aggregates are more expensive than those used in current systems. Table 8-2 shows the SCP material cost per cubic metre at best estimate (Mackechnie, 2011).

One major advantage of SCP production though, is the limited labour component required. As only one mix is batched and then vibrated, the time investment for each panel is less than other thermal panels where one concrete layer must be cast and finished, polystyrene placed, then the final concrete layer cast on top. This reduced labour demand means the overall cost is diminished.

This then means that, although the material cost of SCP is relatively high, especially at this early stage, the overall cost of producing SCP has the potential to be economical.

Table 8-2: SCP material costs

Material	Cost	Quantity	Total Cost
GP Cement	$280/tonne	400 kg	$112.00
Microsilica	$480/tonne	30 kg	$14.40
Aggregate	$20/tonne	555 kg	$11.10
Expanded glass beads	$1300/tonne	155 kg	$201.50
Superplasticiser	$6/litre	1.8 L	$10.80
Total cost/m^3			**$349.80**

Though expanded glass beads are essentially a waste product, the preparation required to make useable beads is expensive. The figure given above for EGB is an average drawn from a range of bulk prices ranging from $800 (2007) to $1800/tonne before shipping costs. Unless EGB is produced locally in the future, $1300/tonne is not a realistic figure for small scale production so SCP will not be competitive with the current market. The current local equivalent would be to use perlite at about $700/tonne. This has similar density but is more difficult in concrete so would most likely need processing in terms of nodulising (Mackechnie, 2011).

Assuming that these figures are achievable in the future, the material costs alone work out at just under $90/$m^2$ for a standard 250 mm thick SCP panel. For SCP to become competitive in the market, this price will have to be reduced to roughly $75/$m^2$ (This is inflated from an estimation of $60/$m^2$ in 2003) (McSaveney, 2003).

More recent figures suggest that basic 150 mm insulating panels currently used in the industry cost approximately $150/$m^2$ including labour costs, about half of which can be attributed to material costs. This concurs with the estimated $75/$m^2$ target for market competition. This style of panel however, does not meet current R-value requirements and must be strapped and lined to do so which incurs extra cost. A similar panel of 200 mm thickness is worth about $200/$m^2$, a price with which SCP can potentially be competitive. These panels, unlike SCP, have the added disadvantage of having thermal mass on the exterior face severely reducing the potential activation of it. At the top end of the range, the superior performance of thermomass panels is worth around $250-300/$m^2$ (Marshall, 2011).

Realistically, for SCP to become established as an industry product, local supply of lightweight material is required. Whether this is in the form of establishing a machine capable of producing EGB or substituting for less preferable but still appropriate perlite aggregates, the cost of SCP will reduce to within a market competitive range.

8.5 Recommendations

To continue work towards commercialising SCP, further research is needed into the vibration energy requirements for accurate and consistent stratification. This requires improving understanding of the frequency and vertical throw needed for sufficient stratification. This could be achieved by characterising the action of the university vibration table with accelerometers and attempting to produce a table of sufficient scale that displays the same action, considering the

weight of the panel to be vibrated. As sufficient power to cause enough vertical shear action for stratification is not generally available from a standard precast yard vibrating table, the easiest way to address this for further experimenting in the short term could be by adding one or more extra vibrating motors to an existing vibrating table.

In the longer term, the most efficient way to produce SCP involves capital investment to set up an assembly line. Here the concrete would be mixed and poured into the formwork before being conveyed onto a vibrating table with sufficient power to stratify one panel. Only one standard panel size would be produced (one storey high) to make the process most efficient with different moulds used where door and window are required in the panels. The panel would then be moved off the vibrating table to harden, leaving room for the next panel to be vibrated.

Of particular importance to this system however, is a means for monitoring the stratification during vibration such that the correct amount of vibration, within a tolerance range, can be reliably provided. This could be achieved using a density probe or other device which reads the change in density as vibration acts.

To optimise the performance of SCP, some substitutions may have to be made for high performance materials such as using fly ash instead of microsilica. This may though add a financial toll; some materials are not as accessible locally and require the concrete workers to work with materials they are not so familiar with. Extra materials may also be required to improve the durability potential of SCP, especially when considering the issue of delamination. A good way to strengthen the boundary between the two strata and improve abrasion resistance would be to use fibres in the mix. Another option would be to insert solar tubes between the heavyweight and lightweight layers for both structural and thermal benefit.

For SCP to gain confidence, or even acceptance in some form, information is required from the point of view of both engineers and the public. To begin to address this, a more robust form of thermal property measurement must be used. This needs to be more objective and less dependent on operator technique. For both technical reasons and the aforementioned public scepticism, static R-values are not an adequate measurement of the total thermal resistance. This measurement is not only potentially inaccurate but the produced values under-estimate the real performance of SCP. Previous work has shown that dynamic R-values are more representative of the true measure of SCP in service as this better considers temperature changes and fluctuations and resistance to this from the panels (Mackechnie and Bellamy, 2011).

The best estimate of the realistic service performance of SCP would be to build a full-scale house using SCP and measure the dynamic R-values over an extended period of time. This would allow the measurements to consider temperature fluctuations with changing weather and environmental effects like sun warmth provided through the windows. Although this would provide an accurate assessment of the total thermal resistance of the panels, it would be a very costly measure to build and monitor.

REFERENCES

ACI 2007. American Concrete Institute, ACI Education Bulletin E1-07: Aggregates for Concrete. *Aggregate properties and test methods.*

ALEXANDER, M. G. & MINDESS, S. 2005. *Aggregates in concrete,* London, Taylor and Francis.

ALONSO, C. & ANDRADE, C. 1994. *Life time of rebars in carbonated concrete: Progress in Understanding and Prevention of Corrosion,* London.

ASGEIRSSON, H. 1994. Helka Pumice in Lightweight Concrete. Reykjavik, Iceland: The Icelandic Building Research Institute.

ASTM 2004. ASTM C1583 / C1583M - 04e1: Standard Test Method for Tensile Strength of Concrete Surfaces and the Bond Strength or Tensile Strength of Concrete Repair and Overlay Materials by Direct Tension (Pull-off Method). West Conshohocken, PA.

ASTM 2006. Standard Test Method for Sieve Analysis of Fine and Coarse Aggregates.

ASTM 2007. ASTM D4580 - 03(2007) Standard Practice for Measuring Delaminations in Concrete Bridge Decks by Sounding. *Road Standards and Paving Standards.* PA, USA.

ASTM 2011. ASTM C469. *Cement Standards and Concrete Standards, Standard Test Method for Static Modulus of Elasticity and Poisson's Ratio of Concrete in Compression.*

BANFILL, P. F. G. 2003. The Rheology of Fresh Cement and Concrete - A Review. *11th International Cement Chemistry Congress.* Durban: School of the Built Environment, Heriot-Watt University, Edinburgh, EH14 4AS, UK.

BASALO, F. J. D. C. Y., MATTA, F. & NANNI, A. 2010. Fiber reinforced cement-based composite for concrete confinement. *Construction and Building Materials*.

BATEMAN, P. 2008. *Delamination of Stratified Concrete Panels.* 3rd Professional Project Report, University of Cantebury.

BELLAMY, L. A. 2010. Concrete Materials ENCI621: Lecture Notes Sustainable buildings: The energy performance of concrete construction. University of Canterbury.

BELLAMY, L. A. & MACKECHNIE, J. R. 2010. An Experimental Assessment of the Energy Performance of High Thermal Mass Concrete Walls in New Zealand. NZCS Conference, Wellington.

BELLAMY, L. A. & MCSAVENEY, L. G. 2003. FRST - Future Building Systems Research Proposal. Christchurch, New Zealand: University of Canterbury.

BERTOLINI, L., ELSENER, B., PEDEFERRI, P. & POLDER, R. P. 2005. *Corrosion of Steel in Concrete: Prevention, Diagnosis, Repair*.

BOBROWSKI 1978. FIP State of Art Report: Principles of thermal insulation with respect to lightweight concrete. Wexham Springs, Brittan: Cement and Concrete Association.

BODDY, A. M., HOOTON, R. D. & THOMAS, M. D. A. 2000. The effect of product form of silica fume on its ability to control alkali-silica reaction. *Cement and Concrete Research,* 30**,** 1139-1150.

BUI, V. K., MONTGOMERY, D., HINCZAK, I. & TURNER, K. 2002. Rapid testing method for segregation resistance of self-compacting concrete. *Cement and Concrete Research,* 32**,** 1489-1496.

CALDARONE, M. A. 2008. *High-strength concrete: a practical guide*, Taylor and Francis.

CCAA 1999. Thermal benefits of 'solid' construction. *In:* AUSTRALIA, C. A. C. A. O. (ed.). Australia.

CCANZ. 2007a. *Cement and Concrete Association of New Zealand, Thermal Performance of High Mass [Concrete] Houses* [Online]. . Available: http://www.ccanz.org.nz/page/Thermal-properties.aspx [Accessed 13 May].

CCANZ 2007b. Cement and ConcreteAssociation of New Zealand, Information Bulletin: IB 87. Concrete Masonary, Compliance with Clause H1 - Energy efficiency. Wellington, New Zealand.

CHIA, K.-S., KHO, C.-C. & ZHANG, M.-H. 2005. Stability of Fresh Lightweight Aggregate Concrete under Vibration. *Materials Journal,* 102**,** 347-354.

CHINNARAJU, K., SUBRAMANIAN, K. & SENTHIL-KUMAR, S. R. R. 2010. Strength properties of HPC using binary, ternary and quatenary cementitious blends. *Structural Concrete,* 11.

CONCRETE-SOCIETY 2003. Concrete Industrial Ground Floors: A guide to design and construction. Third ed.

CONTEC 2003. The ConTec BML Viscometer, Viscometer 4&5, Operating Manual. *In:* LTD, C. (ed.). Laugarvegi 7, Reykjavik, Iceland.

DAYARAM, K. 2010. *The Recarbonation of Crushed Concrete from a New Zealand Perspective.* MSc, The University of Canterbury.

FAXING, D. & ZHIWA, Y. 2006. Strength criterion for plain concrete under multiaxial stress based on damage Poisson's ratio. *Acta Mechanica Solids Sinica,* 19.

FERRARIS, C. F. & GAIDIS, J. M. 1992. Connection Between the Rheology of Concrete and Rheology of Cement Paste. *ACI Materials Journal,* 89**,** 388-393.

GAWIN, D. J., KOSNY, J. & WILKES, K. 2004. Thermal Conductivity of Moist Cellular Concrete - Experimental and Numerical Study. *ASHRAE: Buildings IX*.

GESOGLU, M., OZTURAN, T. & GUNEYISHI, E. 2004. Shrinkage cracking of lightweight concrete made with cold-bonded fly ash aggregates. *Cement and Concrete Research,* 34**,** 1121-1130.

GOLDENBAY. 2009. *Microsilica New Zealand, General Guide to Microsilica* [Online]. Available: http://www.microsilica.co.nz/media/documents/Technical%20Info/general_guide_to_microsilica.pdf [Accessed 24 Aug].

GUSTAVSSON, S. 2005. Hotdisk thermal constants analyzer - Instruction version 5.0. *Unpublished report.* Gothenburg.

HALLIDAY, RESNICK & WALKER 1997. *Fundamentals of Physics Extended*, John Wiley & Sons, Inc.

HOLCIM 2006. Westport Works. *Holcim (New Zealand) Ltd. Christchurch*.

HOLCIM. 2010. *How we make cement (wet process technology)* [Online]. Available: http://www.holcim.co.nz/en/editorials/holcim-new-zealand-cement-operations/uses-of-cement/how-we-make-cement-wet-process.html [Accessed 29 Aug].

HUSSIN, A. & POOLE, C. 2011. Petrography evidence of the interfacial transition zone (ITZ) in the normal strength concrete containing granitic and limestone aggregates. *Construction and Building Materials,* 25**,** 2298-2303.

KELHAM, S. 1988. A water absorption test for concrete. *Magazine of Concrete Research,* 40**,** 106-110.

KOEHLER, E. P. Year. Use of Rheology to Specify, Design and Manage Self-Consolidating Concrete. *In:* Supplementary Proceedings of the Tenth ACI International Symposium on Recent Advances in Concrete Technology and Sustainability Issues, 2009 Spain.

KWAN, A. K. H. & NG, I. Y. T. 2009. Optimum superplasticiser dosage and aggregate proportions for SCC. *Magazine of Concrete Research,* 61**,** 281-292.

LARRARD, F. D. & SEDRAN, T. 2002. Mixture proportioning of high-performance concrete. *Cement and Concrete Research,* 32**,** 1699-1704.

LI, C. Q., LAWANWISUT, W., ZHENG, J. J. & KIJAWATWORAWET, W. 2005. Crack Width Due to Corroded Bar in Reinforced Concrete Structures. *International Jounal of Materials & Structural Reliability,* 3**,** 87-94.

MACKECHNIE, J. R. 2006. Shrinkage of Concrete Containing Greywacke Sandstone Aggregate. *ACI Materials Journal,* 103**,** 390-396.

MACKECHNIE, J. R. 2010a. Course Notes ENCI621: Concrete Materials and Practices. University of Canterbury.

MACKECHNIE, J. R. 2010b. ENCI 621 Course notes - Deformation of Concrete.

MACKECHNIE, J. R. 2010c. Stratified Concrete Mix. University of Canterbury.

MACKECHNIE, J. R. 2011. Allied Concrete. *Personal communication.*

MACKECHNIE, J. R. & ALEXANDER, M. G. 2009. Using Durability to Enhance Concrete Sustainability. *Journal of Green Building,* 4**,** 52-60.

MACKECHNIE, J. R. & BELLAMY, L. A. 2011. Thermal Performance of Variable Density Wall Panels Made Using Portland Cement or Inorganic Polymer Concrete. *Unpublished Work.* Christchurch, New Zealand: University of Canterbury.

MACKECHNIE, J. R., BELLAMY, L. A. & MCSAVENEY, L. G. 2009. Development of stratified concrete wall panels. *Proceedings of the 11th International Conference on Non-conventional Materials and Technologies (NOCMAT 2009).* Bath, UK.

MACKECHNIE, J. R. & FENWICK, R. 2009. Assessing the Dimensional Stability of New Zealand Concrete. *SESOC Journal,* 22.

MACKECHNIE, J. R., KEYTE, L. & LLOYD, R. 2008. Durability of ambient and thermally cured inorganic polymer concrete made with Australasian and South African material, Unpublished Report. University of Canterbury.

MACKECHNIE, J. R. & SAEVARSDOTTIR, T. 2008. New Insulating Precast Concrete Panels. Christchurch, New Zealand: Canterbury University.

MACKECHNIE, J. R., SAEVARSDOTTIR, T. & BELLAMY, L. A. 2007. Stratified Precast Concrete Panels for Buildings. *Concrete Plant International*.

MAILVAGANAM, N. P., SPRINGFIELD, J., REPETTE, W. L. & TAYLOR, D. A. 2000. Curling of Concrete Floors Slabs on Grade - Causes and Repairs. *Journal of Performance of Constructed Facilities,* 15.

MALHOTRA & MEHTA 1996. *Pozzolanic and Cementitious Materials*, Gordon and Breach Publishers.

MARSHALL, J. 2011. Stahlton Engineered Concrete. *Personal communication.*

MCLEOD, R. S. 2005. Ordinary Portland Cement. *Building for a Future***,** 30-33.

MCSAVENEY, L. 2003. Golden Bay Cement/Stresscrete. *Personal communication.*

METSERVICE. 2011. *Past Weather - Christchurch Airport* [Online]. Available: http://www.metservice.com/towns-cities/christchurch [Accessed 19 Sep].

MICROSILICA NEW ZEALAND. 2009. *Microsilica 600* [Online]. Golden Bay. Available: http://www.microsilica.co.nz/mainmenu30/page71/Technical+Info.html [Accessed 25 Aug].

MINDESS, S., YOUNG, FRANCIS, J. & DARWIN, D. 2003. *Concrete,* New Jersey, Pearson Education, Upper Saddle River.

MONTEMOR, M. F., SIMOES, A. M. P. & FERREIRA, M. G. S. 2002. Chloride-induced corrosion on reinforcing steel: from the fundamentals to the monitoring techniques. *Cement and Concrete Composites,* 25**,** 491-502.

NANTHAGOPALAN, P. & SANTHANAM, M. 2010. A new emperical test method for the optimisation of viscosity modifying agent dosage in self-compacting concrete. *Materials and Structures,* 43:203-212.

NEVILLE, A. M. 1995. *Properties of Concrete*, Longman Group Limited, Longman House, Burnt Mill, Harlow Essex, England.

NEWMAN, J. B. 1993. *Properties of Structural Lightweight Aggregate Concrete,* Glasgow, Blackie Academic & Professional.

NEWMAN, J. B. & CHOO, B. S. (eds.) 2003. *Advanced Concrete Technology: Constituent materials,* London: Butterworth-Heinemann.

NILSEN, U. & AITCIN, P.-C. 1992. Properties of High Strength Concrete Containing Light-, Normal-, and Heavyweight Aggregate. *ASTM Journal of Cement, Concrete and Aggregates,* 14**,** 8-12.

NZS3112 1986a. New Zealand Standards, Specification for Methods of Test for Concrete, Part 1, Tests relating to fresh concrete.

NZS3112 1986b. New Zealand Standards, Specification for Methods of Test for Concrete, Part 2, Tests Relating to the Determination of Strength of Concrete.

NZS3122 1995. New Zealand Standard, Specification for Portland and Blended Cements.

NZS4218 2009. New Zealand Standards NZS 4218: Thermal insulation - Housing and small buildings (previously: Energy efficiency - small building envelope). Wellington, New Zealand.

PARK, Y. S. P. 2006. FRST Future Building Systems - Objective 3. Research Report. *Unpublished Report.* University of Canterbury.

PORAVER. 2006. Available: www.poraver.com [Accessed 21 June 2011].

ROGERS, E. M. 1995. Diffusion of Innovations. Free Press.

ROUSSEL, N. 2006. A theoretical frame to study stability of fresh concrete. *Materials and Structures,* 39:81-91.

SAEVARSDOTTIR, T. 2008. *The structural, serviceability and durability performance of variable density panels.* Masters in Civil Engineering, University of Canterbury.

SCHINDLER, A. K. 2003. Prediction of Concrete Setting. Alabama, USA: Department of Civil Engineering, Auburn University.

SHAPIRA, A. & ROSENFELD, Y. 2011. Achieving Construction Innovation through Academia-Industry Cooperation-Keys to Success. *Journal of Professional Issues in Engineering Education and Practice ASCE,* October 2011.

SHAYAN, A. 1985. Warping of Precast, White Concrete Panels. *Cement and Concrete Research,* 15**,** 245-252.

SIKA-CONSTRUCTION 2003. Sika ViscoCrete-5-555 (NZ): Superplasticiser for concrete and mortar. *In:* SIKA (ed.) 03/08 ed. Auckland, New Zealand.

SMITH, I. 2005. *Geology, Rocks and Minerals* [Online]. University of Auckland, School of Geography, Geology and Environmental Science. Available: flexiblelearning.auckland.ac.nz/rocks_minerals/rocks/greywacks.html [Accessed].

SORENSON, K., J.GUTT, T., LANIER, M. W., NIJHAWAN, J., SCHNEIDER, J. A. & WILDEN, H. 2000. Tolerance Manual for Precast and Prestressed Concrete Construction. United States: Precast/Prestressed Concrete Institute (PCI).

SWAMY, R. N. 1992. *The Alkali-Silica Reaction in Concrete*, Taylor and Francis.

THECONCRETECENTRE 2007. High Performance Buildings Using Concrete Frames and Cladding. *School Construction.*

THORNTON, J. 2003. *Field Guide to New Zealand Geology,* Auckland, Reed Publishing.

WALLEVIK, O. & NIELSSON, I. Year. "Rheology - A Scientific Approach to Develop Self-Compacting Concrete" *In:* Proceedings of the 3rd International RILEM Symposium on Self-Compacting Concrete, 2003. O. Wallevik and I Nielsson, RILEM Publications, 23-31.

WHITING, D., LITVIN, A. & GOODWIN, S. E. 1978. Specific Heat of Selected Concretes. *American Concrete Institute,* 75**,** 299-305.

WONG, A. C. L., CHILDS, P. A., TERRY, W., GOWRIPALAN, N. & PENG, G.-D. 2007. Experimental Investigation of Drying Shrinkage and Creep of Concrete Using Fibre-Optic Sensors. *Advances in Structural Engineering,* 10**,** 219-228.

YANG, L. & LI, Y. 2008. Cooling load reduction by using thermal mass and night ventilation. Department of Mechanical Engineering, The University of Hong Kong.

ZHANG, M.-H., LI, L. & PARAMASIVAM, P. 2005. Shrinkage of High-Strength Lightweight Aggregate Concrete Exposed to Dry Environment. *ACI Materials Journal,* 102.

Appendix 1: Temperature Measurements for Warping Testing

Date	T_{max} (°C)	T_{min} (°C)
Jul-22	9.3	-2.3
Jul-23	6.9	1.1
Jul-24	7.2	1.1
Jul-25	5.2	-1
Jul-26	5	-6.3
Jul-27	10.3	-2.7
Jul-28	15.6	-0.9
Jul-29	16.1	3
Jul-30	16.2	4.4
Jul-31	9.4	-3.9
Aug-01	10.5	-4.1
Aug-02	11.3	-2.9
Aug-03	15.3	-2.8
Aug-04	14.2	-3.4
Aug-05	13.4	0.2
Aug-06	12.5	3.4
Aug-07	15.8	1.3
Aug-08	10.1	-3.8
Aug-09	18.3	-3.5
Aug-10	11.6	0.3
Aug-11	12.1	-1.1
Aug-12	9.9	1.6
Aug-13	9.2	5
Aug-14	8.4	3.5
Aug-15	11.2	-1.4
Aug-16	4.6	-0.4
Aug-17	5.1	0.9
Aug-18	5	1.5
Aug-19	7.9	3.5
Aug-20	8.8	-1.5
Aug-21	12.4	-1.7
Aug-22	14.2	-1.3
Aug-23	15.5	-1.2
Aug-24	13.1	-2.2
Aug-25	20.8	-0.6
Aug-26	18	-0.5
Aug-27	14.9	5.2
Aug-28	17.2	3.3
Aug-29	13.6	7.6
Aug-30	12.5	1
Aug-31	17.8	2.5

Date	T_{max} (°C)	T_{min} (°C)
Sep-01	12.7	3.9
Sep-02	12.6	-0.8
Sep-03	12.2	-3
Sep-04	16.5	0.3
Sep-05	15.5	0.1
Sep-06	14.7	0.8
Sep-07	13.5	6.7
Sep-08	12.3	1.4
Sep-09	18.1	5.7
Sep-10	18.6	2
Sep-11	19	9.2
Sep-12	13.5	2.1
Sep-13	14.9	1.6
Sep-14	12	1.3
Sep-15	12.8	1
Sep-16	9.9	-1.8
Sep-17	14.3	2.3
Sep-18	12.3	2
Sep-19	15.7	6.3
Sep-20	11.3	3
Sep-21	11.3	3
Sep-22	11.3	6.6

References

NIWA. (2011). The National Climate Database: Max_min daily, from http://cliflo.niwa.co.nz/pls/niwp/wgenf.genform1_proc

Appendix 2: Thermal Analyser Numerical Data

U1		Sample 1	Sample 2	Sample 3	Average
Thermal Conductivity (W/mK)	Heavyweight	0.459	0.769	1.441	0.889667
	Transition	0.6362	0.6314	0.3729	0.546833
	Lightweight mid	0.4461	0.6596	0.4911	0.532267
	Lightweight top	0.5173	0.5247	0.5155	0.519167
Thermal Diffusivity (mm2/s)	Heavyweight	1.007	0.7082	0.7148	0.81
	Transition	0.5403	0.5717	0.4427	0.518233
	Lightweight mid	0.3122	0.6317	0.5645	0.5028
	Lightweight top	0.4405	0.3701	0.5493	0.4533
Specific Heat (mJ/m3K)	Heavyweight	0.4557	1.086	2.016	1.1859
	Transition	1.177	1.105	0.8424	1.041467
	Lightweight mid	1.429	1.044	0.87	1.114333
	Lightweight top	1.174	1.418	0.9384	1.1768
Probe Depth (mm)	Heavyweight	18	15.1	15.1	16.06667
	Transition	13.2	13.5	11.9	12.86667
	Lightweight mid	10	14.2	13.4	12.53333
	Lightweight top	11.9	10.9	13.3	12.03333
Temp Change (K)	Heavyweight	1.37	0.784	0.413	0.855667
	Transition	0.876	0.892	1.43	1.066
	Lightweight mid	1.08	0.874	1.17	1.041333
	Lightweight top	1.03	0.984	1.08	1.031333
layer thickness	Heavyweight	0.05	0.05	0.025	0.041667
	Transition	0.05	0.05	0.01	0.036667
	Lightweight mid	0.05	0.05	0.0825	0.060833
	Lightweight top	0.05	0.05	0.0825	0.060833
R- value	Heavyweight	0.1089	0.0650	0.0173	0.063767
	Transition	0.0786	0.0792	0.0268	0.061533
	Lightweight mid	0.1121	0.0758	0.1680	0.118625
	Lightweight top	0.0967	0.0953	0.1600	0.117329
		0.3963	**0.3153**	**0.3722**	**0.361254**

U2		Sample 1	Sample 2	Sample 3	Average
Thermal Conductivity (W/mK)	Heavyweight	0.9571	1.255	0.8275	1.0132
	Transition	0.483	0.4624	0.6511	0.532167
	Lightweight mid	0.4683	0.4477	0.3739	0.429967
	Lightweight top	0.4614	0.4199	0.4303	0.4372
Thermal Diffusivity (mm2/s)	Heavyweight	0.8507	0.7838	0.9638	0.8661
	Transition	0.5486	0.4951	0.6224	0.555367
	Lightweight mid	0.5983	0.4098	0.2806	0.429567
	Lightweight top	0.4227	0.377	0.5577	0.452467
Specific Heat (mJ/m3K)	Heavyweight	1.102	1.601	0.8378	1.180267
	Transition	0.8623	0.9339	1.046	0.9474
	Lightweight mid	0.7694	1.083	1.333	1.0618
	Lightweight top	1.092	1.087	0.7715	0.9835
Probe Depth (mm)	Heavyweight	16.5	15.8	17.6	16.63333
	Transition	13.3	12.6	14.1	13.33333
	Lightweight mid	13.8	11.5	9.48	11.59333
	Lightweight top	11.6	11	13.4	12
Temp Change (K)	Heavyweight	0.64	0.478	1.35	0.822667
	Transition	1.18	1.21	0.897	1.095667
	Lightweight mid	1.26	1.18	1.27	1.236667
	Lightweight top	1.24	1.26	1.32	1.273333
layer thickness	Heavyweight	0.035	0.045	0.045	0.041667
	Transition	0.01	0.01	0.01	0.01
	Lightweight mid	0.0775	0.0725	0.0725	0.074167
	Lightweight top	0.0775	0.0725	0.0725	0.074167
R- value	Heavyweight	0.0366	0.0359	0.0544	0.042269
	Transition	0.0207	0.0216	0.0154	0.01923
	Lightweight mid	0.1655	0.1619	0.1939	0.173778
	Lightweight top	0.1680	0.1727	0.1685	0.169705
		0.3907	**0.3921**	**0.4321**	**0.404981**

U3		Sample 1	Sample 2	Sample 3	Average
Thermal Conductivity (W/mK)	Heavyweight	1.033	1.126	1.187	1.115333
	Transition	0.7066	0.4954	0.7033	0.6351
	Lightweight mid	0.3059	0.4424	0.3756	0.374633
	Lightweight top	0.3444	0.4006	0.3076	0.350867
Thermal Diffusivity (mm2/s)	Heavyweight	0.9313	0.5961	0.9081	0.811833
	Transition	0.6017	1.275	0.4629	0.779867
	Lightweight mid	0.3659	0.3228	0.4616	0.383433
	Lightweight top	0.3462	0.318	0.3535	0.339233
Specific Heat (mJ/m3K)	Heavyweight	1.109	2.056	1.307	1.490667
	Transition	1.174	0.3887	1.52	1.027567
	Lightweight mid	0.8634	1.464	0.8354	1.054267
	Lightweight top	0.9946	1.26	0.8703	1.041633
Probe Depth (mm)	Heavyweight	17.3	13.8	17.1	16.06667
	Transition	13.9	20.2	12.2	15.43333
	Lightweight mid	10.8	10.2	12.2	11.06667
	Lightweight top	10.5	10.1	10.6	10.4
Temp Change (K)	Heavyweight	0.574	0.471	0.421	0.488667
	Transition	0.815	1.27	0.772	0.952333
	Lightweight mid	1.35	1.05	1.41	1.27
	Lightweight top	1.46	1.23	1.64	1.443333
layer thickness	Heavyweight	0.07	0.07	0.07	0.07
	Transition	0.01	0.01	0.01	0.01
	Lightweight mid	0.06	0.06	0.06	0.06
	Lightweight top	0.06	0.06	0.06	0.06
R- value	Heavyweight	0.0678	0.0622	0.0590	0.062968
	Transition	0.0142	0.0202	0.0142	0.016186
	Lightweight mid	0.1961	0.1356	0.1597	0.163837
	Lightweight top	0.1742	0.1498	0.1951	0.173017
		0.4523	**0.3678**	**0.4280**	**0.416007**

S3		Sample 1	Sample 2	Sample 3	Average
Thermal Conductivity (W/mK)	Heavyweight	1.689	1.838	1.994	1.840333
	Transition	0.8477	0.7597	0.6371	0.748167
	Lightweight mid	0.3888	0.3451	0.367	0.366967
	Lightweight top	0.3285	0.3239	0.3034	0.3186
Thermal Diffusivity (mm2/s)	Heavyweight	1.673	1.096	1.329	1.366
	Transition	0.7284	0.581	0.5338	0.6144
	Lightweight mid	0.3942	0.3837	0.4109	0.396267
	Lightweight top	0.4484	0.3931	0.3328	0.391433
Specific Heat (mJ/m3K)	Heavyweight	1.009	1.678	1.501	1.396
	Transition	1.164	1.307	1.194	1.221667
	Lightweight mid	0.9862	0.8994	0.893	0.9262
	Lightweight top	0.7326	0.824	0.9119	0.822833
Probe Depth (mm)	Heavyweight	16.4	13.2	14.6	14.73333
	Transition	15.3	13.6	13.1	14
	Lightweight mid	11.2	11.1	11.5	11.26667
	Lightweight top	12	11.2	10.3	11.16667
Temp Change (K)	Heavyweight	1.19	0.931	0.893	1.004667
	Transition	1.4	1.5	1.75	1.55
	Lightweight mid	1.35	2.99	2.88	2.406667
	Lightweight top	3.37	3.23	3.29	3.296667
layer thickness	Heavyweight	0.07	0.07	0.07	0.07
	Transition	0.01	0.01	0.01	0.01
	Lightweight mid	0.085	0.085	0.085	0.085
	Lightweight top	0.085	0.085	0.085	0.085
R- value	Heavyweight	0.0414	0.0381	0.0351	0.0382
	Transition	0.0118	0.0132	0.0157	0.0136
	Lightweight mid	0.2186	0.2463	0.2316	0.2322
	Lightweight top	0.2588	0.2624	0.2802	0.2671
		0.5306	**0.5600**	**0.5626**	**0.5511**

O1		Sample 1	Sample 2	Sample 3	Average
Thermal Conductivity (W/mK)	Heavyweight	1.234	1.283	1.552	1.356333
	Transition	0.458	0.4378	0.9586	0.618133
	Lightweight mid	0.2014	0.2123	0.3295	0.247733
	Lightweight top	0.2056	0.2095	0.2227	0.2126
Thermal Diffusivity (mm2/s)	Heavyweight	1.015	1.114	0.925	1.018
	Transition	0.9942	0.5012	1.023	0.839467
	Lightweight mid	0.2223	0.2255	0.3882	0.278667
	Lightweight top	0.2269	0.2768	0.2161	0.239933
Specific Heat (mJ/m3K)	Heavyweight	1.216	1.151	1.678	1.348333
	Transition	0.4607	0.8736	0.9374	0.757233
	Lightweight mid	0.9061	0.9415	0.8486	0.898733
	Lightweight top	0.9065	0.7569	1.03	0.8978
Probe Depth (mm)	Heavyweight	12.7	13.4	12.2	12.76667
	Transition	12.6	8.96	12.8	11.45333
	Lightweight mid	8.44	8.5	11.2	9.38
	Lightweight top	8.52	9.42	8.32	8.753333
Temp Change (K)	Heavyweight	1.64	2.6	1.07	1.77
	Transition	3.49	3.87	1.82	3.06
	Lightweight mid	3.72	3.55	1.59	2.953333
	Lightweight top	3.67	3.81	3.93	3.803333
layer thickness	Heavyweight	0.055	0.055	0.055	0.055
	Transition	0.1	0.1	0.1	0.1
	Lightweight mid	0.0925	0.0925	0.0925	0.0925
	Lightweight top	0.0925	0.0925	0.0925	0.0925
R- value	Heavyweight	0.0446	0.0429	0.0354	0.040959
	Transition	0.2183	0.2284	0.1043	0.183691
	Lightweight mid	0.4593	0.4357	0.2807	0.391906
	Lightweight top	0.4499	0.4415	0.4154	0.435596
		1.1721	**1.1485**	**0.8358**	**1.0522**

Appendix 3: Water Sorptivity

Water mass accumulation for each of the samples where slice 1 is the bottom layer (most dense) and slice 6 is the top layer (least dense)

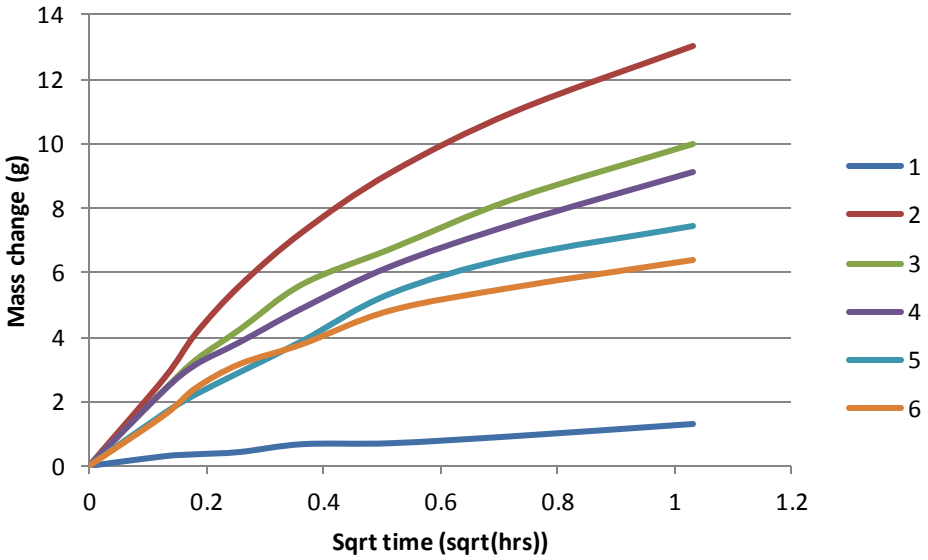

Figure 1: Water Sorptivity Results for Panel U1, test 1

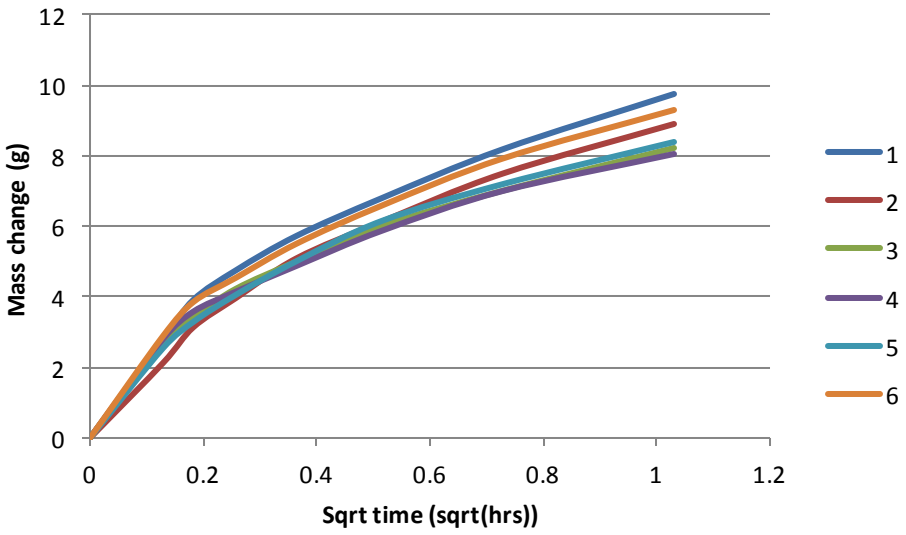

Figure 2: Water Sorptivity Results for Panel U1, test 2

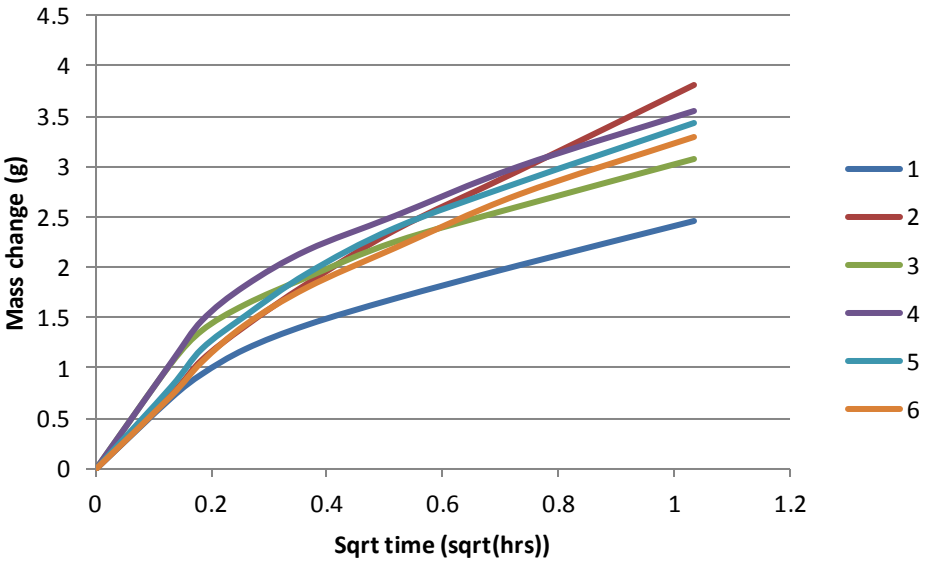

Figure 3: Water Sorptivity Results for Panel U2, test 1

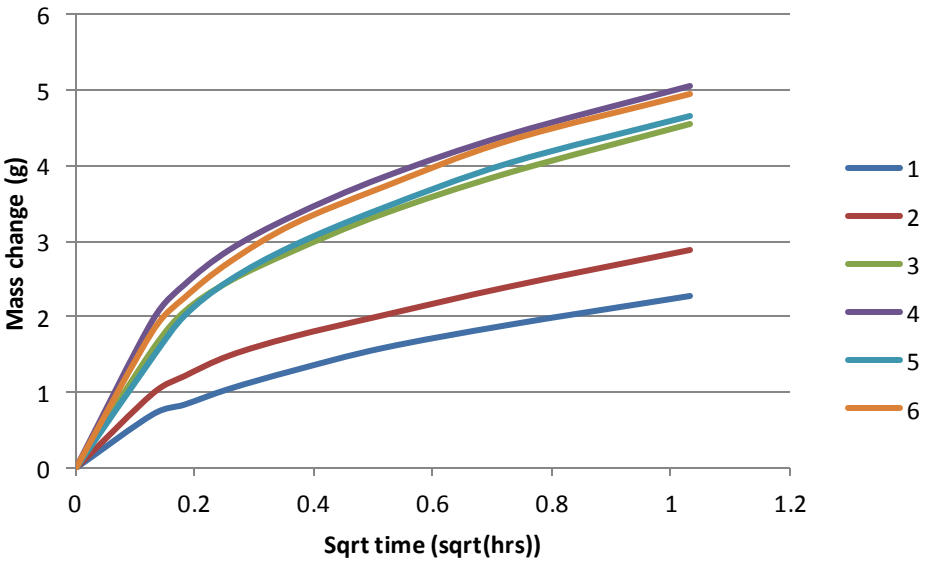

Figure 4: Water Sorptivity Results for Panel U2, test 2

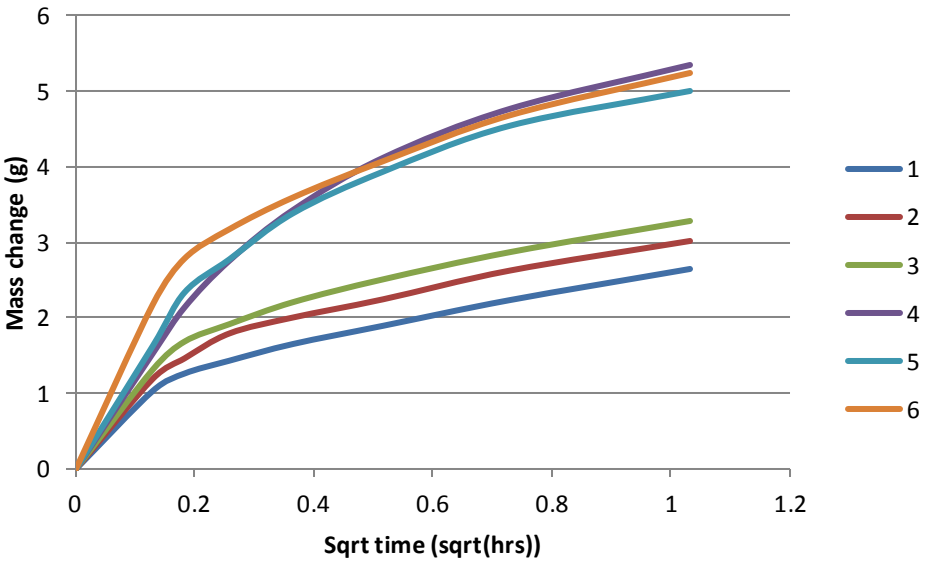

Figure 5: Water Sorptivity Results for Panel U3, test 1

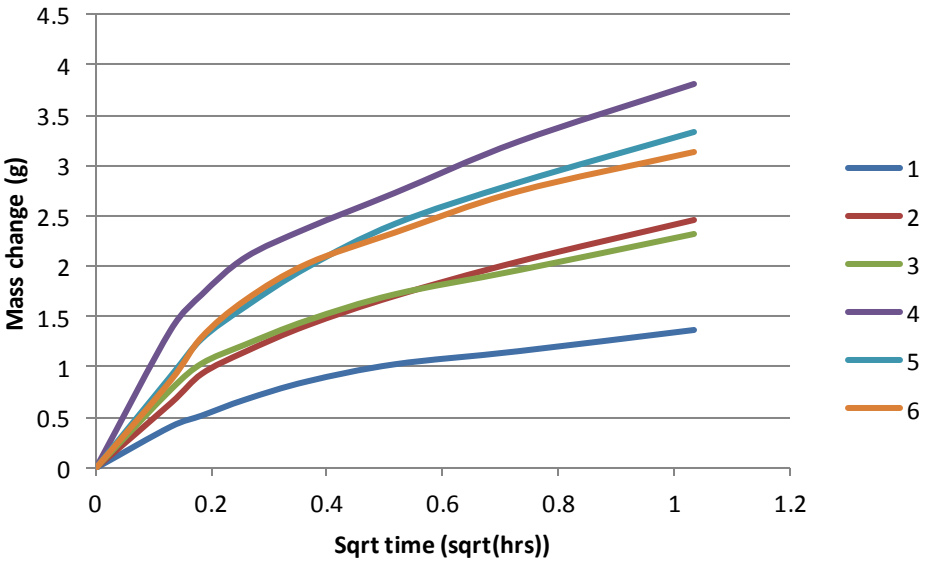

Figure 6: Water Sorptivity Results for Panel U3, test 2

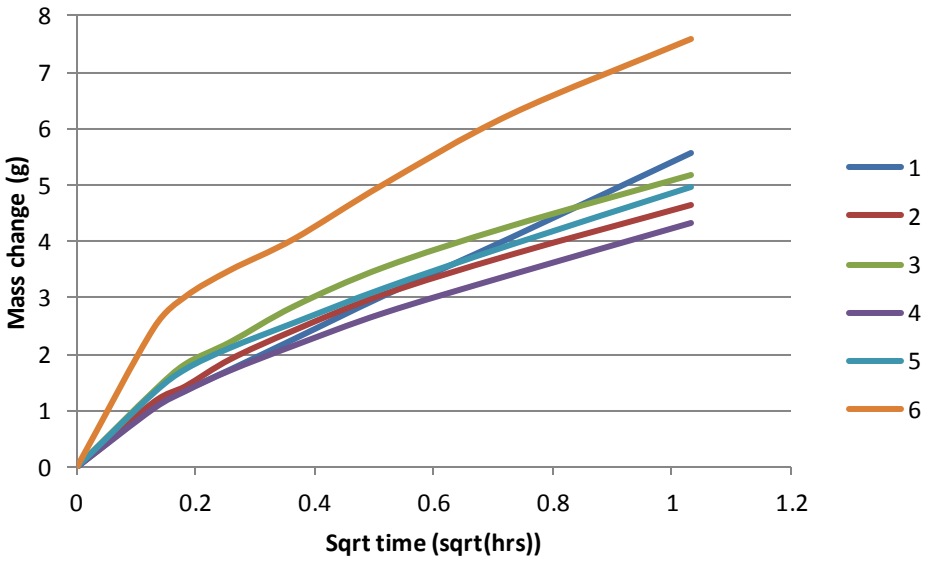

Figure.7: Water Sorptivity Results for Panel S3, test 1

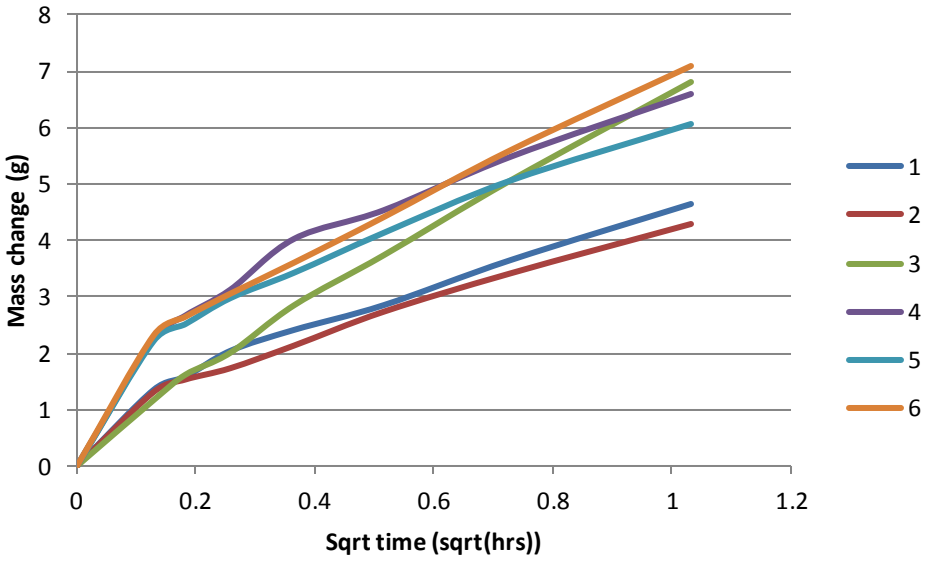

Figure.8: Water Sorptivity Results for Panel S3, test2

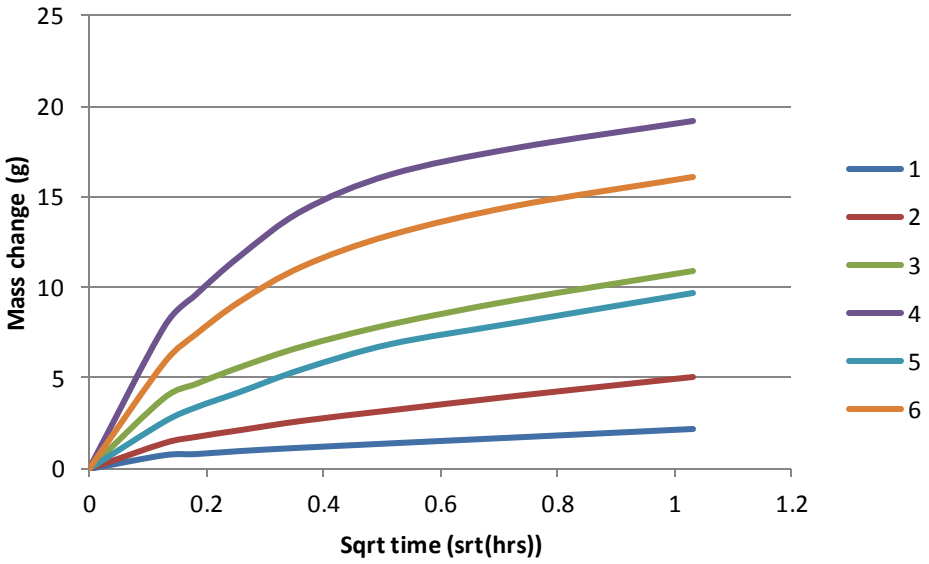

Figure 9: Water Sorptivity Results for Panel O1, test 1

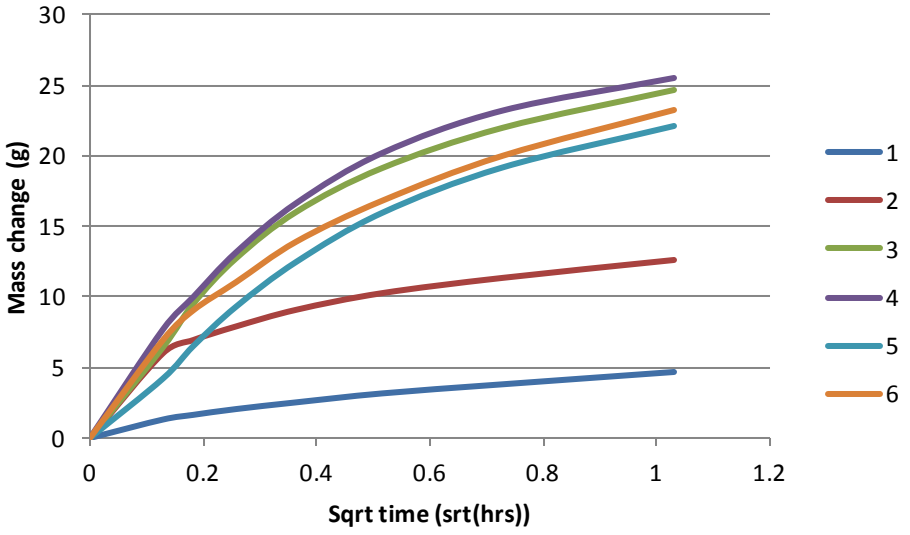

Figure 10: Water Sorptivity Results for Panel O1, test 2